NEUTRALIZATION OF DENGUE VIRUS SEROTYPE II BY POTENT HUMAN MONOCLONAL ANTIBODIES

WANG JIAQI

(*B.Sc.*, *Sun Yat-sen University*)

A THESIS SUBMITTED

FOR THE DEGREE OF DOCTOR OF PHILOSOPHY

DEPARTMENT OF BIOLOGICAL SCIENCES

NATIONAL UNIVERSITY OF SINGAPORE

2015

Declaration

I hereby declare that this thesis is my original work and it has been written by me in its entirety. I have duly acknowledged all the sources of information which have been used in the thesis.

This thesis has also not been submitted for any degree in any university previously.

Name of Candidature: Wang Jiaqi **Date:** 12 Aug, 2015

Signature: 

Acknowledgements

I would like to express my sincere gratitude to my supervisor, Associate Professor Lok Shee Mei for offering me the opportunity to carry out the research project, sharing her valuable knowledge and technical expertise, patient guidance and great encouragement during the last four years.

I would like to give my sincere thanks to my Thesis Advisory Committee members, Associate Professor Ooi Eng Eong, Professor Subhash Vasudevan and Assistant Professor Ashley Lauren St. John for their support and valuable advice. I am extremely grateful to current and former laboratory mates Dr. Zhang Qian, Dr. Guntur Fibriansah, Dr. Victor Kostyuchenko, Dr. Zhang Shuijun, Dr. Petra Kukkaro, Dr. Sebastian Lambert, Mr. Jonathan Ng T.S, Ms. Jaime Lee, Ms. Melissa Wirawan, Ms. Lim Xin Ying Elisa, Ms. Lim Xin Ni, Mr. Justin Ooi, Dr. Phat Vinh Dip, Dr. Joanne Tan Li-Ching and Ms. Pauline Chew for their kind help and assistance.

I thank the National University of Singapore for providing me the scholarship and opportunity to study here. Finally, I would like to thank my parents and wife for their continuous and great support all these years.

Table of Contents

Summary

Dengue virus (DENV) is a mosquito-borne flavivirus and infects approximately 400 million people annually. Currently, there are no approved vaccines or therapeutics available. Recent clinical trials of a tetravalent vaccine revealed a low efficacy, especially against DENV2. Here I have characterized two DENV2-specific neutralizing HMAbs. By using a combination of X-ray crystallography, hydrogen-deuterium exchange mass spectrometry (HDX-MS), and cryo-electron microscopy (cryo-EM) single particle analysis techniques, the epitopes of HMAbs 3F9 and 10.15 were identified to be localized at domain I and III of the envelope (E) protein, respectively. HMAb 3F9 was able to bind to the virus at 4^{o}C. In comparison, efficient binding of HMAb 10.15 to the virus particles can be achieved only at higher temperatures, indicating E protein motion was required to expose the epitope on the virus. The cryo-EM structure of the Fab fragment of HMAb 3F9 complexed with a DENV2 clinical isolate PVP94/07 showed that at saturating antibody concentrations, 120 of the 180 copies of E proteins on the virus surface were bound by Fab fragments. In contrast, Fab 10.15 could only bind to 60 copies of E proteins on the virus. Interestingly, Fab 10.15 is more

potent against another DENV2 strain New Guinea C (NGC) and the binding of Fabs resulted in a higher number of broken particles. Unlike HMAb 3F9, which Fab fragment was as neutralizing as the full-length immunoglobulin G (IgG), IgG 10.15 was approximately 100-fold more potent than Fab 10.15. This was most likely due to the larger steric hindrance caused by the size of a whole immunoglobulin. This unique characteristic of the whole HMAb 10.15 could compensate for its low binding occupancy on the virus surface thus leading to its overall high potency. Together, these findings show the complexity of antibody - flavivirus interaction and provide valuable clues in the selection of neutralizing antibodies for therapeutic purposes.

List of Abbreviations

Å	Angstrom
Ab	Antibody
ADE	Antibody dependent enhancement
ATCC	American Type Culture Collection
BHK-21	Baby hamster kidney 21
BSA	Bovine serum albumin
C	Capsid
CDR	Complementarity determining region
CLEC5A	C-type lectin domain family 5, member A
Cryo-EM	Cryo-electron microscopy
CTF	Contrast transfer function
DC-SIGN	Dendritic Cell-Specific Intercellular adhesion molecule-3-Grabbing Non-integrin
DENV	Dengue virus
DF	Dengue fever
DHF	Dengue Hemorrhagic fever
DLS	Dynamic light scattering
DSS	Dengue Shock Syndrome
DTT	Dithiothreitol
EBV	Epstein-Barr virus

E	Envelope protein
E-DI	Envelope protein domain I
E-DII	Envelope protein domain II
E-DIII	Envelope protein domain III
ELISA	Enzyme linked immunosorbent assay
ESI-Q-TOF MS	Electrospray ionization quadrupole time-of-flight mass spectrometry
EMDB	Electron Microscopy Data Bank
ER	Endoplasmic reticulum
Fab	Fragment, antigen binding
Fc	Fragment, crystallizable
FSC	Fourier shell correlation
H chain	heavy chain
HDX-MS	Amide hydrogen/deuterium exchange coupled with mass spectrometry
HRP	Horseradish peroxidase
Ig	Immunoglobulin
JEV	Japanese encephalitis virus
NGC	New Guinea C
kDa	kilo Daltons
L chain	light chain
log10	logarithm with base 10

M	membrane
MAb	monoclonal antibody
MHC	major histocompatibility complex
NS	Non-structural protein
PBS	Phosphate-buffered saline
PDB	Protein Data Bank
PDI	Polydispersity index
PFU	Plaque forming units
prM	pre-membrane
PRNT	Plaque reduction neutralization test
PVDF	Polyvinylidene fluoride
RC	Replication complex
RNA	Ribonucleic acid
RPMI 1640	Roswell Park Memorial Institute 1640 medium
PCR	Polymerase chain reaction
SD	Standard deviation
SDS-PAGE	Sodium dodecyl sulfate polyacrylamide gel electrophoresis
SNR	Signal to Noise ratio
SPR	Surface plasmon resonance
TBEV	Tick-borne encephalitis virus

WHO	World Health Organization
WNV	West Nile virus
YFV	Yellow fever virus
2D	Two dimensional
3D	Three dimensional

List of Tables

List of Figures

List of Publications

1. Guntur Fibriansah, Kristie D. Ibarra, Thiam-Seng Ng, Scott A. Smith, Joanne L. Tan, Xin-Ni Lim, Justin S. G. Ooi, Victor A. Kostyuchenko, **Jiaqi Wang**, Aravinda M. de Silva, Eva Harris, James E. Crowe Jr., Shee-Mei Lok. Cryo-EM structure of an antibody that neutralizes dengue virus type 2 by locking E protein dimers. *Science.* 3 July 2015: Vol. 349 no. 6243 pp. 88-91.
   I prepared the purified virus of mouse-adapted strain S221 used in the cryo-EM imaging for Fig. S2.

2. Satoru Watanabe, Kitti Wing Ki Chan, **Jiaqi Wang**, Laura Rivino, Shee-Mei Lok, Subhash G. Vasudevan. Dengue Virus Infection with Highly Neutralizing Levels of Cross-Reactive Antibodies Causes Acute Lethal Small Intestinal Pathology without a High Level of Viraemia in Mice. *Journal of Virology.* 2015, Jun; 89 (11):5847-61.
   I purified the virus of mouse-adapted strain S221 and also performed the dynamic light scattering experiment for measurement of the size of the antibody – virus complex. I also prepared the Figure 4 in this paper.

3. Guntur Fibriansah, Joanne L Tan, Scott A Smith, Adamberage R de Alwis, Thiam-Seng Ng, Victor A Kostyuchenko, Kristie D Ibarra, **Jiaqi Wang**, Eva Harris, Aravinda de Silva, James E Crowe Jr, & Shee-Mei Lok. A potent anti-dengue human antibody preferentially recognizes the conformation of E protein monomers assembled on the virus surface. *EMBO Mol Med.* 2014, Mar; 6 (3):358-71.
   I prepared the recombinant envelope protein of DENV1 used in this study.

4. Guntur Fibriansah, Thiam-Seng Ng, Victor A. Kostyuchenko, Jaime Lee, Sumarlin Lee, **Jiaqi Wang** and Shee-Mei Lok. Structural Changes in Dengue Virus When Exposed to a Temperature of 37°C. *Journal of Virology.* 2013, 87(13):7585.
   I prepared the purified virus sample of DENV2 strain NGC used in this study.

Manuscript in preparation

Jiaqi Wang, Thiam-Seng Ng, Victor A Kostyuchenko, Shuijun Zhang, Guntur Fibriansah, , Petra Kukkaro, Ganesh Anand, Paul A. MacAry, Brendon J. Hanson, and Shee-Mei Lok. A cryptic epitope in dengue serotype 2 virus captured by a potent human antibody.

Patent disclosure

A Fully Human Anti-Dengue Serotype 2 Antibody and Uses Thereof. Paul Anthony MacAry, En Wei Teo, Shee Mei Lok, **Wang Jiaqi,** Brendon John Hanson, Conrad En Zuo Chan. Invention Disclosure submitted October 2014

Chapter I. Literature review

1.1 Dengue virus

Dengue virus (DENV) was first independently isolated by Kimura et al. and Sabin et al back in the 1940s. It belongs to the virus genus *Flavivirus* of the family *Flaviviridae*, which also encompasses several other important human pathogens, such as West Nile virus (WNV), tick-borne encephalitis virus (TBEV), yellow fever virus (YFV) and Japanese encephalitis virus (JEV) (Fig. 1-1). As arboviruses (arthropod borne viruses), their main method of transmission is through the bite of infected arthropods (mosquito or tick). There are four serotypes of DENV, defined by their reactivity to anti-dengue antibodies. The nucleotide sequences of these serotypes share about 65% identity (Kuno et al., 1998)**.** DENV can be further classified into genotypes within each serotype based on their nucleic acid sequences (Rico-Hesse, 1990, Rico-Hesse, 2003). The diameter of the DENV particles is about 50 nm and its surface glycoproteins are arranged in icosahedral symmetry. The glycoprotein shell surrounds the lipid bilayer membrane which encloses the nucleocapsid. The nucleocapsid consists of multiple copies of capsid proteins complexed with the 11Kb single-stranded positive sense RNA genome.

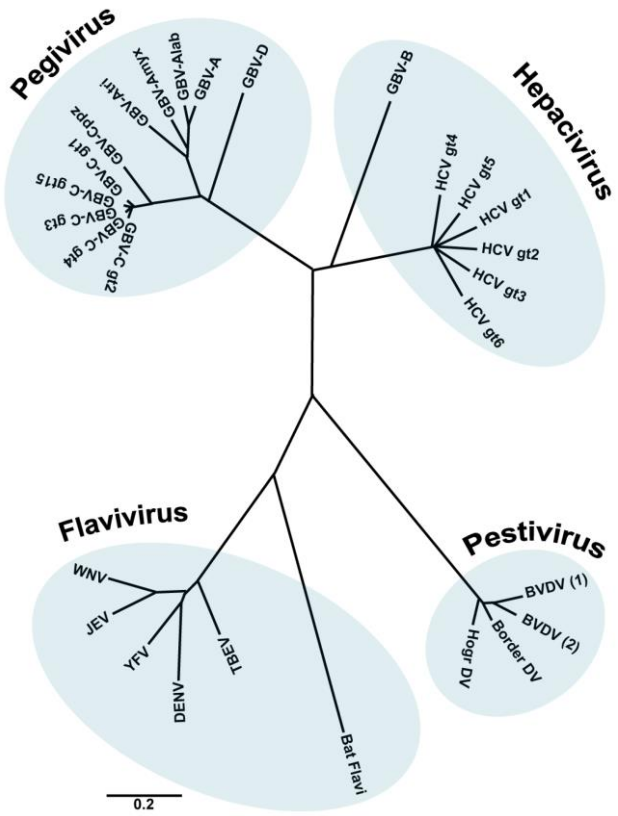

Figure 1-1 Phylogenetic tree of the family *Flaviviridae*. *Flaviviridae* composed of *Flavivirus, Pestivirus, Pegivirus* and *Hepacivirus* genera (Figure adapted from (Romero-Brey and Bartenschlager, 2014)).

There are two distinct DENV transmission cycles: (1) an endemic and epidemic cycle involving human hosts and transmission mainly by *Aedes aegypti* and *Aedes albopictus* mosquitoes, and (2) a cycle in sylvatic habitats, involving non-human primate hosts and several different *Aedes* mosquitoes (Gubler, 1988). Phylogenetic analysis of both endemic/epidemic and sylvatic DENV strains suggests that the endemic/epidemic forms evolved between 100 and 1,500 years ago

(Wang et al., 2000). Infected humans, in which the virus can propagate, serve as a source of the virus for uninfected mosquitoes.

1.2 Characteristics of dengue

Dengue virus infection typically causes a flu-like illness, which in rare cases, can develop into lethal complication called dengue hemorrhagic fever (DHF) or dengue shock syndrome (DSS). The symptoms start to appear after an incubation period of 3-14 days (Gubler, 1998). Dengue symptoms include fever, severe headache, pain behind the eyes, muscle and joint pains, nausea, vomiting, swollen glands or rash. Severe dengue is potentially fatal due to capillary leakage accompanied by thrombocytopenia, altered hemostasis, and liver damage (John et al., 2013). The pathogenesis of dengue remains unclear due to a complex interaction of viral and host factors. An infection with one dengue serotype renders lifelong protection against that particular serotype and short-term protection against the other serotypes. Secondary infection by a heterologous DENV serotype has been hypothesized as the greatest risk factor for severe dengue (Halstead, 1988).

1.3 Epidemiology of dengue

Dengue is endemic in tropical and subtropical regions, affecting half of the world's human population, with explosive outbreaks occurring more and more frequently (Guzman et al., 2010). It is estimated that 500,000 people with severe dengue require hospitalization annually and 2.5% of the affected die, a large proportion of whom are children (WHO, 2009). A recent estimate suggests that there are 390 million dengue infections each year with 96 million of them manifesting clinically (Bhatt et al., 2013). There is currently no approved specific treatment or vaccine for dengue.

1.4 Structure of dengue virus

Mature DENV particles has a spherical shape, and the virus surface is composed of 180 copies of envelope (E) proteins and the same number of membrane (M) proteins arranged in icosahedral symmetry. Envelope proteins form homodimers and a set of three homodimers lay parallel to each other, which forms a raft (Fig. 1-2d). There are 30 rafts on the virus surface. There are three individual E proteins (molecules (mols) A, B, C) in one asymmetric unit (Fig. 1-2d). They have different local chemical microenvironments. After viral RNA replication, dengue virus assembles in the endoplasmic reticulum (ER) as immature virus.

The virus surface contains pre-membrane (prM) protein, a precursor of the M protein (Lindenbach and Rice, 2003). The pr domain of the prM caps the fusion loop of E protein. This prevents the newly synthesized virus particles from fusing back into the cell during the maturation process (Li et al., 2008, Kostyuchenko et al., 2013) (Fig. 1-2b). The prM-E heterodimers are organized as trimers, each forming one of the 60 spikes on the surface of the immature virion.

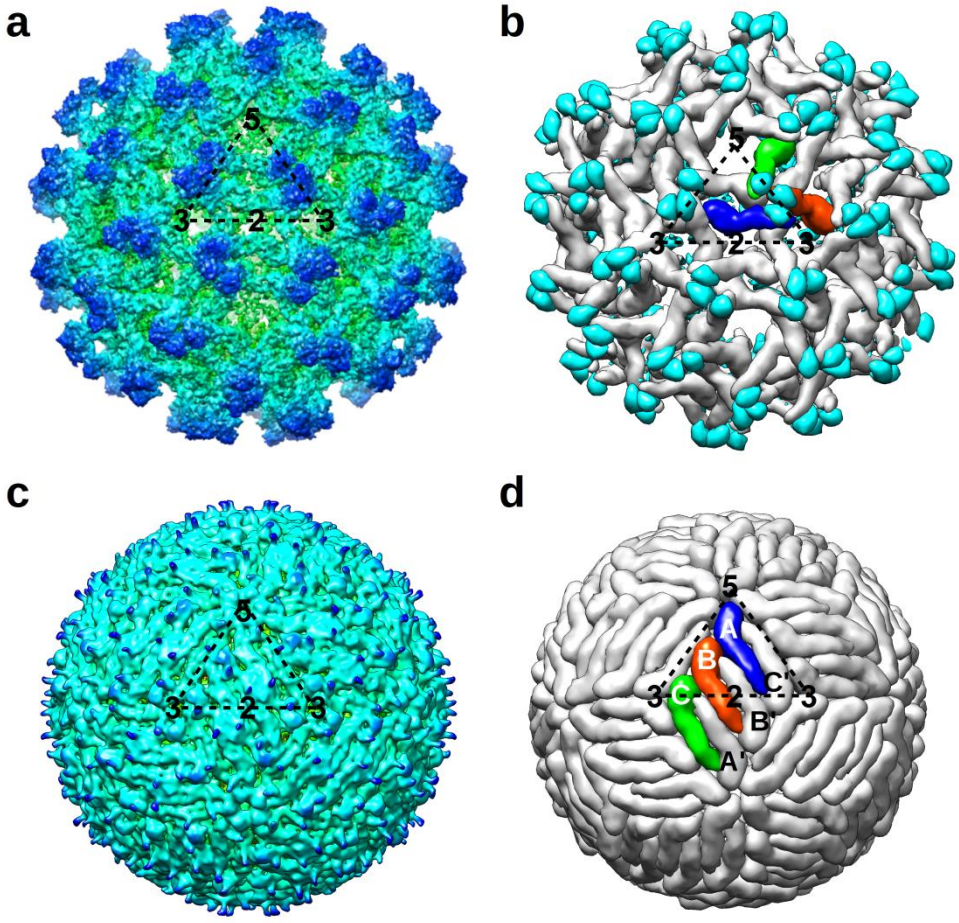

Figure 1-2 The cryo-EM structures of mature and immature DENV. Surface view of the cryo-EM density map of immature virus (a) and mature virus (c) are shown. Cryo-EM maps are colored radically: green,

0-200 Å; cyan, 201-235 Å; blue, 236 Å above. Organization of the surface proteins in the immature virus (b) and mature virus (d) structures. E protein mols A, B and C in an asymmetric unit are colored as green, red and blue, respectively. Symmetry-related E proteins are shown as grey surfaces, and prM proteins are shown as cyan surfaces. Black dotted triangles represent one asymmetric unit, the 5-, 3- and 2-fold vertices are indicated. For the mature virus in (d), mols A, B and C are labelled, mols in the nearby asymmetric unit forming the other half of the raft are labeled as A', B' and C'. Cryo-EM map of the mature and immature viruses are based on EMDB entry 5520 and 2141, respectively. The fitted models of mature and immature viruses are from PDB code 3J27 and 4B03, respectively.

The E protein layer of three DENV2 strains have been found to expand at elevated temperatures (Fibriansah et al., 2013, Zhang et al., 2013). Four classes of particles have been observed at higher temperatures for the DENV2 New Guinea C (NGC) strain (Fibriansah et al., 2013) (Fig. 1-3). Class I particles are similar to the compact unexpanded DENV2 structure while, the class II and III particles have larger radius. The E protein shell of class IV particles was shown to lose icosahedral symmetry. Temperatures above 33^{o}C (Zhang et al., 2013) was required to induce structural changes of virus particles.

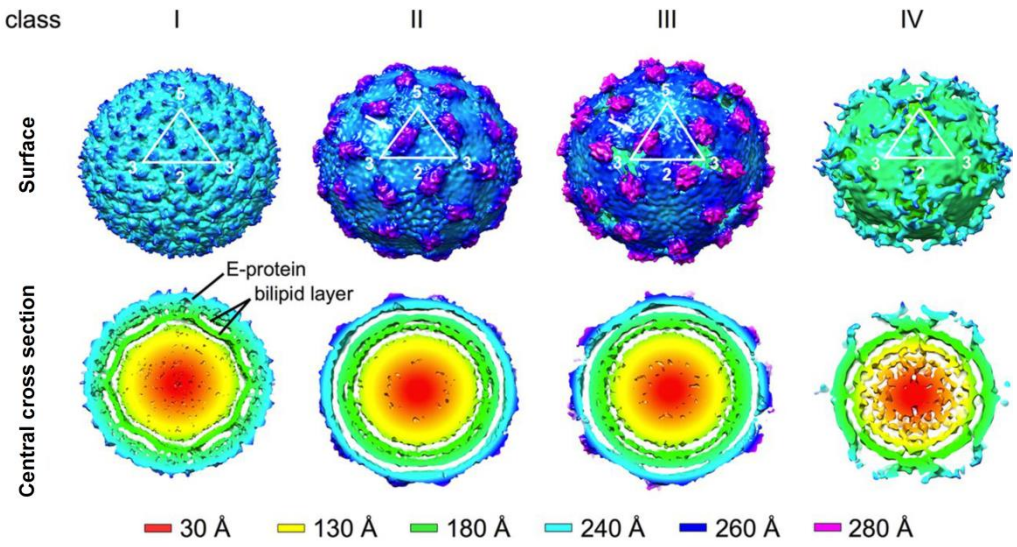

Figure 1-3 The Cryo-EM maps of class I to IV particles when DENV2 strain New Guinea C (NGC) sample was incubated at 37°C. The surfaces of the maps (above) and the central cross-sections (below) are colored radically (shown in the lower panel). The white triangle represents an icosahedral asymmetric unit, and the corresponding 2-, 3-, and 5-fold symmetry vertices are indicated (Figure extracted from (Fibriansah et al., 2013)).

1.5 Structure of proteins

The dengue virus genome is translated to one polypeptide which is subsequently processed into 3 structural (E, prM, C) and 7 non-structural proteins (NS1, NS2A, NS2B, NS3, NS4A, NS4B, NS5) by several host and viral proteases (Fig. 1-4) (Lindenbach and Rice, 2003). Structural proteins are the building blocks of the virus particle, while non-structural proteins mainly help the transcription, translation of the viral genome and post-translational modifications of the viral proteins. Detailed descriptions of each protein are below.

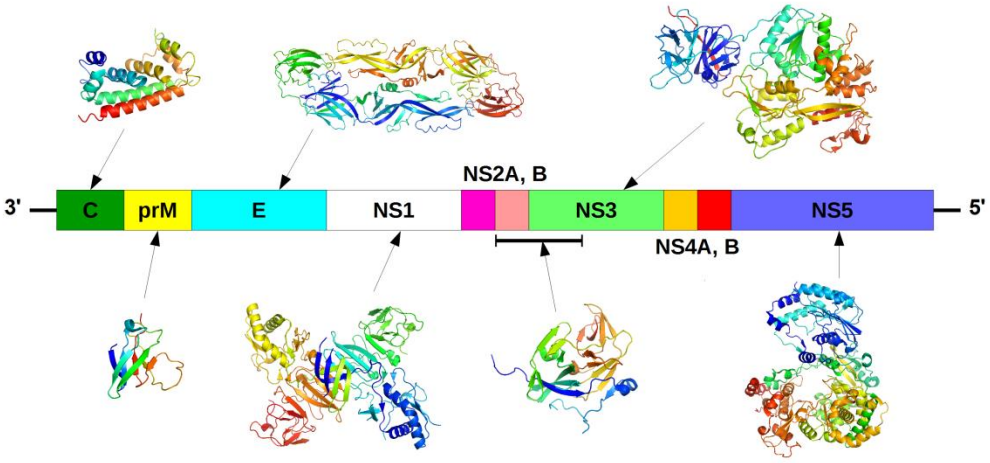

Figure 1-4 The known protein structures for dengue virus. From left to right: Capsid protein, PDB code 1R6R; prM protein (prM part of prM-E chimera), 3C6E; Envelope protein, 1OAN; NS1, 4O6B; NS2B-NS3 protease, 2FOM; NS3, 2VBC; NS5, 4VOQ.

1.5.1 Capsid protein

Capsid protein is a highly basic protein with a molecular weight of 12 kDa. The C-terminal hydrophobic signal peptide is removed by the NS2B-NS3 protease (Amberg et al., 1994, Yamshchikov and Compans, 1995). The RNA genome forms a complex with capsid proteins, which is encapsulated by the virus bilayer lipid membrane. Crystal and NMR structures of the capsid protein showed that it exist as dimers in solution (Jones et al., 2003, Ma et al., 2004). A capsid protomer consists of four helices: α1, α2 and α3 which form a three-helix core and a long α4 extending outwards. The capsid structure is stabilized by a large dimerization surface between the two protomers, contributed by α2-α2'

and α4-α4’ helix pairs. The charge distribution on its surface is asymmetric with a hydrophobic patch at the exposed surface of the α2-α2’ interface and a positive charge patch at the solvent-exposed edge of α4-α4’. The hydrophobic patch is assumed to interact with the lipid bilayer (Markoff et al., 1997), while the positive charge side is proposed to interact with the negatively-charged RNA genome (Wang et al., 2002, Ma et al., 2004).

1.5.2 The prM protein

The prM protein acts like a chaperone for envelope protein folding. It is cleaved by host protease furin to M and pr molecules when the immature virus is exposed to the low pH environment of the TGN (Stadler et al., 1997). The M part contains an ectodomain of about 20 amino acids, a stem region and two transmembrane helices (Zhang et al., 2003). In the mature virus surface, the M protein lies below the E protein shell (Zhang et al., 2003).

1.5.3 The E protein

The E protein has an elongated shape and a molecular weight of about 54 kDa. This multifunctional protein participates in receptor binding and membrane fusion processes (Rey et al., 1995). An E protein consists of the ectodomain, the transmembrane domain and a

stem region connecting these two domains (Fig. 1-5a). E protein ectodomain is further divided into three domains, domain I, II and III (Rey et al., 1995, Modis et al., 2003) (Fig. 1-5b). Domain I forms a β-barrel with eight β-strands and domain II has an elongated shape with the conserved hydrophobic fusion loop at its distal end. Domain I-II hinge facilitate the flipping of domain II so as to expose the fusion loop (Modis et al., 2004, Bressanelli et al., 2004). Domain III, which has an immunoglobulin fold, contains seven β-strands forming two β-sheets facing each other. The DI-III hinge facilitates the changes of position of DIII relative to DI as observed in the post-fusion E protein structure when exposed to low pH. E protein is glycosylated at one or two residues, depending on the cell line in which the virus is propagated (Lee et al., 1997). One of the glycosylated residue, N67, is demonstrated to be involved in the binding to the receptor DC-SIGN on dendritic cells (Mukhopadhyay et al., 2006). In low pH environment and with presence of liposomes, E proteins form the post-fusion trimeric structure, (Modis et al., 2004, Bressanelli et al., 2004) (Fig. 1-5c). In this structure, E protein domains undergo major rearrangements: domain II rotates ~30^{o} relative to domain I about the DI-II hinges, while domain III rotates ~70^{o} with respect to domain I. The changes result in the

formation of the packing interfaces and increased buried surface area of each monomer in the trimer compared to that in the dimer. The fusion loops are assembled at the tip of the trimer (Fig. 1-5c).

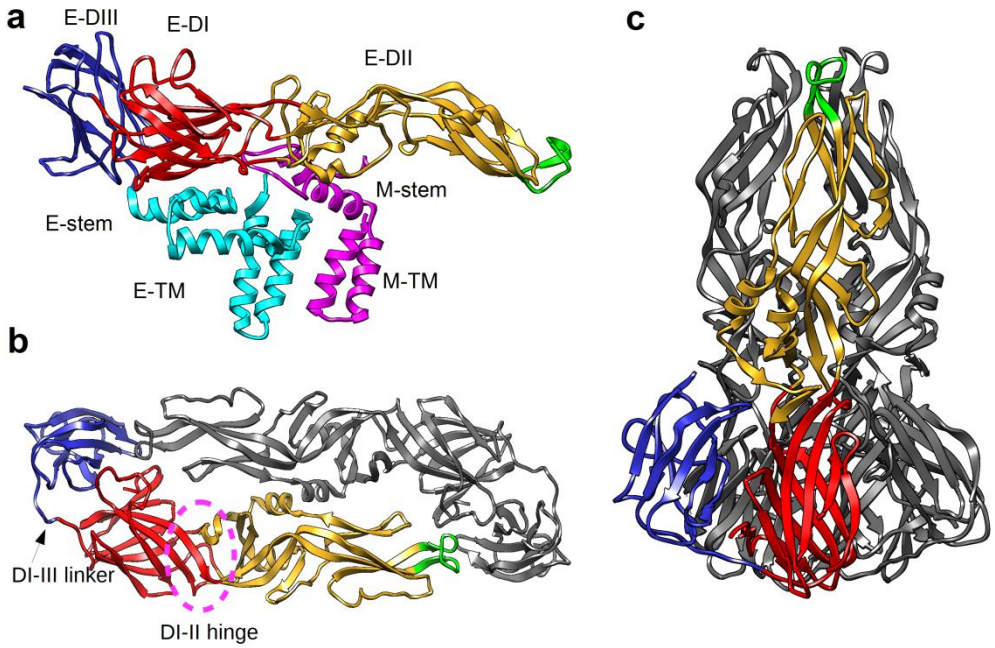

Figure 1-5 The Envelope protein of dengue virus.
(a) Cryo-EM structure of E protein and the M protein on mature virus (PDB code 3J27). E protein stem and transmembrane (TM) regions are colored as cyan. M protein stem and transmembrane (TM) regions are colored as magenta. (b) Crystal structure of dimeric E proteins at neutral pH (PDB code 1OAN), with DI-III linker and DI-II hinge highlighted. (c) Crystal structure of trimeric post-fusion E protein at low pH (PDB code 1OK8). Domain I, II and III of one of the E proteins are colored in red, yellow and blue, respectively. The fusion loop is colored in green. Symmetry-related E proteins in (b) and (c) are colored in grey.

1.5.4 Non-structural proteins

All non-structural proteins are involved in the formation of the replication machinery. They are assembled mostly on the cytoplasmic side of the ER membrane with only NS1 protein on the ER lumen side

(Muller and Young, 2013). In the replication complex, the NS3 and NS5 function on a scaffold form by the other four non-structural proteins (Fig. 1-6).

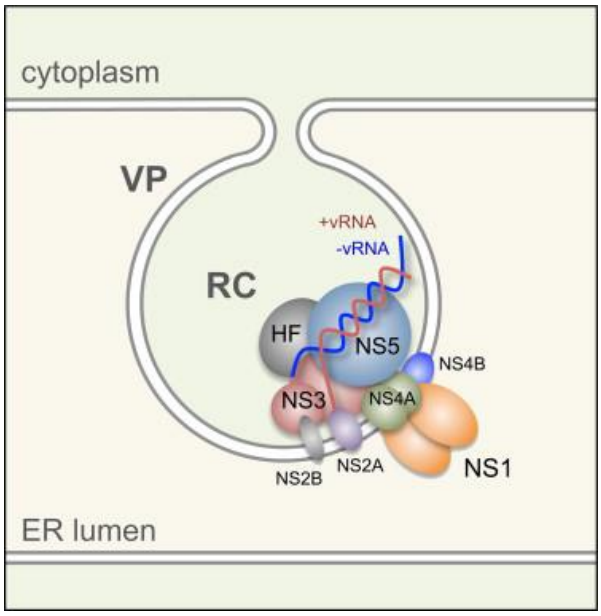

Figure 1-6 Hypothetical model of the dengue virus replication complex. The replication complex resides inside the membranous vesicle packets in infected cells. All seven non-structural proteins together with some host factors, forming the replication complex. This figure is adopted from (Muller and Young, 2013).

1.5.4.1 NS1

NS1 protein has three domains and its molecular weight that ranges between 46-55 kDa is dependent on the degree of glycosylation at three glycosylation sites: N130, N175 and N207 (Akey et al., 2014). NS1 glycoprotein exists in three different forms in infected cells: the intracellular dimeric form at the site of the viral replication complex on the ER membrane, the cell surface-associated form that might be

involved in signal transduction, and the secreted hexameric form that interacts with components of the complement-mediated immune system (Muller and Young, 2013). NS1 is essential for the replication of the flavivirus genome (Mackenzie et al., 1996, Lindenbach and Rice, 1997, Lindenbach and Rice, 1999), and involved in immune system evasion and pathogenesis (Chung et al., 2006, Avirutnan et al., 2010). Full-length NS1 protein has been crystallized as a hexamer (Akey et al., 2014), and is consistent with the electron microscopy structures (Gutsche et al., 2011, Muller and Young, 2013). NS1 hexamer forms an open-barrel protein shell with lipids in its central channel, which has been proposed a role in hijacking lipid metabolic pathways to result in endothelium dysfunction (Gutsche et al., 2011). It has also been postulated that cross-reactivity of anti-DENV NS1 antibodies to host proteins and endothelial cells can cause autoimmune reaction and endothelium dysfunction (Lin et al., 2003, Lin et al., 2005). NS1 is also a major target of the humoral immunity (Dejnirattisai et al., 2010, Beltramello et al., 2010).

1.5.4.2 NS3

NS3 carries out several enzymatic reactions, which are essential for

viral replication. The NS3 N-terminal domain together with the 40 residues long segment of NS2B serves as a serine protease, responsible for the cleavage of the viral polyprotein (Lindenbach and Rice, 2001, Bera et al., 2007). The C-terminal domain of NS3 is an ATPase/helicase can provide energy for the helicase domain to untangle the viral RNA for amplification (Li et al., 1999). Also, NS3-NS2A complex has been proposed to play a role in virus assembly (Patkar and Kuhn, 2008).

1.5.4.3 NS5

NS5 is a multifunctional enzyme that comprises of 900 amino acid residues. Its N-terminal portion contains an S-adenosyl-L-methioinine (SAM)-dependent methyltransferase (MTase) domain, which caps the viral RNA genome for stability and facilitates translation (Egloff et al., 2002). Methylations of the Guanine N-7 atoms and ribose 2'-OH also help evade the host innate immune response (Ray et al., 2006, Zhou et al., 2007). Residues 273-900 at the C-terminus end of NS5, is the RNA-dependent RNA polymerase (RdRp), which synthesizes the viral genome (Yap et al., 2007). NS5 can also antagonize the host interferon response by promoting degradation of STAT2 (Ashour et al., 2009).

1.5.4.4 NS2A, 2B, 4A, 4B

NS2A, NS4A and NS4B are small hydrophobic proteins with multiple transmembrane regions embedded in the ER membrane (Miller et al., 2006, Miller et al., 2007, Xie et al., 2013, Xie et al., 2014). NS2A participates in RNA synthesis and virion assembly/maturation (Xie et al., 2013). NS4A and NS4B co-localize with other DENV proteins and dsRNA, suggesting they may form part of the membrane-bound viral replication complex (Miller et al., 2007, Miller et al., 2006). They are thought to anchor other components of the replication complex to the cytoplasmic site of ER-derived membrane. For example, NS4B has been found to directly interact with NS1 (Youn et al., 2012) while NS2B mainly act as a cofactor of NS3 protease (Lindenbach and Rice, 2003). In addition, NS2A and NS4A are capable of blocking IFN-mediated signal transduction (Muñoz-Jordán et al., 2003, Muñoz-Jordán et al., 2005).

1.6 Life cycle of dengue virus

DENV has been shown to be able to infect various human cell types: dendritic cells, monocytes, macrophages, B cells, T cells, endothelial cells, hepatocytes, and neuronal cells, as well as a number of others

which can be used for viral propagation (Anderson, 2003). From clinical and autopsy studies, dendritic cells, monocytes and macrophages are found to be the primary targets for DENV infection in *vivo* (Jessie et al., 2004, Durbin et al., 2008).

It is hypothesized that during entry into the cell, the domain III of the E protein of DENV bind to a receptor (Crill and Roehrig, 2001, Rey et al., 1995). Several mammalian cell receptors or attachment factors have been identified, suggesting that DENV might be able to enter cells using more than one molecule. The identified receptors or attachment factors include heparan sulfate (Chen et al., 1997, Liu and Thorp, 2002), heat shock protein 70 and 90 (Reyes-del Valle et al., 2005), GRP78/BiP (Jindadamrongwech et al., 2004), CD14 (Chen et al., 1999), laminin receptor (Thepparit and Smith, 2004), mannose receptor (Miller et al., 2008) as well as DC-specific intercellular adhesion molecule 3 grabbing non-integrin (DC-SIGN) (Tassaneetrithep et al., 2003, Lozach et al., 2005, Navarro‐Sanchez et al., 2003). These receptors demonstrate different affinities and interactions to DENV. For example, DC-SIGN interacts with the virus via carbohydrate moieties on E protein (Pokidysheva et al., 2006). DENV can also interact with a C-type lectin receptor named CLEC5A, which stimulates the release of

proinflammatory cytokines (Chen et al., 2008).

Upon virus attachment to receptor, clathrin-mediated endocytosis ensues (van der Schaar et al., 2007). The virus is subsequently transported from the early endosomes to the late endosomes (van der Schaar et al., 2008), where the low pH environment and the anionic lipids of the endosomes induce the rearrangement of the virus surface proteins (Zaitseva et al., 2010). The E proteins rearrange from dimers to trimers and the fusion loop is inserted into the host-cell membrane. The movement of domain III relative to domain I/II folds the C-terminus of E protein towards the fusion loop, which bends the membranes to form a lipid fusion pore (Modis et al., 2004, Bressanelli et al., 2004). The viral genomic RNA is released into the cytoplasm and translated into polyprotein, which is then processed to form structural and non-structural proteins. As described in section 1.5.4, the non-structural proteins form replication complex, which initiates replication of the viral genome (Lindenbach and Rice, 2003). The newly synthesized RNA genome and structural proteins are assembled into immature virus and the virus is then transported through the TGN where the prM protein gets cleaved by the host protease furin. The pr peptide only falls off from the virus surface when the virus gets released to the extracellular

neutral pH environment (Stadler et al., 1997, Yu et al., 2008). This completes the maturation process.

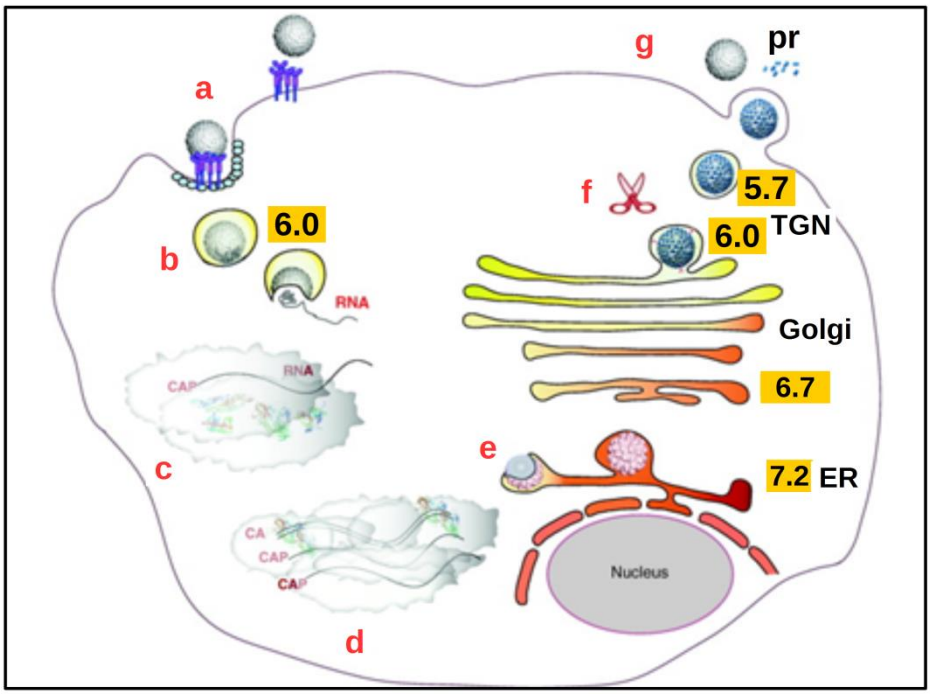

Figure 1-7 Life cycle of dengue virus.
(a) Virions enter the cell via receptor-mediated endocytosis. (b) In the endosome at acidic pH, E protein facilitates the fusion between virus and endosomal membranes, releasing the virus genome into the cytoplasm. (c) Viral RNA is translated. (d) Viral genomic RNA is replicated. (e) Immature virus particles are assembled at the ER membrane. (f) prM is cleaved by furin in TGN. (g) Mature virus is released into the extracellular environment, and the pr domain falls off the virus completing the maturation process. The numbers in colored boxes refer to the pH values in the respective compartments. Figure extracted from (Rodenhuis-Zybert et al., 2011).

1.7 Human immune response to dengue infection

Recovery from a dengue infection by one serotype provides lifelong immunity against that particular serotype, but cross-serotype protection

is only partial and temporary (Halstead, 1988). More importantly, subsequent infection with a second serotype, can result in the development of dengue hemorrhagic fever (Rothman, 2004, Halstead and O'Rourke, 1977a).

1.7.1 Cellular immune responses to dengue infection

The role of cellular response in dengue protection is complex. T cells recognize viral antigen presented by the MHC molecules in infected cell instead of intact virion and the main target of T cell response during a natural dengue infection has been found to be NS3 and NS5 (Rivino et al., 2012, Duangchinda et al., 2010). After recognizing virus-infected cells, T cells respond to DENV infection with diverse effector functions: proliferation of T cells, lysis of infected-cells and production of cytokines (Rothman, 2011). The cytokines produced include interferon-γ (IFNγ), tumour necrosis factor (TNF) and interleukin-2 (IL-2) (Rothman, 2011). IFNγ produced by stimulated CD4+ T cells was shown to be able to augment DENV infection *in vitro* in cooperation with antibody-virus immune complex (Kurane et al., 1989). This can be explained by a theory called “the original antigenic sin”, in which the cellular immune response is skewed to primary infection and is less effective for the clearance of a heterologous

secondary infection (Mongkolsapaya et al., 2003). The cross-reactive DENV-specific T cells offer suboptimal degranulation and high cytokine production, which contributes to the development of vascular leakage (Duangchinda et al., 2010). Inhibition of the central cytokine regulator CLEC5A was able to rescue mice from vascular permeability in a DHF/DSS mouse model (Chen et al., 2008). However, recent findings have presented a controversial view that pre-existing DENV-specific T cells are protective (Weiskopf et al., 2013, Dung et al., 2010). Additionally, it is important to note that the original antigenic sin alone cannot be the only risk factor for severe dengue disease, because infants, who do not have a pre-existing T cell memory, can also suffer from severe dengue (Kliks et al., 1988).

1.7.2 Humoral immune response to dengue infection

Antibody plays a key role in long-term protection against dengue (Sabin, 1952). This is supported by vaccine studies using inactivated Japanese encephalitis virus and yellow fever virus (Monath et al., 2002, Hoke et al., 1988). In a primary DENV infection, immunoglobulin M (IgM) antibodies are the first to be generated, peak at ~2 weeks following fever onset and subsequently decrease to undetectable levels over the next 2-3 months, whereas immunoglobulin G (IgG) antibodies start to

be detectable at low titer at the end of the first week of illness (Guzman et al., 2010) (Fig. 1-8). In contrast, during a secondary infection, high levels of IgG antibodies which are cross-reactive to many flaviviruses are already detectable even during the acute phase (Innis et al., 1989).

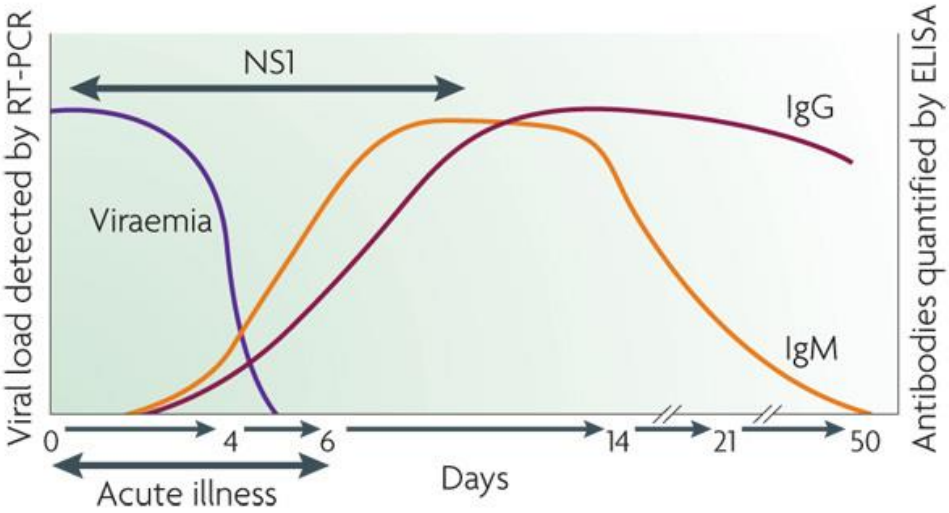

Figure 1-8 Antibody responses in primary dengue infection.
After dengue infection, NS1 can be first detected as well as viraemia. As viraemia wanes, IgM antibodies are first produced followed by IgG antibodies produced at the later stage. Figure adapted from (Guzman et al., 2010).

Antibodies against DENV can be protective but at lower concentrations, it can become detrimental to the patient due to a mechanism called antibody-dependent enhancement (ADE). One strong evidence for ADE is that maternal antibodies can induce DHF in newborn baby (Kliks et al., 1988). This phenomenon can also be observed both *in vitro* (Halstead and O'rourke, 1977b, Halstead and

O'Rourke, 1977a) and *in vivo* with animal models (Goncalvez et al., 2007, Zellweger et al., 2010). In this phenomenon, non-neutralizing antibodies, or neutralizing antibodies at sub-neutralizing concentration, were shown to ligate Fc-γ receptors on monocytes or macrophages to suppress innate immunity (Chan et al., 2011, Balsitis et al., 2010).

Serotype-specific DENV antibodies bind to only one serotype; DENV complex reactive antibodies cross-react with different serotypes. Most of the IgG antibodies generated from natural infection are cross-reactive and weakly neutralizing and only a small subset of them is serotype-specific and highly neutralizing (Beltramello et al., 2010, de Alwis et al., 2011, Dejnirattisai et al., 2010). These antibodies react with E, prM and NS1. Antibodies targeting NS1 can be protective. They can stimulate complement-mediated lysis of infected cells or Fc-γ receptor-mediated phagocytosis following antibody recognition of cell surface-bound NS1 (Muller and Young, 2013). Due to molecular mimicry, NS1 can also elicit antibodies, which cross-react with host cell components, such as platelets and components of extracellular matrix. This could cause damage to the endothelial cells. Antibodies targeting prM are mostly cross-reactive, non-neutralizing and ADE-promoting (Rodenhuis-Zybert et al., 2010, Dejnirattisai et al., 2010). Antibodies

targeting E proteins are protective and produced at a level sufficient for neutralization of all DENV serotypes during early convalescence following acute infection (Sabin, 1952). However, as antibody levels decline, only serotype-specific antibodies remains neutralizing and are able to protect the host from re-infection. Serotype-specific antibodies have hence been suggested to play a key role in the life-long protection against dengue infection.

An ideal therapeutic antibody should render strong neutralization while at the same time minimize or even eliminate enhancement across serotypes. Neutralization is defined here as the abolition of virus infection without a need for leukocytes (except production of the antibody). There are two strategies to develop an antibody therapy for DENV infection. One of which is to generate cross-reactive antibodies that can bind to and neutralize all four serotypes of dengue virus. This requires the identification of antibodies that bind to functional epitopes conserved between all four serotypes. The other strategy is to generate highly neutralizing serotype-specific antibodies, and combine antibodies each specific to a serotype into a cocktail.

1.7.3 Neutralization of dengue virus by monoclonal antibodies

Highly neutralizing murine monoclonal antibodies have been

extensively studied. They are mainly mapped to E protein domain III (E-DIII), including lateral ridge and A-strand (Crill and Roehrig, 2001, Sukupolvi-Petty et al., 2007, Nybakken et al., 2005, Lok et al., 2008, Cockburn et al., 2012a) (Fig. 1-9a). However, a previous study has also showed that the E-DIII lateral ridge antibody was detected at low levels and did not correlate with clinical outcomes (Oliphant et al., 2007). It has also been found that one highly neutralizing chimpanzee antibody bound to E-DI and the same epitope region was demonstrated to be immunogenic in humans by the same study (Cockburn et al., 2012b) (Fig. 1-9b).

With the recent technological developments in isolating human monoclonal antibodies (MAbs) from memory B cells and plasmablasts, neutralizing epitopes recognized by human monoclonal antibodies can be characterized. Although some of the neutralizing antibodies from humans are still mapped to E-DIII A-strand (Beltramello et al., 2010), anti-DIII antibodies have been shown to form only a small fraction in the repertoire of human antibodies. This is consistent with another study showing that human serum depleted of E-DIII targeting antibodies remained highly neutralizing against dengue virus (Crill et al., 2009, Wahala et al., 2009, Williams et al., 2012). Compared to murine

neutralizing antibodies, human serotype-specific neutralizing antibodies target quaternary structure-dependent epitopes present only on intact compact mature dengue virus (de Alwis et al., 2012, Teoh et al., 2012, Kaufmann et al., 2010, Fibriansah et al., 2014, Fibriansah et al., 2015b) (Fig. 1-9d). Also, a new class of epitope that is recently identified is the E protein dimer epitope (Fig. 1-9c). Antibodies targeting this class of epitopes can be either cross-reactive or serotype-specific (Fibriansah et al., 2015a, Dejnirattisai et al., 2015, Rouvinski et al., 2015). However, the majority of antibodies in the human serum are cross-reactive and poorly neutralizing and they target either prM protein or E-DI/II, especially the fusion loop region (Dejnirattisai et al., 2010, Beltramello et al., 2010, de Alwis et al., 2011, Lai et al., 2008, Smith et al., 2012). Although antibodies targeting the fusion loop or adjacent regions isolated from patients from primary infection are generally poorly neutralizing, its neutralization capacity seemed to improve in patients in secondary infection (Tsai et al., 2013).

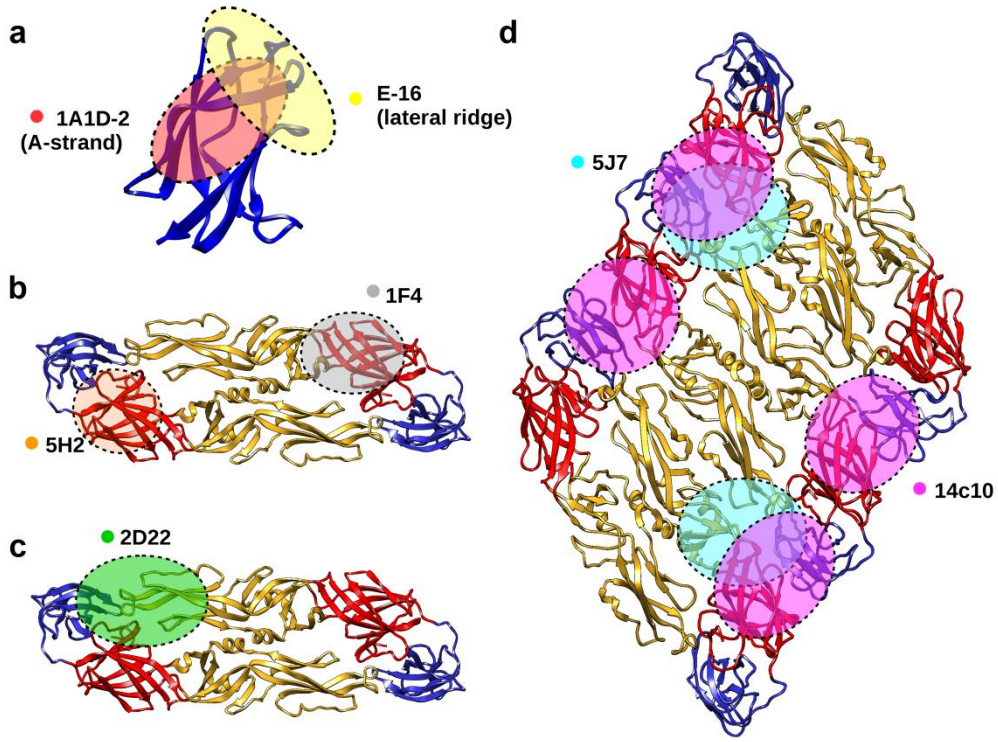

Figure 1-9 Major neutralizing epitopes of DENV antibodies. Highly neutralizing epitopes are classified as anti E-DIII lateral ridge and A-strand (a), E-DI (b), envelope dimer epitope (EDE) (c), and quaternary structure-dependent antibodies (d). The epitope is highlighted with a circle of the same color as the dot near the name of a typical antibody from that class. In (b), the antibody 1F4 binds to E-DI and DI/II hinge with its footprint restrained to E protein monomer. But it only recognizes the E protein on the virus surface with the correct hinge angle, thus it can also be considered as a quaternary structure-dependent antibody.

The potency of antibodies can partially be determined by its affinity to the epitope and also the accessibility of the epitope on the virus particle (Pierson et al., 2007). Antibody affinity, defined as the strength of the antibody-antigen interaction, has been found to correlate with neutralizing activity *in vitro*. Lower binding affinities of the same

antibody to various virus strains or genotypes can result in the reduction of its neutralization potency (Sukupolvi-Petty et al., 2010, Wahala et al., 2010). However, differences in antibody neutralizing capabilities against different virus strains cannot always be fully explained by the variation of antibody affinity alone (Shrestha et al., 2010, Austin et al., 2012).

Epitope accessibility, defined as the number of epitopes accessible for binding on the virion, has therefore been suggested to explain for this discrepancy. The number of antibodies which was required to neutralize a virion was suggested to be determined by the accessibility of the particular epitope (Pierson et al., 2007). For a more potent MAb, a lower fraction of all accessible epitope sites was required to be bound for neutralization. In addition, weakly neutralizing MAbs with less accessible epitope sites on the virus surface were suggested to require almost complete occupancy. Antibody needs to achieve a critical number of occupancy for neutralization, lower occupancy than that was thought to result in the enhancement of infection in cells bearing Fc-γ receptors. For instance, the occupancy on the virus particle in order to neutralize WNV, a closely related flavivirus, was suggested to be 30 out of 180 copies of its surface E proteins. Epitope accessibility can be influenced by (1) steric hindrance caused by the different domains

within a protein or by the neighboring E proteins on the virus structure, (2) the different E protein arrangement due to various virus maturation state, and (3) the dynamics of virus structure (Dowd and Pierson, 2011, Lee et al., 2013, Dowd et al., 2014). For example, the epitope of cross-reactive non-neutralizing murine antibody, 2H12, was found to be centered on the E-DIII AB loop, which was blocked by steric obstruction by the fusion loop from the opposing E protein molecule in the E dimeric structure (Midgley et al., 2012). Another antibody E53, was shown to be unable to bind to mature virus since its epitope, the fusion loop, is hidden in this conformation. It however, binds to E proteins in the immature virions as the epitope is exposed (Cherrier et al., 2009). Recent findings showing that the mature DENV2 can undergo structural changes when incubated at human physiological temperatures (Fibriansah et al., 2013, Zhang et al., 2013) and therefore can alter epitope accessibility.

Anti-DIII antibodies can neutralize DENV by inhibiting attachment (Crill and Roehrig, 2001) or the fusion process (Thompson et al., 2009). Binding of antibodies to E-DIII was also suggested to trap virus at its transition fusion structure (Kaufmann, 2006). On the other hand, antibodies that bind quaternary structure-dependent epitopes can

cross-link virus surface preventing E protein rearrangement required for different stages of entry into cells, such as attachment or fusion (Fibriansah et al., 2014, Teoh et al., 2012). Lastly, another class of antibodies that bind to partially hidden epitopes, such as murine antibody 1A1D-2, neutralizes virus by disrupting the virus surface structure (Lok et al., 2008). While various neutralization mechanisms have been identified, there are still many unknowns, as such, a complete understanding of DENV - human antibody interaction would provide important information for vaccine and therapeutics development.

1.8 Dengue vaccine

The development strategy for dengue vaccine can be generally categorized into four types, each with its own advantages and drawbacks. The four types of vaccines are inactivated virus, live attenuated virus, recombinant protein vaccine and DNA vaccine. Successful vaccines had been developed for other flavivirus such as, the yellow fever virus (YFV), Japanese encephalitis virus (JEV), and tick-borne encephalitis virus (TBEV). Among them are the YF17D (for YFV), and SA14-14-2 (for JEV) live attenuated vaccines, and the

inactivated TBEV vaccine. There is also an inactivated virus vaccine for JEV. Significant progress has been made in the development of tetravalent DENV vaccine. There is currently one vaccine candidate in phase III clinical trials, and others at earlier stages of clinical development (Thomas, 2014).

1.8.1 Inactivated virus vaccine

The inactivated virus vaccine does not replicate in patients and is therefore likely to be safe. However, the immune response elicited is generally weaker than when live attenuated vaccine is used. Some candidate inactivated DENV vaccine has been developed and the result shows that it can induce highly neutralizing antibody response that protects against viraemia in a primate model (Putnak et al., 1996).

1.8.2 Live attenuated virus vaccine

Live attenuated vaccine contains virus with reduced replication capability, so that it will not cause disease, but is able to elicit adaptive immune responses. Live-attenuated vaccines can be generated by two strategies, either by continuous passaging of the virus in tissue culture, or constructing mutant virus with its RNA backbone modified.

A tetravalent live attenuated vaccines, ChimeriVax from Sanofi Pasteur, has completed the phase III clinical trial (Guy et al., 2011). It

consists of DENV prM and E structural genes inserted into the yellow fever vaccine (YF17D) backbone (Guirakhoo et al., 2001). The safety of this vaccine has been proven in phase I trial, which also showed relatively low viraemia in vaccinated individuals (Capeding et al., 2011). Phase II trial of this vaccine confirmed its safety but showed varied efficacy against different serotypes, with essentially no protection against DENV2, leading to an average efficacy of only 30.2% (Sabchareon et al., 2012). Phase III trial of this vaccine in Asia showed that it could reduce the incidence of symptomatic infection and hospital admission with a efficacy of 56.5%, However, the efficacy against DENV2 was lower, consistent with the observations in phase II trial (Capeding et al., 2014). The vaccine trials showed vaccinated volunteers above the age of 9 did not have disease enhancement after natural infection with dengue and also hospitalization is reduced (Hadinegoro et al., 2015). However, vaccinated children below the age of 9 year showed increased hospitalization.

In another case, attenuated DENV vaccine candidate developed by Mahidol University had not been successful due to adverse side effects observed in the phase I and II clinical trials (Kanesa-Thasan et al., 2001, Sabchareon et al., 2004, Kitchener et al., 2006). This vaccine was

produced by passaging the different DENV serotypes multiple times in either primary dog kidney cells or primary African green monkey kidney cells and combining them into a tetravalent formulation (Bhamarapravati and Sutee, 2000).

Similarly, a tetravalent vaccine developed by the Walter Reed Army Research Institute (WRAIR) was produced by passaging all dengue virus serotypes in primary dog kidney cell (PDK-53) and then a final passage in fetal rhesus lung cell (Butrapet et al., 2000). This vaccine induced differing immunogenicity and reactogenicity towards the four different serotypes (Sun et al., 2003, Edelman et al., 2003, Sun et al., 2009). In this vaccine, DENV1, DENV3 and DENV4 were not attenuated enough to prevent development of disease. The PDK-53 vaccine strain of DENV2 was then used as a backbone to engineer chimeric vaccine whereby its structural protein genes were swapped with those from DENV1, 3 or 4. This formulation was named DENVax (Huang et al., 2003). Phase I trial of this vaccine showed low side effects and can induce immunogenicity in healthy, flavivirus-naive adults (Osorio et al., 2014). However, further clinical trials in different age groups and in dengue-endemic areas are needed.

Site-directed mutagenesis of the viral genome could also be used as

an attenuation strategy. DENV1 and DENV4 with their 30-nucleotide deleted (Δ30) in the 3'-UTR, retained their immunogenicity (designated DEN1Δ30 and DEN4Δ30) (Men et al., 1996, Whitehead et al., 2003). The DEN4Δ30 was then used as a backbone to engineer chimeric DENV2 and DENV3 vaccines. Various tetravalent mixtures are currently being tested in Phase I clinical trial (Kirkpatrick et al., 2015, Durbin et al., 2013). After vaccination, the characteristics of HMAbs derived from memory B cells were similar to those generated in a natural infection (Smith et al., 2013).

1.8.3 Recombinant protein vaccine

Similar to inactivated vaccine, recombinant E protein vaccine is expected to have a better safety profile. Induction of an equally protective immune response against the different serotypes can also be controlled by differing dosage of E proteins from each serotype. However, since the protein is small in size, addition of adjuvants and multiple injections are required to stimulate immune response. E protein constructs, developed by Hawaii Biotech (later acquired by Merck & Co), contain prM and 80% of E protein. These recombinant proteins are expressed with Drosophila melanogaster Schneider 2 (S2) cells in their native structures (Clements et al., 2010, Coller et al., 2011). This

vaccine is currently undergoing phase I clinical trial. There are also other dengue protein constructs developed to be vaccine candidates. The domain III of E protein as a fusion protein (Hermida et al., 2006, Bernardo et al., 2008, Leng et al., 2009), or E-DIII plus capsid (Zuest et al., 2015), have been developed and served as proof-of-concept that a fragment of the DENV structural proteins can induce protective immunity in various animal models.

1.8.4 DNA vaccine

DNA constructs can also be used as vaccines. Peptides of antigens are expressed after these DNA constructs are introduced into cells. Compared to conventional vaccines, its advantages include ease of production, better stability at room temperature and the possibility to vaccinate against several pathogens in a single vaccination (Beckett et al., 2011). Nevertheless, adjuvants, multiple doses and specialized injection equipment are needed (Thomas, 2014). Although protection has been shown in non-human primate model (Raviprakash et al., 2003), a recent clinical phase I trial with a DENV1 DNA construct (encoding prM and E proteins) given in three doses shows induction of neutralizing antibodies in less than 50% of recipient (Beckett et al., 2011).

Table 1-1 Dengue vaccines under development.

Vaccine name	Vaccine type	Description	Vaccine developers	Clinical testing status
CYD Dengue Vaccine	Live attenuated virus	Yellow fever 17D virus backbone with prM and E replaced with	Sanofi Pasteur	Phase III
DENVax	Live attenuated virus	DENV-2 PDK-53 backbone and DENV-1/2, -3/2,	Takeda Pharmaceutical Company Limited	Phase II
TetraVax-DV-TV003 (TV003)	Live attenuated virus	Attenuated by directed mutagenesis and chimeras	National Institute of Allergy and Infectious	Phase II
TDEN-PIV	Inactivated virus	Purified inactivated vaccine	Walter Reed Army Institute of Research	Phase I
V180	Recombinant protein	Recombinant protein 80% of DENV-1–4 E protein	Merck Sharp & Dohme Corp.	Phase I
Tetravalent Dengue Vaccine (TVDV)	DNA	Plasmid DNA vaccine	U.S. Naval Medical Research Center	Phase I

1.9 Aim of the project

Recent dengue vaccine phase II and III trials by Sanofi Pastuer showed no protection against DENV2. DENV2 particles have been observed to change in structure when shifting from an incubation temperature of 28^{o}C to 37^{o}C. To aid in the rational design of effective antiviral therapeutics and vaccines, it is necessary to understand the neutralization of different morphologies of DENV2 by human neutralizing antibodies at molecular level.

The specific aims of this thesis are to

1. Characterize epitopes recognized by DENV2-specific highly neutralizing human monoclonal antibodies.
2. Investigate the impact of structural dynamics of DENV2 on antibody-mediated neutralization.
3. Provide a structural basis for understanding the mechanisms of antibody-mediated neutralization of DENV.

Chapter II. Materials and Methods

2.1 Antigen production and purification

2.1.1 Recombinant E protein ectodomain cloning, expression and purification

Recombinant E protein soluble ectodomain construct was based on DENV2 strain 16681. In general, the virus RNA genome was extracted using QIAamp viral RNA mini kit (Qiagen) and the gene encoding E protein ectodomain (amino acid 1-394) was reverse transcribed to cDNA using the cDNA synthesis kit (Life Technologies). The product was amplified and flanked by sequences of *BgI* II and *Xho* I restriction sites by PCR. This PCR product was then ligated to pMT/BiP/V5-His A vector. The resulting plasmid and a hygromycin resistant plasmid (Life Technologies) were used to co-transfect *Drosophila* Schneider 2 cells. The cells were subsequently cultured and selected to generate a stable cell line. Protein expression was induced with $CuSO_4$ at a final concentration of 500 μM at a minimum cell concentration of $1X10^6$ cells per ml for 6 days. Upon which, the culture supernatant was harvested by centrifugation and filtered prior to purification with a homemade affinity column. Briefly, DENV cross-reactive monoclonal antibody IgG 4.8A (Costin et al., 2013) was covalently immobilized to agarose beads

using AminoLink Immobilization Kit (Thermo Scientific) and the beads were then packed into a low-pressure Glass Econo chromatography column (Bio-Rad). The filtered supernatant was allowed to flow through the column by a gravity-flow method and non-specific binders were washed away from the column. The protein was finally eluted with a low pH elution buffer (0.1 M glycine-HCl, pH 2.7) and the pH was instantly adjusted to neutral using 1 M Tris-HCl buffer, pH 9.0. The eluted protein was further dialyzed in 10 mM Tris-HCl pH 7.5 and 150 mM NaCl, and then further purified by size-exclusion chromatography using a Superdex 200 10/300 GL column (GE Healthcare).

2.1.2 E protein domain III cloning, expression, refolding and purification

Residues 291-395 of DENV2 E protein (strain PVP94/07) were cloned into pET16b vector (Novagen) fused with an N-terminal 10X Histidine tag (Moreland et al., 2012). To generate the E-DIII construct representing strain NGC, residue 390 was mutated from serine to asparagine by site-directed mutagenesis with primers (forward: 5’-GGACAACTGAAGCTCAACTGGTTTAAGAAAGG-3’, and reverse: 5’-CCTTTCTTAAACCAGTTGAGCTTCAGTTGTCC -3’) using Quickchange kit (Stratagene).

To facilitate protein crystallization, four flexible N-terminal residues (291-294) of this E-DIII construct were removed and only residues 295-395 were amplified with primers (forward, 5'-CTGTATTTTCAGGGCGCCGGCAAAGGAATGTCATATTCTATGTG TACAGG-3', and reverse, 5'-GCGACTAGTGAGCTCGTCGACTTATCC TTTCTTAAACCAGCTGAG-3') and cloned into pProEx HTb plasmid using ligation-independent cloning methods (Aslanidis and de Jong, 1990). The expressed construct includes a 6X His-tag and a Tobacco Etch Virus (TEV) protease cleavage site fused at the N-terminus of this construct.

The recombinant E-DIII constructs were transformed to *Escherichia. coli* BL21-CodonPlus strain (Stratagene) and the bacteria were grown in LB medium containing 34 µg/ml chloramphenicol at 37^{o}C to an absorbance of 0.6-0.8 at 600 nm wavelength. Protein expression was induced with 1 mM Isopropyl β-D-1-thiogalactopyranoside (IPTG) at 37^{o}C in a shaker for 4 hrs. Cells were harvested by centrifugation at 8000g for 30 min at 4^{o}C. Bacteria containing over-expressed proteins were passed through a French cell press twice (Thermo Electron Corp) pre-cooled to 4°C. E-DIII was detected in the inclusion body fraction as previously described (Moreland et al., 2012). The inclusion body was

clarified with washing buffer (0.1M Tris-HCl pH 8.5, 200 mM NaCl, 1 M Urea, 20% Triton X-100) for three times and re-pelleted each time by centrifugation. The inclusion body was then dissolved in 0.1 M Tris-HCl pH 8.5, 200 mM NaCl, 8 M Urea, 10 mM imidazole, 10 mM β-mercaptoethanol (buffer A) overnight at 4^{o}C and loaded into a HisTrap FF Crude column in AKTA protein purification systems (GE Healthcare). After a washing step with 20 mM imidazole, the protein was eluted with an imidazole gradient (0 – 500 mM) in buffer A and refolded by dialysis with refolding buffer (0.2 M Tris-HCl pH 8.5, 200 mM NaCl, 100 mM arginine, 10 mM EDTA, 5 mM reduced glutathione, 0.5 mM oxidized glutathione) (Moreland et al., 2012). The refolded protein was further purified over a Superdex 75 16/60 size exclusion column (GE Healthcare) equilibrated in 20 mM Tris-HCl pH 7.5, 150mM NaCl. Recombinant E-DIII for crystallization was cleaved by TEV protease overnight at 4°C and the product was purified by passing through HisTrap FF Crude column (GE Healthcare).

2.1.3 Virus sample preparation

DENV2 strains NGC and PVP94/07 were used in this study. Strain PVP94/07 (DEN2/SG/07K3598DK2/2007) was obtained from the EDEN patient cohort (Low et al., 2006) and was a kind gift from Associate

Professor Ooi Eng Eong. All viruses were grown in C6/36 mosquito cells at 28°C and the virus used in cryo-EM and dynamic light scattering study was purified as described (Kuhn et al., 2002). Briefly, C6/36 cells was grown with RPMI 1640 medium (HyClone) containing 10% FCS at 28°C. Cells were infected at a MOI of 0.1, and culture medium was harvested 96 hrs post-infection. To purify the virus, the culture medium was clarified by centrifugation at 6000g for 30 min, and the supernatant was precipitated by incubating overnight at 4°C with 8% PEG 8000 (Sigma-Aldrich). The mixture was centrifuged at 7000g, and the pellet was resuspended in NTE buffer (12 mM Tris pH 8.0, 120 mM NaCl, 1 mM EDTA). The virus was then purified through a 24% sucrose cushion and a 10 to 30% potassium tartrate-glycerol linear gradient. The virus band was extracted and subjected to buffer-exchange into NTE buffer, and concentrated in an Amicon Ultra-4 concentrator (100 kDa; Millipore). The purity of the virus sample was evaluated by SDS-PAGE (Fig. 2-1). Purified virus sample showed very faint pre-membrane (prM) protein band, corresponding to lower percentage of immature particles in the sample. The virus concentration was estimated by comparing the viral E protein band with a bovine serum albumin (BSA) protein standard of known concentrations.

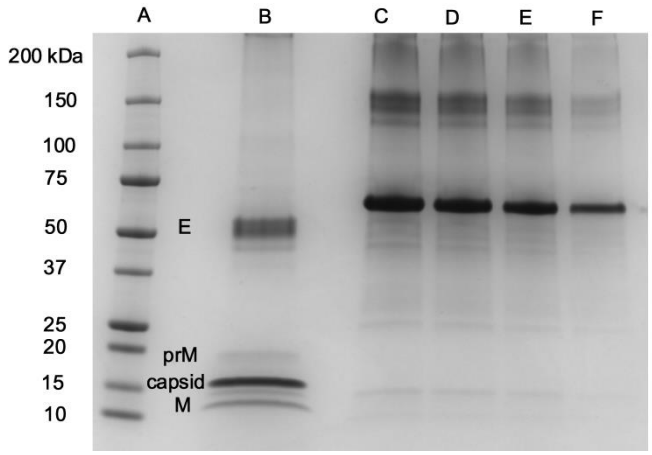

Figure 2-1 SDS-PAGE gel of the purified DENV2 strain PVP94/07. Lane A: Protein standard; B: virus sample; C-F: BSA protein concentration standard at 2, 1.5, 1, 0.5 mg/ml, respectively. Virus protein bands corresponding to E, prM, capsid and M proteins are labeled.

2.2 Antibody IgG and antigen binding fragment (Fab) generation

Both HMAb 10.15 (Teo, 2014) and 3F9 (Smith et al., 2014) were isolated from B cells of convalescent dengue patients using two different methods. For generation of 3F9, human B cells from a dengue patient were transformed with Epstein-Barr virus (EBV) and screened for virus specificity in ELISA and neutralizing activity in a flow-cytometry based assay. Selected cells were cryofused with myeloma cells to generate hybridomas (Smith et al., 2014). For generation of HMAb 10.15, genes of both antibody heavy and light chains were amplified from B cells, which were isolated from a convalescent patient, and combined as random pairs to construct an antibody-library. The library

was expressed on phage surface and panned for DENV2 binding specificity. Constructs with desired specificity were further cloned and expressed as full-length IgG monoclonal antibodies. Both antibodies were proven to be extremely potent against DENV2 *in vitro*.

To obtain Fab used for crystallization and cryo-EM study, IgG of HMAb 10.15 (IgG 10.15) and 3F9 (IgG 3F9) were digested by immobilized papain resin (Pierce) for 22 and 18 hrs in a 37^{o}C shaker, respectively. The digestion time was pre-optimized to obtain a high yield of Fab and avoid over-digestion. Digested antibodies were separated from the resin and the supernatant was dialyzed against 10 mM Tris-HCl pH 7.5, 1 mM Dithiothreitol (DTT). Fab was separated from the cleaved Fc fragments and undigested IgG by eluting with a linear gradient of 0 to 1 M NaCl in 10 mM Tris-HCl pH 7.5 buffer from a Resource Q column (GE Healthcare). Fab fragments of both antibodies were collected in the flow-through and the purity of the Fab preparation was determined by running SDS-PAGE gels. Fab of HMAb 10.15 (Fab 10.15) used in PRNT assay were generated by our collaborators directly as a recombinant protein with a His-tag at the C-terminus of the heavy chain.

Hybridoma expressing mouse anti-EDIII MAb 3H5 (Gromowski and

Barrett, 2007), anti-prM MAb 2H2, 1A1D-2 (Roehrig et al., 1998) and anti-fusion loop MAb 4G2 (Henchal et al., 1985) were used in the studies. Hybridoma cells were grown in BD Cell MAb Medium in the CELLine device (BD Bioscience) and the culture supernatant containing secreted antibodies were harvested weekly. The supernatants was centrifuged at 2000g for 10 min to remove cell debris and then dialyzed to 20 mM sodium phosphate buffer at pH 7.0 at 4°C before filtered through a 0.22 μm membrane. The filtered sample was passed through HiTrap Protein G HP column (GE Healthcare) and eluted using 100 mM glycine-HCl at pH 2.7. The purified Ab was immediately neutralized by adding 1 M Tris-HCl at pH 9.0 and then dialyzed against 20 mM sodium phosphate buffer at pH 7.0 with 150 mM NaCl.

2.3 Enzyme-linked immunosorbent assay (ELISA)

Microtiter plates (Nunc MaxiSorp, Thermo Scientific) were coated with purified antigens (E and E-DIII, 0.25 μg/well) overnight at 4^{o}C. The plate was then blocked at room temperature for 1 hr with 5% BSA in PBST buffer (137 mM NaCl, 2.7 mM KCl, 10 mM Na_2HPO_4, 1.8 mM KH_2PO_4, pH 7.4, 0.05% (v/v) Tween 20). Purified IgG 10.15 and 3F9 (0.25 μg/well) were added to each well and incubated at room

temperature for 1 hr. Same amounts of murine monoclonal antibodies 1A1D-2, 3H5, 4G2 and 2H2 were included as controls for domain binding specificity. The plates were washed 4 times with PBST buffer prior to incubation with goat anti-human IgG (H+L) HRP-conjugated secondary antibodies (Thermo Scientific) for HMAb and goat anti-mouse IgG Fc HRP-conjugated secondary antibodies (Thermo Scientific) for murine MAb at room temperature for 1hr. The plates were washed 4 times with PBST before the reaction was developed by adding 3,3',5,5'-tetramethylbenzidine (TMB) substrates (Bio-Rad) and quenched with 1M hydroxide chloride. The absorbance at 450 nm was read in Infinity200 microplate reader (Tecan). All ELISA experiments were repeated at least twice in duplicates.

2.4 Western blot

Purified antigens (E and E-DIII) were either mixed with sample loading buffer (10% (w/v) SDS, 0.2 M Tris-HCl pH 6.8, 20% (v/v) glycerol, 0.05% (w/v) Bromophenolblue) or mixed with reducing sample loading buffer (sample loading buffer with 10 mM DTT) and boiled. The samples were separated on SDS-PAGE at 200 V for 30 min. The proteins were then transferred from the gel onto Polyvinylidene fluoride

(PVDF) membrane at 15 V for 30min using Trans-Blot Semi-Dry Transfer Cell (Bio-Rad). The membrane was blocked in PBST with 5% BSA at room temperature for 1 hr and then probed with IgG 10.15 at 4^{o}C overnight. After four 10-min wash steps with PBST, the membrane was incubated with HRP-conjugated goat anti-human IgG H+L secondary antibody (Thermo Scientific) at room temperature for 1 hr. The membrane was developed with ECL Plus western blotting detection reagent (GE Healthcare) and imaged by ImageQuant ET-RCL (Bio-rad).

2.5 Plaque reduction neutralization test

Plaque reduction neutralization assay (PRNT) was performed for HMAb 10.15 and 3F9 with the two DENV2 strains (NGC and PVP94/07) on baby hamster kidney 21 cells (BHK-21) as described (Morens et al., 1985). Full-length IgG and Fab fragment of both antibodies were tested in PRNT. BHK-21 (ATCC CCL-100) cells were maintained in RPMI 1640 (HyClone) supplemented with 10% FCS at 37°C with 5% CO_2. Eleven 4-fold serial dilutions of each antibody starting from a maximum concentration of 100μg/ml were mixed with 30 plaque-forming units of DENV2 (pre-determined by standard plaque assay for virus stocks).

The mixtures were incubated at 37°C for 1 hr and 100 µl of these mixtures were added to a monolayer of BHK-21 cells in each well of a 24-well plate in duplicate and incubated at 37°C for another 1 hr. The inoculum was removed after incubation and the cells were further incubated at 37°C for 3-4 days before they were fixed and stained with 0.5% (w/v) crystal violet dissolved in 25% (v/v) formaldehyde for visualization of the plaques. Percentage of neutralization was determined by comparing the numbers of plaques in various antibody concentrations to that in the control without presence of antibodies. $PRNT_{50}$ values were defined as the concentration of antibodies causing 50% reduction of the plaque numbers and determined by non-linear regression in GraphPad Prism version 6.01.

2.6 Surface plasmon resonance (SPR)

Kinetic parameters of the interaction between HMAb 10.15 and recombinant E protein/E-DIII at pH 7.4 were determined by using ProteOn™ XPR 36 Surface Plasmon Resonance system (Bio-Rad). Approximately 200 response units (RU) of IgG or Fab were immobilized to ProteOn™ GLC sensor chip (Bio-Rad) using amine coupling. Negative controls were set up where no antibody was immobilized.

Once stabilized, two-fold serial dilutions of antigens in PBST (0.05% (v/v) Tween 20) were injected over the chip at a flow rate of 100 µl/min for 180 sec and allowed to dissociate for 600 sec. For interactions with E-DIII, the dissociation was not complete at the end of the dissociation period. Therefore the chips were regenerated by a wash step with glycine-HCl at pH 2.5 at a flow rate of 120µl/min for 15 sec. The sensorgrams were double-referenced to correct the response from both reference flow cell and blank buffer. The binding kinetic parameters were then determined by fitting to a nonlinear 1:1 Langmuir binding model in the ProteOn^{TM} manager software (Bio-rad). Each interaction was repeated at least three times.

2.7 Amide hydrogen/deuterium exchange coupled with mass spectrometry (HDX-MS)

HDX-MS measures the kinetics of deuterium exchange of amides at protein backbone because the side chain deuterons will be back-exchanged to hydrogen during the washing step in mass spectrometry. After deuterium exchange, the reaction is quenched and the protein is rapidly digested by proteases such as pepsin. The mass of the peptides generated is analyzed by liquid chromatography–mass spectrometry and the result shows the kinetics of deuterium exchange

throughout a protein. Amides that are heavily solvent occluded or stably engaged in hydrogen bonds through the secondary structure are protected from exchange, which results in slow deuterium uptake (Englander and Kallenbach, 1983, Guttman et al., 2015). Ligand-binding which involves large changes in solvent protection can be monitored by HDX-MS with three to five short time points (less than 30 min) (Baerga- Ortiz et al., 2002, Pandit et al., 2012, Kim et al., 2011, Yamada et al., 2002, Paterson et al., 1990).

To probe the epitope of HMAb 10.15 on DENV2 E protein, HDX-MS was performed with antigens (recombinant E ectodomain and E-DIII) in both absence and presence of Fab 10.15. All antigens were purified by size-exclusion chromatography and concentrated to approximately 100 μM before the experiment. The antigen was mixed with Fab 10.15 at a molar ratio of 1:1.5 followed by 1-hr incubation on ice. Samples (antigen alone or antigen-antibody mixture) were diluted 10 times with D_2O buffer (20 mM Tris-HCl pH 7.5, 150 mM NaCl, 99.9% D_2O) and incubated for various time points (0.5, 1, 2, 5 and 10 min) at room temperature. Undeuterated sample of just the antigen alone was included as negative control. The reactions were slowed down by adding pre-chilled quenching buffer (0.1% (v/v) trifluoroacetic acid (TFA)

solution with 2.5 M guanidine hydrochloride) to reach a final pH of 2.5. The protein was then reduced by a 3-min incubation at near 0^{o}C with immobilized TCEP disulfide reducing gel (Pierce) before mass analysis, which was conducted by Electrospray ionization quadrupole time-of-flight mass spectrometry (ESI-Q-TOF MS) as described elsewhere (Wang et al., 2012).

Briefly, the quenched sample was injected into a pre-cooled nano-ACQUITY UPLCs system (Waters Corporation) and digested in an immobilized pepsin column (Applied Biosystems) in the system. Digested peptides were eluted using an 8–40% (v/v) gradient of acetonitrile in 0.1% (v/v) formic acid and resolved with ACQUITY UPLC BEH C18 column (Waters Corporation). The masses of the peptides were measured using a SYNAPTs High Definition Mass Spectrometer (Waters Corporation) acquiring in MS^{E} mode (Shen et al., 2009). Deuterium-exchange pattern of each peptide from the antigen in the presence and absence of antibody was compared.

2.8 Structure determination of Fab 10.15 – E-DIII complex by X-ray crystallography

X-ray crystallography is currently the most powerful technique to determine the structure of biological macromolecules to high resolution.

Generally the major bottleneck in crystallography is to obtain a crystal that will diffract to high resolution.

2.8.1 Basic theory

A protein crystal is composed of an ordered array of protein molecules. A unit cell is a smallest volume, which when repeated in three dimensional space forms the whole crystal. The general shape of the unit cell can be described by using six parameters: the lengths of the unit cell edges (**a, b, c**) and the angles between them (**α, β, γ**) (Fig. 2-2).

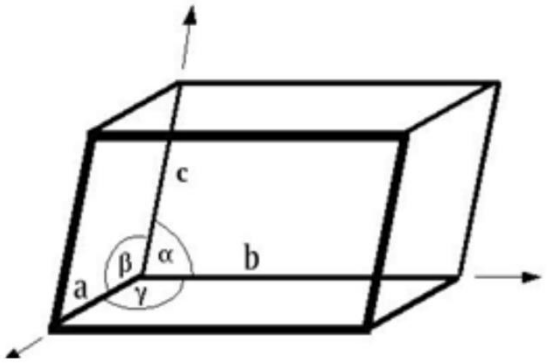

Figure 2-2 The dimensions of a unit cell. Axes a, b and c and inter-axial angles α, β and γ are labeled.

Since the unit cell is repeated to produce a crystal, the electron density of the protein molecules in a crystal can be described mathematically by a 3D periodic function, each period covering one unit cell. The aim of X-ray crystallography experiment is to find this mathematical function. It can be shown, that a diffraction pattern from a

crystal is related to the Fourier transform of the electron density within the crystal unit cell, known as structure factor, which can be sampled by collecting the diffraction pattern in reciprocal space and represented as a Fourier series. To this end, a crystal can be viewed as series of parallel planes separated by a constant distance. Each set of parallel planes can be specified with Miller indices (*hkl*) where each number refers to how many times each plane will cut the respective unit-cell edges. *W. L. Bragg* showed that X-ray beam reflected from each series of these planes will interfere constructively only at some specific angles. These angle θ can be described with an equation

$$2d_{hkl}sin\theta = n\lambda \qquad (2.1)$$

In which, d_{hkl} is the interplanar spacing for a particular set of parallel planes (*hkl*) and λ is the wavelength of the incident X-ray beam.

In a diffraction experiment, locations and intensities of the diffracted beams on the detector are recorded. The location of the diffraction spot depends on the dimension of the unit cell, whereas the intensity of diffraction beam depends on the electron density ρ on planes (*hkl*) and the internal symmetry within the unit cell. The structure factor (the Fourier transform term) for particular directions, determined by the

Miller indices, which represents the waves that result from the diffraction which can be expressed as

$$F(\boldsymbol{s}) \sim \int_{space} \rho(\boldsymbol{r}) exp\,(2\pi i \boldsymbol{s} \cdot \boldsymbol{r}) d\boldsymbol{r} \qquad (2.2)$$

In this equation, each reflected wave is represented by a complex number. Since the crystal is just multiple repeats of the unit cell, the formula can be limited to the unit cell only. ***r*** is the position vector in real space and defined as fractions of the unit cell axes, expressed as

$$\boldsymbol{r} = x\boldsymbol{a} + y\boldsymbol{b} + z\boldsymbol{c} \qquad (2.3)$$

While ***s*** is the reciprocal vector and equal to

$$\mathbf{s} = h\boldsymbol{a}* + k\boldsymbol{b}* + l\boldsymbol{c}* \qquad (2.4)$$

Where ***a*, b**** and ***c**** are three axes of the reciprocal lattices, which are perpendicular to the plane bc (meaning plane formed by axis b and c in real space), ac and ab, respectively. Therefore

$$\begin{aligned} \boldsymbol{s} \cdot \boldsymbol{r} &= (h\boldsymbol{a}* + k\boldsymbol{b}* + l\boldsymbol{c}*) \cdot (x\boldsymbol{a} + y\boldsymbol{b} + z\boldsymbol{c}) \\ &= hx + ky + lz \\ &= h \cdot x \end{aligned} \qquad (2.5)$$

From equation (2.2-2.5), one can deduce that:

$$F(h) = \int_{cell}^{d} \rho(x)\, exp(2\pi i h \cdot x)\, dx \qquad (2.6)$$

Note that the structure factor is expressed in terms of Miller indices (*hkl*) which can be related to the individual spots in the diffraction pattern. As the structure factor is a Fourier transform of the electron distribution in real space, the electron density can be regenerated from the structure factors with an inverse Fourier transform. This equation called electron density equation is expressed as:

$$\rho(x) = \frac{1}{V}\sum_{h} F(h) exp(-2\pi i h \cdot x) \qquad (2.7)$$

All information of the diffracted waves, including their Miller indices, amplitudes and phases, is required in order to produce the electron density function and solve the crystal structure. The Miller indices are determined from the observed diffraction spots positions, and the amplitude is measured in the experiment. However, the phase is not directly recorded in a diffraction experiment. The estimation of the phase can be obtained in various ways: the direct methods, Multiple-wavelength Anomalous Diffraction (MAD), Multiple Isomorphous Replacement (MIR), Molecular Replacement (MR). If there are available crystal structures homologous to the protein being studied, MR is the most straightforward approach for solving the phase problem. In short, the technique tries to model the unit cell composition

using the existing homologous structures, calculating the diffraction pattern and comparing them with the experimental data.

Since both DENV envelope protein and human Fab structures are available, molecular replacement has been used for the determination of DENV E-DIII- antibodies complex crystal structure in this thesis. An initial model is built and used to refine the estimates of the phases for the data, which should lead to an improved model. The positions of the atoms and their respective Debye-Waller factors (B-factor, accounting for the thermal motion of the atom) can be refined to fit the observed diffraction data to obtain more accurate phases. The refinement is done iteratively and the correlation between the diffraction data and the model is measured by an R-factor defined as

$$R_{work} = \frac{\sum_{all\ reflections}|F_o - F_c|}{\sum_{all\ reflections}|F_o|} \qquad (2.8)$$

Where F_o is the structure factor observed with the data and F_c is the structure factor calculated from the fitted model. A similar quality criterion R_{free}, developed to prevent over-fitting of the data, is usually calculated from a subset (~5-10%) of reflections that are not used in the structure refinement. Chemical bonding features are also used to validate the structure. They include stereochemistry, hydrogen bonding

and distribution of bond lengths and angles. Omit maps (*Fo-Fc*) is also used to check for phase bias.

2.8.2 Crystallization of Fab 10.15 – E-DIII complex

DENV2 E-DIII was mixed with Fab 10.15 in a molar ratio of 1.5:1 and incubated on ice for 1 hr. Complex was separated from excessive E-DIII with a Superdex 75 10/60 size exclusion column (GE Healthcare) pre-equilibrated with 20 mM Tris-HCl pH 7.5 and150 mM NaCl. The purified complex was concentrated to 12 mg/ml for crystallization screen.

Initial screen was set up in Intelli 96-well sitting drop plates with Phoenix crystallization robot (Hampton Research) and incubated at 20^{o}C. Drops were composed of 0.3 µl protein solution and 0.3 µl crystallization solution. Crystals were found in two conditions of the PACT *premier*^{TM} HT-96 screen (Molecular Dimensions) (Fig. 2-3): condition B12 (0.1M MES, pH=6.0, 20% PEG6000 and 0.2mM Zinc Chloride) and condition D12 (0.1M Tris-HCl pH 8.0, 20% PEG6000 and 2mM Zinc Chloride). The second condition was used for further optimization.

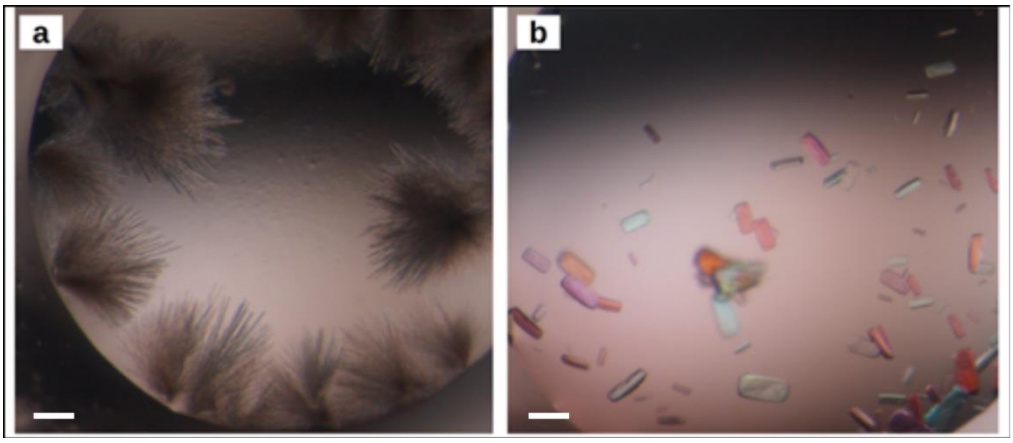

Figure 2-3 Morphology of the crystals obtained in initial screen. (a) Crystal grown as needle clusters at condition B12 in PACT *premier*™ HT-96 screen. (b) Crystal grown at all three dimensions at condition D12 in PACT *premier*™ HT-96 screen. Scale bar represents 100 µm.

The optimization was done manually by hanging-drop vapor diffusion technique with a bigger drop size comprising of 1 µl protein solution plus 1 µl crystallization solution. Parameters that were optimized include PEG6000 concentration (5% to 25% in steps of 2.5%), buffering pH (7.5 to 8.5 in steps of 0.25), zinc chloride concentration (0-2.5 mM in steps of 0.5 mM), protein concentration (3, 6, 9 and 12 mg/ml) and temperature (4^{o}C and 20^{o}C). Larger, diffracting crystals were obtained in presence of 0.1 M Tris-HCl pH 8.0, 9% PEG6000 and 2 mM zinc chloride. However, very few spots were observed in the diffraction pattern, indicating that the crystals were not well packed. Therefore, additive screen HT (Hampton Research) was used to further improve crystal quality. Crystal diffraction quality was improved by

adding cadmium chloride hydrate to the crystallization solution at a final concentration of 10 mM. Crystals appeared on the second day and grew to a maximum size within one week. For data collection, the crystals were flash-frozen with mother liquor supplemented with 30% glycerol as cryo-protectant.

2.8.3 X-ray diffraction of Fab 10.15 – E-DIII crystal

Diffraction data were collected with an in-house X-ray source of a wavelength of 1.54178 Å and a Saturn 944 CCD detector (Rigaku) set at a distance of 70 cm. One hundred and eighty degrees rotation data were collected at 1^{o} oscillation range. The detector to crystal distance was set up by considering the balance between maintaining reasonable spot separation and preserving higher resolution signals. The exposure time was set up to 30 sec per frame to achieve a good intensity for higher resolution data while also avoiding pixel overload at the low resolution range. The oscillation angle was determined by considering factors such as the overlaps of lunes at high resolution and the mosaicity of the crystal.

2.8.4 Crystal structure determination

The diffraction data were indexed, integrated and scaled using HKL2000 (Otwinowski et al., 1997) (Table 3-2). Indexing involved

determining the unit cell dimension, assigning a Miller index to each diffraction spot and finding the unit cell symmetry (the space group). Integration over multiple images further refines the crystal, beam and detector parameters. Moreover, as symmetry-equivalent data are collected multiple times in the data collection process due to the symmetry of the crystals, merging and scaling these images put the data to a consistent intensity scale. Symmetry-related R-factor (R_{sym}) is used to evaluate how similar the measured intensities of symmetry equivalent reflections are and also act as an indicator for data quality.

The crystal of Fab 10.15 – E-DIII complex diffracted to 2.65-Å and belonged to monoclinic C-centered space group C2. Matthews coefficient was calculated and number of molecules within one asymmetric unit was estimated to be two with an estimated solvent content of 50.63%. Using the program Phaser (McCoy et al., 2007), initial phase was obtained by MR method using the coordinates of DENV-2 E-DIII (extracted from PDB code 2R69) and the Fab fragment of an anti-influenza virus IgG 1F1 (PDB code 4GXU) as search models. Iterative cycles of model building and refinement were performed by using the program Coot (Emsley et al., 2010) and Phenix.refine (Afonine et al., 2012), respectively. The quality of the structure was

analyzed using Molprobity (Chen et al., 2009). The details of the parameters for the final structure are listed in Table 3-2.

2.9 Cryo-EM study of virus – antibody complex

2.9.1 Introduction of cryo-EM single particle analysis

Cryo-electron microscopy (cryo-EM) is a powerful technique in structural biology. In cryo-EM experiment, the sample suspended in buffers is frozen into vitreous ice on cryo-EM grids and thus imaged in a near native state. Biological macromolecules (proteins, RNA, etc.) are composed of mostly light atoms: carbon, oxygen, nitrogen, sulfur, and phosphorus, which do not interact strongly with electron beam. Because of that, vitrified biological specimens produce very low contrast images in the electron microscope. Hence, in order to improve contrast, vitrified sample is imaged at a range of underfocus value. This imaging technique takes advantage of the wave properties of the electron beam where the phase contrast generated by the interaction of the beam and sample is converted into amplitude contrast, which is recorded by the detector. Several factors are important for optimization of data collection, such as electron dose, defocus range, energy of electrons used etc. Due to the distortions introduced by out of focus imaging, the further

away from focus will result in the loss of high resolution signal but increased in contrast. Defocus range used therefore depends on whether contrast or obtaining high resolution signal is preferable. Electron dose for data collection is also another important factor as increased dose also increases contrast but the radiation can damage the structure of the particle leading to a loss in resolution. Typically, a dose of about $20e^{-}/Å^{2}$ is considered acceptable (Cheng, 2015).

There are three common cryo-EM techniques to obtain 3D reconstruction of macromolecule, namely 2D crystallography, tomography and single particle analysis. The 2D crystallography determines the structure of macromolecules arranged in the form of 2D crystals. In tomography, a series of images of the same object tilted at different angles around a fixed axis is taken and then computationally processed to obtain a 3D reconstruction of the macromolecule. This thesis employs the use of the third technique: single particle analysis. It involves a collection of 2D projections of many different views of the same macromolecule. The orientations of these 2D projections are determined and then computationally aligned to each other to obtain a 3D reconstruction of the structure. With the newly developed CMOS

camera and reconstruction algorithms, single particle analysis can now achieve atomic resolution (Bartesaghi et al., 2015, Campbell et al., 2015, Grant and Grigorieff, 2015, Jiang et al., 2015, Fischer et al., 2015).

Basic steps of single particle analysis are: particle selection, contrast transfer function (CTF) correction, 2D classification, initial model generation, model-based 3D classification and refinement, resolution assessment, and interpretation of the 3D density maps. More detailed introduction of these procedures can be found in some recent reviews (Cheng, 2015, Bai et al., 2014, Henderson et al., 2012).

2.9.1.1 Correction of contrast transfer function (CTF)

The CTF must be first corrected in order to properly recover the high resolution information recorded in a cryo-EM image. An electron beam is considered as a wave whose phase and amplitude are subject to change upon passing through materials with altering properties. The CTF describes the influence of imperfections of the microscope and choice of imaging conditions on the final image. These include angular spread of the electron beam, spherical and chromatic aberration from

the lenses, specimen drift, specimen vibration, underfocus, noise from the microscope, and the detector's nonlinearity of response and its own noise. To obtain a faithful 3D reconstruction of the structure to a resolution better than 10 – 15 Å, the images should be corrected for the influence of the CTF. As stated in (Ludtke et al., 1999), the data measured in a transmission electron microscope can be described as:

$$M(s)^2 = F(s)^2 CTF(s)^2 E(s)^2 + N(s)^2 \qquad (2.9)$$

In which *s* is the spatial frequency, *M*(*s*) is the measured data, *F*(*s*) is the structure factor of the molecule, *CTF*(*s*) *i*s the contrast transfer function, *E*(*s*) is the envelope function and *N*(*s*) is the mean noise intensity. The CTF can be estimated by using the averaged power spectrum of the image and summarized as

$$CTF(s) = -k(\sqrt{1 - A^2}\sin\gamma + A\cos\gamma) \qquad (2.10)$$

Where

$$\gamma = -2\pi\left(\frac{C_s\,\lambda^3 s^4}{4} - \frac{(Z_0+Z)\,\lambda\, s^2}{2}\right) \qquad (2.11)$$

In which *k* is the scaling factor, *A* is the percentage of amplitude contrast, C_s is the spherical aberration coefficient, λ is the electron wavelength, Z_0 is the object lens defocus and *Z* is the focal difference due to axial astigmatism. The CTF oscillates between -1 (negative contrast transfer)

and +1 (positive contrast transfer) as it goes from low to high spatial frequencies with some locations having zero crossings and resulting in information loss (Fig. 2-4)

The major contributors to the envelope functions are the spherical aberration C_s and the current/voltage instabilities, which limits the spatial and temporal coherency of the beam, respectively. The envelope function can usually approximate Gaussian envelope function:

$$\mathrm{E(s)} = e^{-Bs^2} \qquad (2.12)$$

The combined effects of CTF and envelope function become more noticeable at higher spatial frequencies, ultimately limiting the achievable resolution (Fig. 2-4).

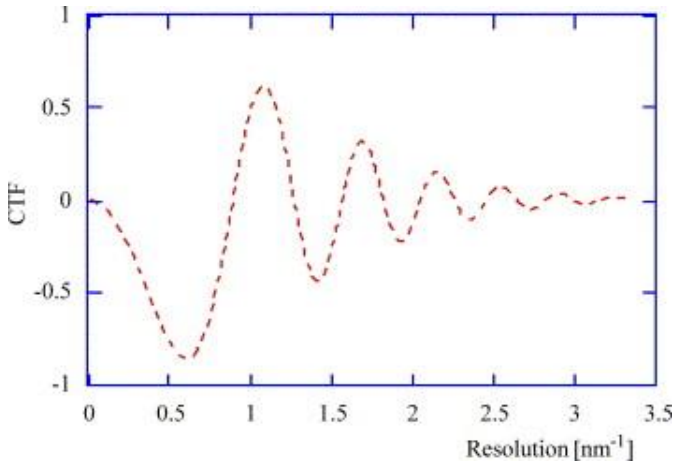

Figure 2-4 The contrast transfer function and envelope function. The CTF of an electron microscope produces periodic phase reversals.

The amplitude of the CTF is attenuated towards higher resolution by a near Gaussian envelope function. Figure extracted from (Mindell and Grigorieff, 2003).

In addition, noise should be properly estimated to retrieve the signal in the micrographs. There are many ways to estimate the noise. For example, in the EMAN software package (Ludtke et al., 1999), the noise profile is approximated by an empirical four parameters function:

$$N_2(s) = n_1 \exp\left(n_2 s + n_3 s^2 + n_4 s^{1/2}\right) \qquad (2.13)$$

In summary, defocus is the only arbitrary parameter for the same sample during cryo-EM imaging. Features of the object at different resolutions appear distorted in the image depending on the defocus setting. Images are usually collected at several different defocus values to allow for proper recovery of information at all spatial frequencies (Penczek et al., 1997).

2.9.1.2 Particle alignment

Besides CTF correction, another fundamental step to obtain the 3D structure of the molecule is particle alignment. Particle images need to be aligned relative to each other and averaged to obtain an image with higher signal to noise ratio (SNR). An image of a particle is defined by

five alignment parameters: three orientation Euler angles (θ, ϕ and ω) defining the direction of view of the object (Fig. 2-5) and two translation parameters (x, y) defining the center position of the object in the image. One of the methods used for particle alignment is the common lines method (Crowther et al., 1970). A common line is the intersection line where the Fourier transforms of any two projections coincide. The central section theorem states that Fourier transform of a 2D projection of a 3D object forms a central section in the 3D Fourier transform of the same object. Therefore it is possible to estimate a relative orientation of a projection when compared to a projection that has a defined orientation. The method to derive orientation by comparing projections of different particles is called cross-common line method. For highly symmetric objects, such as icosahedral viruses, there are many self-common lines, allowing determining the approximate alignment parameters from a single image (Baker et al., 1999). This method is called the self-common line method.

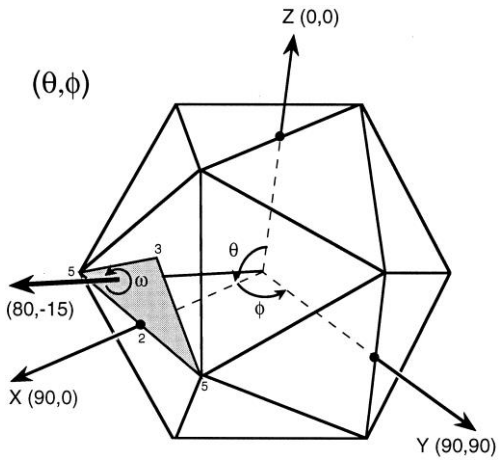

Figure 2-5 Definition of particle orientation of an icosahedron object. θ, φ, and ω angles together define the orientation in which an icosahedral particle is viewed. Any view vector can be transformed to a view of the single asymmetric unit (shaded region) due to the icosahedral symmetry. Figure from (Baker et al., 1999).

Search for the orientation is usually conducted using either the self-common line or the cross-common line method. This initial search for the center and orientation can be done either sequentially (first to find the center and then search for orientation with the pre-fixed center) or simultaneously (procedures implemented in Multi-Path Simultaneously Annealing (MPSA), the algorithm used in 3D reconstruction of the DENV2 - Fab 10.15 samples) (Liu et al., 2007). Refinement of the center and orientation is generally conducted locally using cross-common lines between particle images and reference projections generated from a 3D model that has known orientations.

Considering that signal from the sample is low in the cryo-EM image, particle alignment based on cross-correlation can sometimes produce unreliable result. To tackle this, different strategies are implemented in various algorithms. One of the algorithms, MPSA, validates the correctness of the determined orientation of a particle image by checking for consistency in the result when the orientation search is repeated several times. Particles with inconsistent orientations are discarded from further processing. In another method based on maximum likelihood approach, all possible orientations are tested, by comparing systematically with all projections of a 3D model. Each orientation is assigned a weight and with the weights taken into consideration, all possibilities are used to make a 3D map. This approach is implemented in Relion (Scheres, 2010b, Scheres, 2010a).

Once the center and orientation of each particle image is determined, they are combined together to generate a 3D structure using the projection-slice theorem. An iterative routine using the generated 3D map as a model for next cycle of particle alignment is proven to be useful to obtain a more precise alignment, leading to the convergence and also attainment of a higher resolution cryo-EM map.

Some samples can be heterogeneous in structure. To sort particles into different structural groups, maximum-likelihood approach can be applied at both 2D (Scheres et al., 2005) and 3D levels (Scheres et al., 2007). The 2D classification is also used to remove broken and abnormal particles from the image reconstruction process.

2.9.1.3 Resolution assessment

For resolution estimation of cryo-EM density map, Fourier shell correlation (FSC) is currently the most accepted method. It is defined as the spatial frequency at which two reconstructions each generated from a different half of a dataset are comparable with each other at a chosen correlation threshold. Different correlation threshold cutoff have been proposed. The accepted value is 0.5 for low to intermediate resolution (worse than 10 Å), and 0.143 for higher resolution structures (Rosenthal and Henderson, 2003). Recently, the method termed “gold standard FSC” has been proposed (Henderson et al., 2012), where comparison are done with the half datasets that are reconstructed independently from the beginning of the iterative cycles of orientation search and 3D reconstruction procedure. In this thesis, resolution assessment was done using the “gold standard FSC” method.

2.9.2 Preparation of DENV2 – Fab complex and cryo-EM data collection

Both DENV2 strains NGC and PVP94/07 were mixed with Fab 10.15 at a molar ratio of three Fab molecules for every two E proteins on the surface of the virus. Both these complexes were incubated at 4, or 28, or 37°C, followed by 2 hrs at 4°C. The control samples without Fab were incubated at the same temperatures. For HMAb 3F9, only DENV2 PVP94/07 strain was used and the virus was mixed with Fab 3F9 at a similar molar ratio as when preparing the Fab 10.15 sample. The complexes were incubated at either 4 or 37°C for 2 hrs prior to freezing on cryo-EM grids.

Approximately 2.5 µl drop of each sample was pipetted onto ultra-thin carbon-coated lacey carbon grids (Ted Pella). The grids were then blotted with filter papers for 2 sec and flash-frozen in liquid ethane using the Vitrobot Mark IV plunger (FEI). The frozen grids were kept at liquid nitrogen prior to imaging. The sample was imaged using a 300-kV Titan Krios electron microscope (FEI) at 47,000X magnification with an electron dose of 18 $e^-/Å^2$. At a range of underfocus value to provide phase contrast. The images were collected on a direct electron detector (Falcon, FEI) at a pixel size of 1.71 Å.

Since Fab 10.15 was found to bind more efficiently to both DENV2 strains NGC and PVP94/07 at 37^{o}C as compared to other temperatures (Fig. 3-11), images of Fab 10.15 complexed with both NGC and PVP94/07 incubated at 37°C were used for manual data collection. Fab 3F9 bound equally well to DENV2 PVP94/07 at both 4^{o}C and 37^{o}C. The sample at 4^{o}C was used for data collection due to additional consideration that at low temperature the complex might be less mobile, which may lead to the attainment of a higher resolution map. Similar microscopic parameters were used to collect images of DENV2 - Fab 3F9 sample as the DENV2 – Fab 10.15 sample, except automated data collection software, Leginon, was employed (Carragher et al., 2000).

2.9.3 Single particle analysis of DENV2 – Fab complexes

Firstly, cryo-EM micrographs were analyzed and those showing obvious drift and astigmatism were discarded. Micrographs with defocus values between 0.5 to 3.5 μm were used for image reconstruction process (Table 2-1). Images of individual particles were manually selected in the micrograph and extracted using e2boxer from EMAN2 software package (Tang et al., 2007). Pixels containing extreme intensities were removed from the extracted images and the particles were normalized. A CTF estimation algorithm that accounts for

astigmatic defocus implemented in program CTFFIND3 was used for determination of the CTF parameters (Mindell and Grigorieff, 2003). For all datasets, before icosahedral reconstruction, particles were always sorted through reference free 2D classification to remove broken and abnormal particles using maximum likelihood method implemented in Relion (Scheres, 2012).

For HMAb 10.15, the sample of DENV2 NGC – Fab 10.15 complex was more heterogeneous than PVP94/07 – Fab 10.15 complex (Fig. 3-12, Fig. 3-14). This could be due to the structural flexibility of the DENV2 NGC strain. Orientation assignment was performed using MPSA (Liu, 2007) followed by 3D reconstruction using the Make3D program from EMAN (Ludtke et al., 1999). Resolutions of the maps were determined by plotting the FSC coefficient between reconstructions from two half datasets refined independently from the start with a cutoff value of 0.5. Initial models and statistics of final reconstructions are listed Table 2-1.

Unlike the approach in analyzing the DENV2 - Fab 10.15 datasets, a maximum likelihood method implemented in Relion was used throughout the processing of DENV2 – Fab 3F9 dataset (Scheres, 2012). After the selected particles and CTF information were imported

to this program, particles were first sorted by reference free 2D classification, followed by 3D classification. After the 3D classification runs (with parameter K=5, i.e. request the algorithm to generate 5 classes) with different initial models, majority of the particles were always sorted into a single class. Since the 3D maps which were reconstructed from these particles were always similar to each other, one of these maps was used as the initial model for 3D refinement. To avoid the problem of over-fitting in iterative reconstruction, the 3D refinement was conducted whereby the dataset was divided into random halves and reconstructed separately. An FSC curve between the two independent reconstructions is calculated at the end of every cycle to estimate the resolution-dependent SNR, which is then used to filter the maps. The convergence of the final structure is monitored by the accuracy of rotation and translation assigned to the particle images. Only upon convergence, the two halves of the data were then combined to calculate a single map accounting for all particles. The resolution is reported as the spatial frequency at a cut-off of 0.143 correlation of the gold-standard FSC curve (Rosenthal and Henderson, 2003).

Table 2-1 Information of cryo-EM 3D reconstruction of Fab in complex with DENV2.

Sample	PVP94/07- Fab 10.15	NGC- Fab 10.15	PVP94/07 – Fab 3F9
Sofeware	Refine2D in Relion + MPSA + Make3D in EMAN	Refine2D in Relion + MPSA + Make3D in EMAN	Relion
Starting model	Unexpanded mature virus	Unexpanded mature virus	Map generated from 3D classification in Relion
No. of micrographs	285	361	791
No. of particle selected	2351	8292	8652
No. of particle used in orientation search	2186 (93.0%)[a]	3831 (46.2%)	4891 (56.5%)
No. of particle in final reconstruction	1463 (62.2%)	2762 (33%)	4891 (56.5%)
Resolution (Å)	24	22	22

[a] Numbers in the parentheses indicate the percentage of the particles in all selected particles.

2.9.4 Fitting of the DENV2 - Fab 10.15 cryo-EM density map

The pixel size of the map was confirmed by comparing the radius of its lipid bilayer with a low-pass filtered high-resolution DENV2 mature virus cryo-EM map. Due to its low resolution, interpretation of the Fab 10.15 – PVP94/07 map was done by manually fitting the Cα chain of the

DENV2 mature virus structure (PDB code 3J27) and the crystal structure of E-DIII and Fab 10.15 into their corresponding cryo-EM densities in the program “O” (Jones et al., 1991).

For the DENV2 – Fab 3F9 complex, the interpretation of the cryo-EM density map was carried out by manually fitting with the Cα chain of the E protein and a Fab (using the structure of Fab 10.15 as a substitute) by using the program “O” (Jones et al., 1991). All structural figures were made using the program “Chimera” (Pettersen et al., 2004).

2.10 Dynamic light scattering to determine size of immune complex

The size of the immune complex was determined by using dynamics light scattering (DLS) (Stieh et al., 2014). This technique utilizes a time-correlation function to determine the sizes of particles which diffuse in a solution due to Brownian motion. Sample that self-correlates for a longer period is larger in size than those of which time-correlation functions decrease more rapidly. The slope of the time-correlation function reflects the polydispersity of the sample and a steeper slope of the time-correlation function indicates more homogeneous sample with lower polydispersity index (PDI). The

diameter obtained from this method is the diameter of a sphere with the same diffusion coefficient as the sample.

In our experiment, purified virus particles in NTE buffer were used at a concentration of 50 µg/ml of E proteins. Serial dilutions of IgG were mixed with the purified virus in a 1:1 volume ratio and the mixtures were incubated at 37^{o}C for 30 min before the measurement. A volume of 15 µl for each reaction was loaded into a Quartz cuvette for measurement at 37^{o}C by Zetasizer Nano S machine (Malvern instrument). Data were analyzed using Zetasizer Nano software version 6.01. Ten readings were collected for each measurement of one duplicate and the reported diameters are averages of duplicate measurements.

2.11 Structural analysis

Buried surface areas of the antibody-antigen interface were calculated with the PISA server (Krissinel and Henrick, 2007). LSQ superpose in COOT was used for superimposition of protein structures. Electrostatic properties of the protein were presented based on Coulomb potential surface coloring using Chimera (Pettersen et al., 2004). Epitope accessibility was represented as the percentage of epitope solvent-accessible surface area (SSA) buried by the

neighboring E proteins. This was calculated by dividing the sum of the SSA of all residues of the epitope in presence of neighboring E proteins by the corresponding sum in absence of neighboring E proteins. The SSA was calculated using CCP4 program AREAIMOL with a 1.4-Å radius sphere as a probe.

2.12 Sequence variation analysis

In total, 1,097 DENV2 E protein sequences were downloaded from NCBI database and submitted to ViPR web server for protein sequence variation analysis (Pickett et al., 2012).

2.13 Statistical analysis

Unpaired t-test was used to check whether any difference in means observed in the experiment was statistically significant ($P<0.05$). All calculations were done using GraphPad Prism version 6.01 (GraphPad Software Inc).

Chapter III. DENV2-specific Neutralizing HMAb 10.15

3.1 HMAb 10.15 binds to recombinant E protein and E-DIII

HMAb 10.15 was previously found to be DENV2-specific and its neutralization potency was evaluated in a standard PRNT assay with various DENV2 strains. Some DENV2 strains, both laboratory-adapted and clinical isolates, were neutralized by this antibody at picomolar concentrations (Teo, 2014). In addition, this antibody can significantly increase the survival rate of AG129 mice infected by DENV2 strain D2Y98P-PP1 at concentration of 250 μg per mouse (Teo, 2014)

As shown in Fig. 3-1, anti-prM antibody 2H2 did not bind to either recombinant E protein or E-DIII. In comparison, anti-DIII antibody 3H5, could bind to both E protein and E-DIII whereas an anti-DII fusion loop antibody 4G2 only recognized E protein but not E-DIII. HMAb 10.15 behaved similarly to 3H5 with binding specificity to both E protein and E-DIII, suggesting that its binding target was E-DIII.

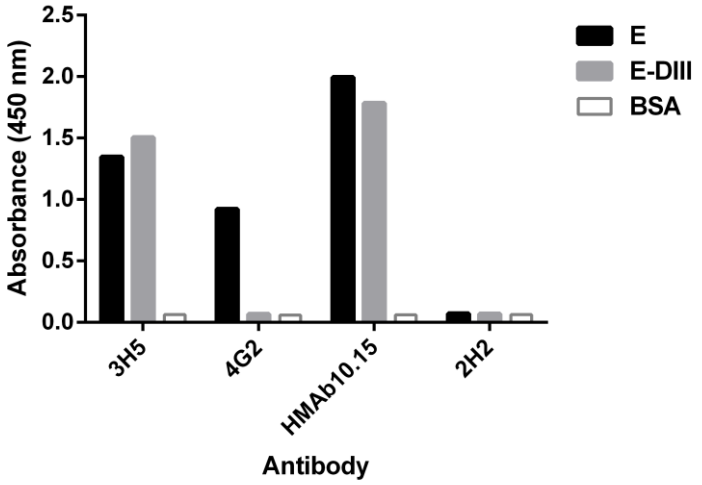

Figure 3-1 HMAb 10.15 binds to both recombinant E and E-DIII. Binding of murine MAbs 3H5, 4G2 and 2H2 and, HMAb 10.15 to recombinant DENV2 E protein and E-DIII. BSA was employed as a control antigen in this indirect ELISA.

In western blot analysis, HMAb 10.15 bound strongly to the non-reduced form of recombinant E and E-DIII in semi-denaturing condition. The binding to the reduced form of both proteins, on the other hand, was much weaker (Fig. 3-2). This suggested that HMAb 10.15 recognize a conformational dependent epitope within E-DIII. HMAb 10.15 bound to the E protein with an affinity of 8.85 nM and a half-life of approximately 33 sec (Fig. 3-3, Table 3-1) as determined by SPR.

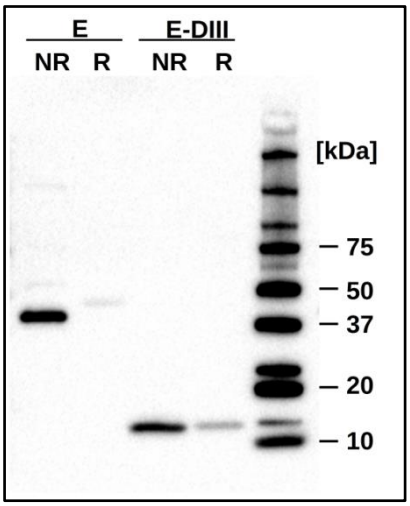

Figure 3-2 Binding analysis of HMAb 10.15 by western blot. Binding of HMAb 10.15 to recombinant DENV2 E protein and E-DIII at non-reducing (NR) and reducing (R) conditions.

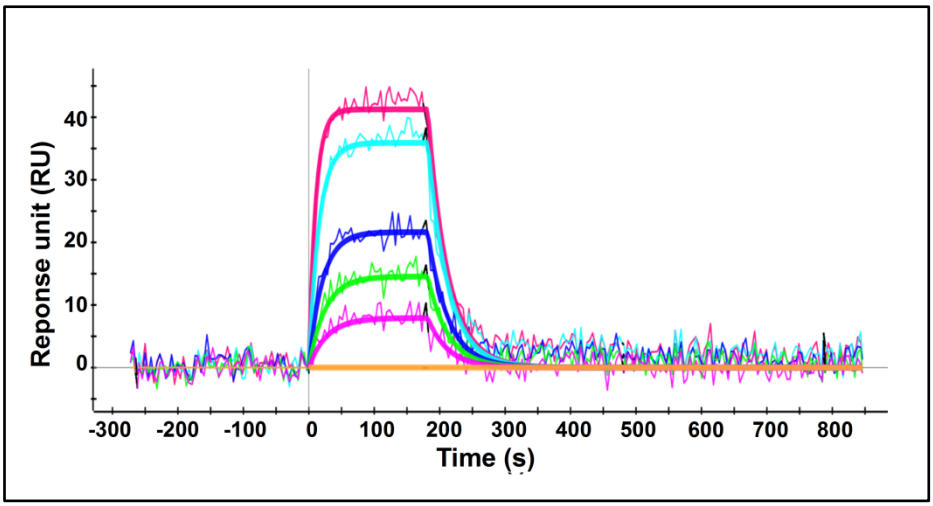

Figure 3-3 Kinetics analysis of HMAb 10.15 interaction with DENV2 recombinant E protein. SPR traces are presented of HMAb 10.15 interacting with E protein. The experimental curves were fitted using 1:1 Langmuir analysis to determine the kinetic parameters presented in Table 3-1. Binding curves at different antigen concentrations are labelled pink (40 nM), cyan (20 nM), blue (10 nM), green (5nM), magenta (2.5nM) and orange (no antigen).

Table 3-1 Kinetics of HMAb 10.15 binding to E protein measured by surface plasmon resonance.

Antigen	Association constant k_a (10^6 $M^{-1}s^{-1}$)	Dissociation constant k_d (10^{-3} s^{-1})	Affinity k_D (nM)[a]	Half-life $t_{1/2}$(sec)[b]
E	2.13±0.18	11.82±1.13	8.85±1.25	32.94±9.19

[a] $k_D = k_d/k_a$

[b] $t_{1/2} = \ln(2)/K_d$

3.2 Crystal structure of Fab 10.15 - E-DIII complex

Fab 10.15 was complexed with E-DIII (amino acid 295-395) from DENV2 strain PVP94/07 and the crystal structure of this complex was determined to 2.65-Å resolution (model statistics in Table 3-2). The observed root mean square deviation (r.m.s.d.) of only 0.75 Å between all equivalent Cα atoms in E-DIII and crystallized DENV2 E protein (Modis et al., 2003) suggested that binding of Fab 10.15 caused no major perturbation to the E-DIII structure.

The surface areas of the interface were 656.4 $Å^2$ and 679.2 $Å^2$ in E-DIII and Fab 10.15, respectively. The paratope of the Fab consisted of all six complementary determining regions (CDRs), H1 - H3 and L1 - L3, resulting in a total of 13 residues (nine from heavy chain, four from light chain) (Fig. 3-4a). Sixteen residues in E-DIII constituted the epitope and they were mostly located in A-strand, FG loop and G-strand except for a single residue in BC loop (Fig. 3-4a). The epitope mainly

interacted with the heavy chain of the Fab and it was centered on a hydrophobic groove formed by residues from A- and G-strands (Fig. 3-4b). Two residues, Lys305 and Lys307, interacted with both heavy and light chains of Fab 10.15, whereas residues Glu327 and Pro384 interact only with the light chain (Fig. 3-4b). There were twelve hydrogen bonds and some hydrophobic interactions in the interface (Table 3-3). Six of these hydrogen bonds involved main chain atoms, Phe306(O), Val308(O), Ile312(N), Gln386(O), Lys388(N) and Ser390(N), of E-DIII (Table 3-3). The CDR-H3 of HMAb 10.15 made extensive interactions with both A- and G-strands of DIII. For instance, side chains of two bulky hydrophobic residues Tyr105 and Trp109 in CDR-H3 could bind to the hydrophobic groove formed by A- and G-strands (Fig. 3-4c). This hydrophobic interaction was further stabilized by hydrogen bonds formed between residues in CDR-H3 and residues in both A- and G- strand of E-DIII (Table 3-3). The epitope and paratope were highly complementary in shape (i.e. shape complementarity value = 0.656), typical for antibody-antigen interactions (Lawrence and Colman, 1993).

Table 3-2 Data collection and refinement statistics (molecular replacement) for Fab 10.15 - E-DIII complex.

	Fab 10.15 – E-DIII
Data collection	
Space group	C2
Cell dimensions	
a, b, c (Å)	129.509, 53.208,91.283
α, β, γ (^{o})	90, 108.911, 90
Resolution (Å)	23.21 – 2.65 Å (2.74 – 2.65 Å)
R_{sym} or R_{merge}	0.054 (0.312)
I / σI	19.668 (4.857)
Completeness (%)	99.0 (96.8)
Redundancy	3.4 (3.2)
Refinement	
Resolution (Å)	23.21 – 2.65 Å (2.74 – 2.65 Å)
No. reflections	17084
R_{work} / R_{free}	0.24 / 0.28
No. atoms	
Protein	4017
Ligand/ion	1
Water	23
B-factors	
Protein	68.654
Ligand/ion	59.390
Water	44.962
R.m.s. deviations	
Bond lengths (Å)	0.003
Bond angles (^{o})	0.79

Values in parentheses are for highest-resolution shell.

R_{work} = Σhkl||Fobs| - |Fcalc||/Σhkl |Fobs|, which is the crystallographic R-factor and calculated with 90% of the data used in the refinement; R_{free} is another crystallographic R-factor calculated with 10% randomly selected data which is not used in the refinement for cross validation.

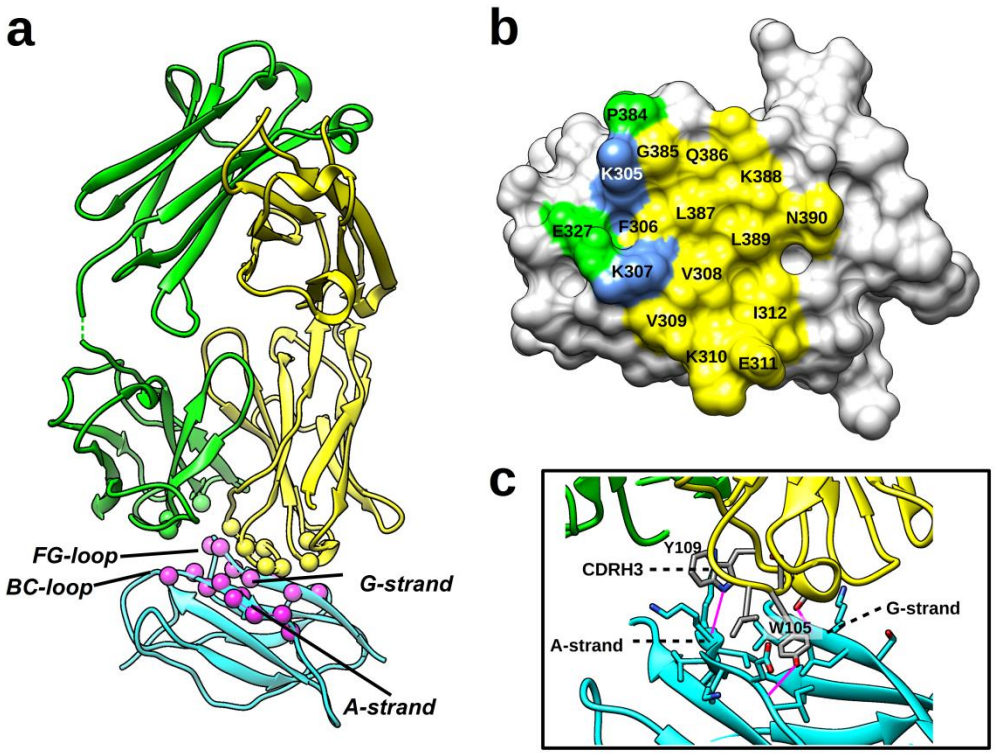

Figure 3-4 The crystal structure of Fab 10.15 complexed with DENV2 E-DIII.

(a) A ribbon diagram showing the crystal structure of Fab 10.15 - E-DIII complex. The light chain and heavy chain are colored in green and yellow, respectively, with residues constituting the paratope as spheres. The E-DIII is colored in cyan with the residue forming the epitope as magenta spheres. (b) Surface representation of the epitope with surface contacted exclusively by light chain, heavy chain and both chains colored as green, yellow and blue, respectively. Residue numbers and amino acids are labelled. (c) A close-up view of the CDR-H3 binding to the hydrophobic groove formed between A- and G-strands of E-DIII, with the same color scheme as (a). Side chains of contact residues are shown as sticks with hydrogen and oxygen atoms colored as blue and red, respectively. Residues W105 and Y109 in CDR-H3 with hydrophobic side chains are labelled. Potential hydrogen bonds are highlighted with magenta lines.

Table 3-3 List of potential hydrogen bonds based on the 2.65-Å resolution crystal structure of Fab 10.15 – E-DIII complex.

E-DIII		Fab fragment			Distance (Å)
Position	**Residue**	**CDR**	**Position**	**Residue**	
305	Lys (NZ)	L3	114	Asp (OD1)	2.58
		L1	52	Asn (OD1)	2.37
306	Phe (O)	H3	109	Trp (NE1)	3.01
307	Lys (NZ)	L2	71	Ser (OG)	4.00
308	Val (O)	H3	104	Leu (N)	3.96
311	Glu (OE2)	H1	33	Asn (ND2)	3.36
312	Ile (N)	H3	105	Tyr (OH)	3.06
327	Glu (OE1)	L1	53	Thr (OG1)	3.86
	Glu (OE2)	L2	71	Ser (OG)	3.68
386	Gln (O)	H3	108	Gly (N)	3.55
388	Lys (N)	H3	107	Ser (OG)	3.44
390	Ser (N)	H2	55	Tyr (OH)	2.96
	Ser (OG)	H2	56	Asp (OD1)	3.00

Red color highlights DIII main chain atoms potentially involved in the hydrogen bond interaction with Fab 10.15

This epitope was highly conserved in DENV2 with only residue 390 showing significant polymorphism. Of 1097 DENV2 sequences analyzed, 86% have an asparagine (e.g. NGC) at residue 390 while 10% have a serine (e.g. PVP94/07) and 4% aspartic acid. In contrast, DENV1, DENV3 and DENV4 have more non-conserved substitutions in

this epitope region (Fig. 3-5e). These changes might disrupt the shape and charge complementarity between HMAb 10.15 and E-DIII, explaining the serotype specificity of this antibody (Fig. 3-5a, b, c, d).

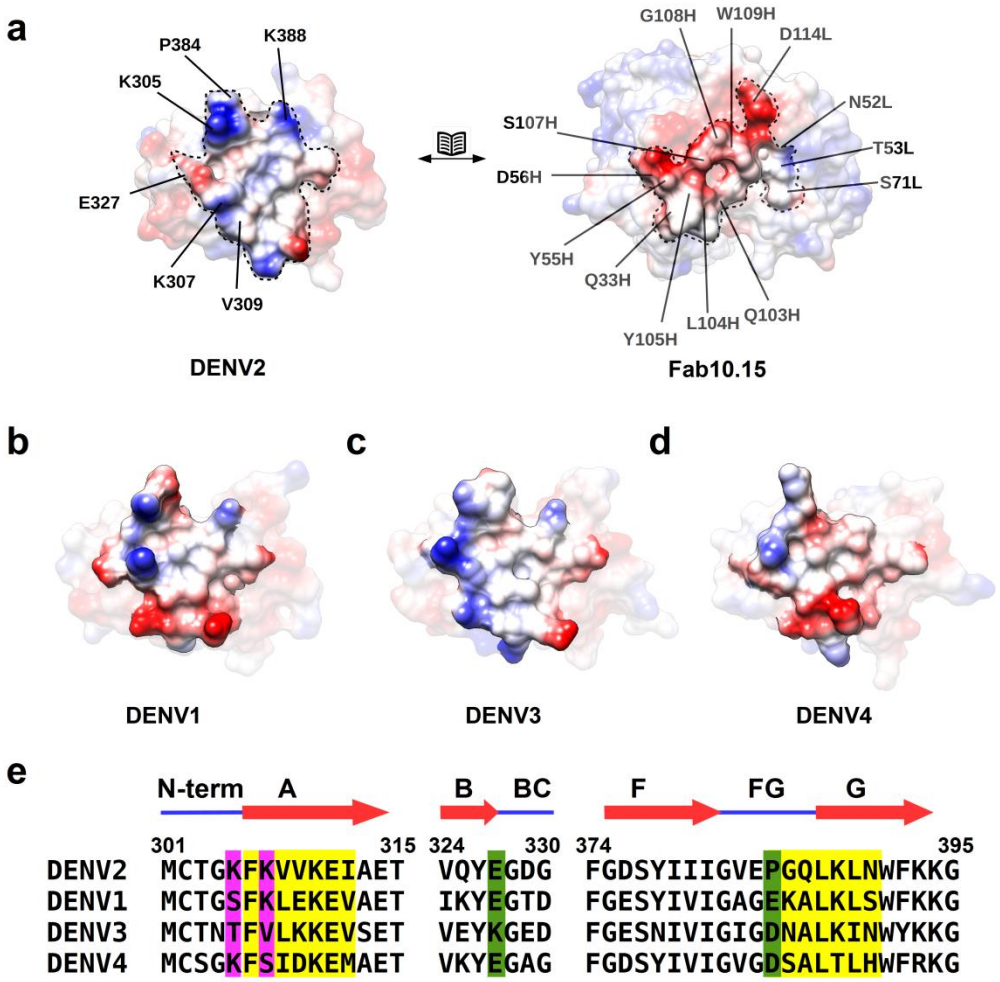

Figure 3-5 Comparison of electrostatic charges of the epitope across DENV serotypes. Electrostatic potential surfaces of E-DIII are colored blue (positive), red (negative) and white (neutral). (a) Representation of the electrostatic potential of DENV2 E-DIII (left) and Fab 10.15 (right) interface. Borders of the epitope and paratope are indicated with dashed line. Residues in the epitope that were mutated in other serotypes, which might reduce the charge complementarity, are highlighted (left). Residues in the paratope are labeled (right), with heavy (H) and light (L) chains indicated after the residue numbers. The electrostatic potentials of E-DIII of (b) DENV1, (c) DENV3 and (d)

DENV4 of the same region as epitope in DENV2 are shown. (e) Sequence alignment of the epitope region of DENV1-4. Residues interacting with heavy, light and both chains are highlighted in yellow, green and magenta boxes, respectively. Secondary structure and residue numbers are indicated above the sequence. Electrostatic potential surface were calculated using PDB code 4FFZ (DENV1), 3VVT (DENV3) and 3WE1 (DENV4) and their sequences were also used for alignment.

3.3 HDX-MS result is consistent with the crystal structure

In the HDX-MS experiment using E-DIII, the coverage of pepsin-digested peptides was 67.7% of the E-DIII sequence. One peptide in A-strand (residues 307-313) and multiple peptides extending from F-strand to G-strand (from residues 377 to 391) showed significant reductions of deuterium uptakes (with cut-off value = 0.5 Da) in presence of Fab 10.15 (Fig. 3-6a). As there were overlapping peptides for this region, comparisons of their deuterium-uptake differences could be conducted. Alterations of deuterium uptakes for peptide 378-387 and peptide 378-389 showed approximately one dalton difference, similar to the difference observed between those of peptide 377-387 and 377-389 (Fig. 3-6b). Similar result was also observed between peptide 378-389 and peptide 378-391. These differences indicated that residues 388-389 and 390-391, located in G-strand, became much more buried when E-DIII was complexed with Fab 10.15. This result

was consistent with our crystal structure which showed that the amides of residues 388 and 390 directly formed hydrogen bonds with the side chains of Ser107 and Tyr55 in heavy chain of Fab 10.15, respectively (Table 3-3).

One peptide (residues 312-322) which extended from AB loop to B-strand showed increased deuterium uptake in the presence of Fab 10.15 (Fig. 3-7a). Comparison of the alterations of deuterium uptakes between this peptide and two overlapping peptides (peptides 312-321 and 313-321) suggested that residue 322 located in the B-strand might be the residue that contributed to this increase. When the E-DIII structure in the complex was compared with the E-DIII in the DENV2 E protein crystal structure (PDB code 1OAN), a positional shift of A-strand was noticed. This conformational change was presumably caused by the binding of Fab 10.15 (Fig. 3-6c) which resulted in changes of the hydrogen bonding network around residue 322.

There was another area with peptides (peptides 352-366, 352-377 and 360-377) showing reduction of deuterium exchange larger than 0.5 Da. A closer examination of shorter peptides (including peptides 352-359, 360-366, 360-367, 367-377) in the same region did not show significant reductions of deuterium uptakes (Fig. 3-6d). The information

of deuterium exchange for the first residue in any peptide is lost due to peptic cleavage. Considering this, comparison of the overlapping peptides suggested that residue 360, located in the DE loop, might be the key residue causing the reduction. However, examination of this residue in our crystal structure did not show obvious conformational change from its conformation in the unbound E protein.

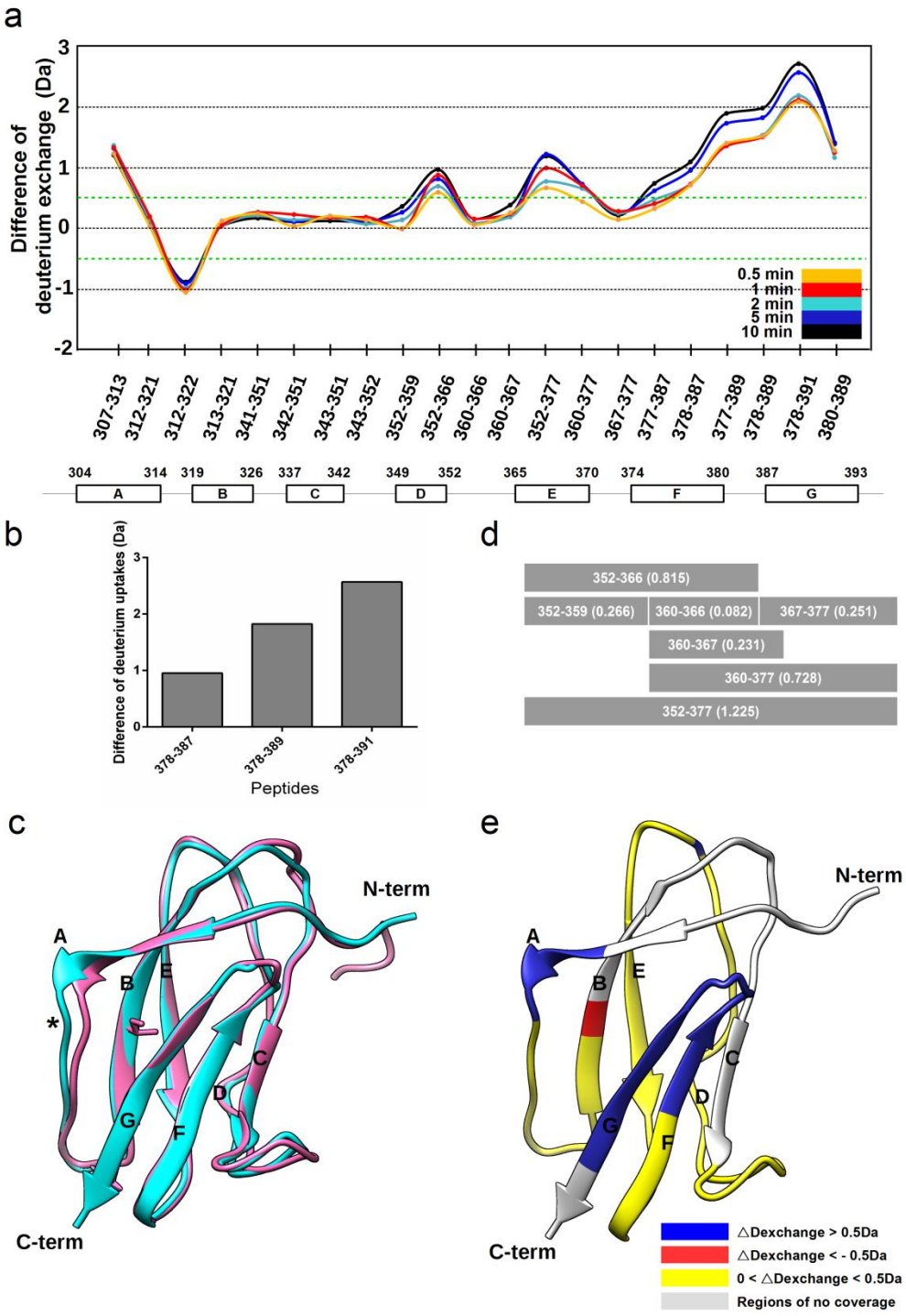

Figure 3-6 Comparison of deuterium exchange between E-DIII in absence and presence of Fab 10.15.

(a) The difference plot of the deuterium exchange of E-DIII in presence and absence of Fab 10.15. Coloring scheme of the results at different time points are indicated by the color key. A positive value of the different plot means less deuterium uptake in presense of Fab,

suggesting that the peptides are more buried, whereas the negative value means the opposite. Peptides are numbered according to the sequence of full-length E protein and the secondary structure of E-DIII is attached below with the numbers indicating the start and end residues of the β–strands. A difference larger than 0.5 Da is considered significant, highlighted as green dashed line in the plot. (b) Comparison of deuterium exchange differences for multiple peptic peptides at the N-terminus of E-DIII. (c) Superimposing the E-DIII structure (cyan) of the Fab 10.15 – E-DIII complex with the unbound E-DIII structure (pink) (extracted from PDB code 1OAN). The * highlighted the region where conformational changes happen and residue 322 showing increased deuterium uptake was shown in sticks. (d) Overlapping peptides in region 352-377 with sequence numbers plus deuterium exchange difference in parenthesis. (e) Results from HDX-MS mapped onto the crystal structure of E-DIII in the Fab 10.15 – E-DIII complex. Color keys are indicated in the figure.

Another HDX-MS experiment was conducted by using recombinant E protein ectodomain instead of E-DIII. In this experiment, pepsin-digested peptides covered 69% of the E protein ectodomain (amino acid 1-395) sequence. Region 378-389 consistently showed reduction of deuterium uptake in presence of Fab 10.15 (Fig. 3-7a). However, there was no obtained peptide covering A-strand in this experiment. In addition, peptide 313-322 did not show increase of deuterium uptake. Thereby residue 322 might not show increase of deuterium uptake similar as in the experiment with E-DIII. Moreover, the reduction of deuterium uptake for peptides spanning DE loop (where residue 360 is located) was also smaller compared to that in the

experiment with E-DIII as antigens (Fig. 3-6a, Fig. 3-7a). These results could be due to varied protein dynamics of E-DIII in absence or presence of E-DI/II. Besides, this experiment also provided information about the protein dynamics for DI/II of E protein after it was bound by Fab 10.15. There was reduced deuterium uptake in peptide 131-159 in presence of Fab 10.15, indicating that this region had become more buried. This peptide is close to the DE loop of DIII in the E protein crystal structure (Fig. 3-7b).

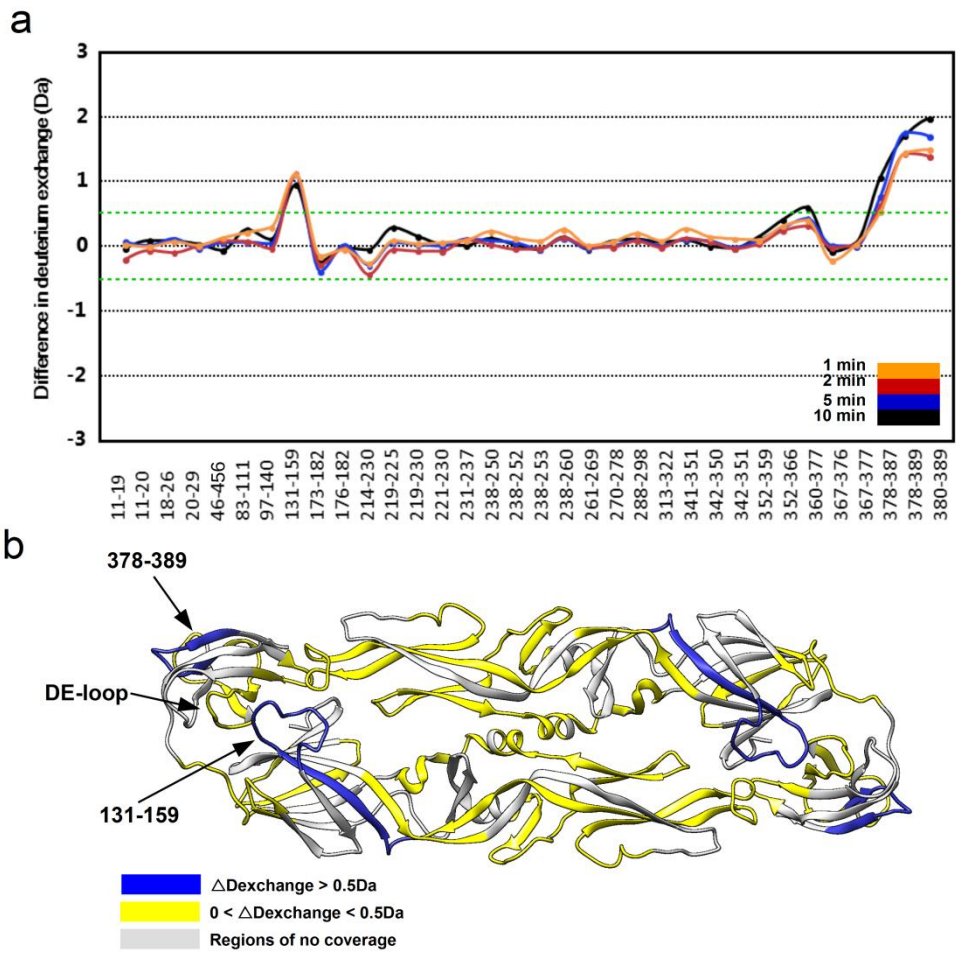

Figure 3-7 Comparison of deuterium exchange between E proteins in absence and presence of Fab 10.15.
(a) The difference plot of the deuterium uptake of E protein in presence and absence of Fab 10.15. Coloring scheme of the results at different time points are indicated by the color key. The meaning of positive and negative values are the same as Fig. 3-6. Peptides are numbered according to the full-length E protein. The 0.5 Da cut-off is highlighted as dashed line. (b) HDX-MS results are mapped onto DENV2 E protein structure (PDB code 1OAN) in ribbon view with color key attached below.

3.4 The amount of HMAb 10.15 required to neutralize DENV2 strains NGC and PVP94/07 differs

There were significant differences ($P < 0.001$) in the $PRNT_{50}$ value for HMAb 10.15 with DENV2 strain NGC (3.5 ± 0.5 ng/ml) and strain PVP94/07 (59.4 ± 12.1 ng/ml) (Fig. 3-8a). Similar trend was observed with the Fab of this HMAb except that much more Fab were required ($PRNT_{50}$ NGC; 293.6 ± 67.5 ng/ml, $PRNT_{50}$ PVP94.07; 3649 ± 1090 ng/ml) (Fig. 3-8b, Table 3-4).

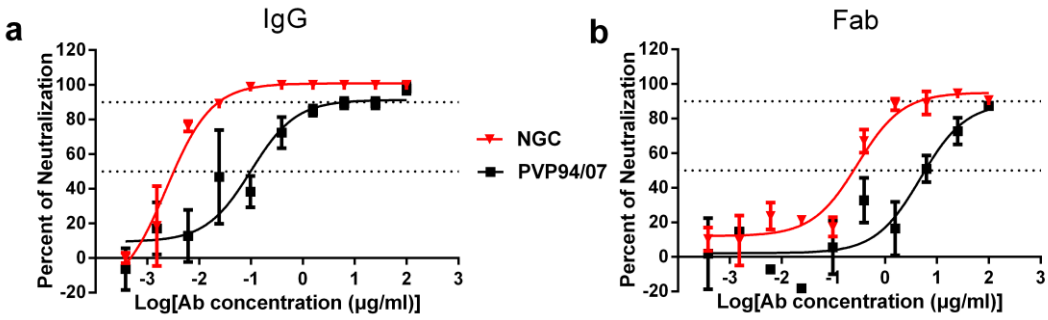

Figure 3-8 Neutralization of DENV2 strains NGC and PVP94/07 by HMAb 10.15 and Fab 10.15 in BHK-21 cell. Neutralizations of 50% and 90% of the infectivity were highlighted by dashed lines.

Table 3-4 Summary of $PRNT_{50}$ values for HMAb 10.15.

$PRNT_{50}$ (μg/ml) **HMAb 10.15**	**NGC**	**PVP94/07**	**PVP94/07 : NGC**
Fab	293.6 ± 67.5	3649 ± 1090	12
IgG	3.5 ± 0.5	59.4 ± 12.1	17
Fab : IgG	84	61	

3.5 Neutralization potency difference is not due to variation of the binding affinity

Variation within the epitope site and surrounding regions might affect the binding of HMAb 10.15 to the virus, leading to the difference between sensitivity of NGC and PVP94/07 to neutralization. Sequence alignment of the epitope on E-DIII between DENV2 strains PVP94/07 and NGC showed that only one residue, 390, was different. While strain NGC has an asparagine, PVP94/07 has a serine at this position. Although the bulkiness of their side chains is different, both are uncharged polar residues. The binding kinetics of HMAb 10.15 to these two virus strains were measured using recombinant E-DIII bearing sequences of these two strains as mobile analyte through the immobilized antibodies, either full-length IgG or Fab, in surface plasmon resonance (SPR) experiment.

The results showed that IgG 10.15 had a higher affinity towards E-DIII from strain PVP94/07 than that of the NGC strain (Table 3-5).

Similar result was obtained when Fab fragment was immobilized on the chip to capture E-DIII in the flowing phase (Table 3-5). HMAb 10.15 has higher neutralization potency towards NGC than PVP94/07. In contrast, the opposite is true in terms of the affinity. In conclusion, the different neutralization potencies of HMAb 10.15 against NGC and PVP94/07 are not due to its differences in binding affinities to the different E-DIII DENV2 strains. It is thus possible that the mobility of the quaternary E protein structures on the virus surface may expose its epitope and lead to the observed differences in neutralization.

Table 3-5 Kinetics of HMAb 10.15 binding to recombinant E-DIII from both DENV2 strains PVP94/07 and NGC measured by surface plasmon resonance.

Interaction	Association constant k_a (10^6 $M^{-1}s^{-1}$)	Dissociation constant k_d (10^{-3} s^{-1})	Affinity k_D (nM)[a]	Half-life $t_{1/2}$(sec)[b]
	IgG			
E-DIII (PVP94/07)	3.08 ± 1.64	0.87 ±0.44	0.29±0.09	996 ± 529
E-DIII (NGC)	1.21 ± 0.31	1.16 ± 0.16	0.97± 0.11	604 ± 75
	Fab			
E-DIII (PVP94/07)	1.95±1.10	1.06±0.27	0.60±0.20	677±173
E-DIII (NGC)	1.09±0.39	1.13±0.29	1.14±0.51	641±160

[a] $k_D = k_d/k_a$

[b] $t_{1/2} = \ln(2)/K_d$

3.6 Analysis of epitope accessibility of HMAb 10.15 on DENV2 mature virus structure

Analysis of the epitope accessibility on DENV2 compact unexpanded mature virus structure at 28^{o}C (PDB code 3J27) revealed that 35%, 26% and 25% of this epitope were buried in molecules A, B and C, respectively, due to intra-dimeric, inter-dimeric and inter-raft interactions (Fig. 3-9a, b). However, as the E protein shell expanded of the NGC strain at human physiological temperatures, this epitope became more exposed. The proportions of the buried epitopes in molecules A, B and C were reduced to 7%, 0% and 1%, respectively (Fig. 3-9b). Although E-DIII of molecule B has been elevated in this expanded structure with the binding site of HMAb 10.15 becoming fully exposed, epitopes in molecules A and C were still occluded by their adjacent E proteins (Fig. 3-9b, right).

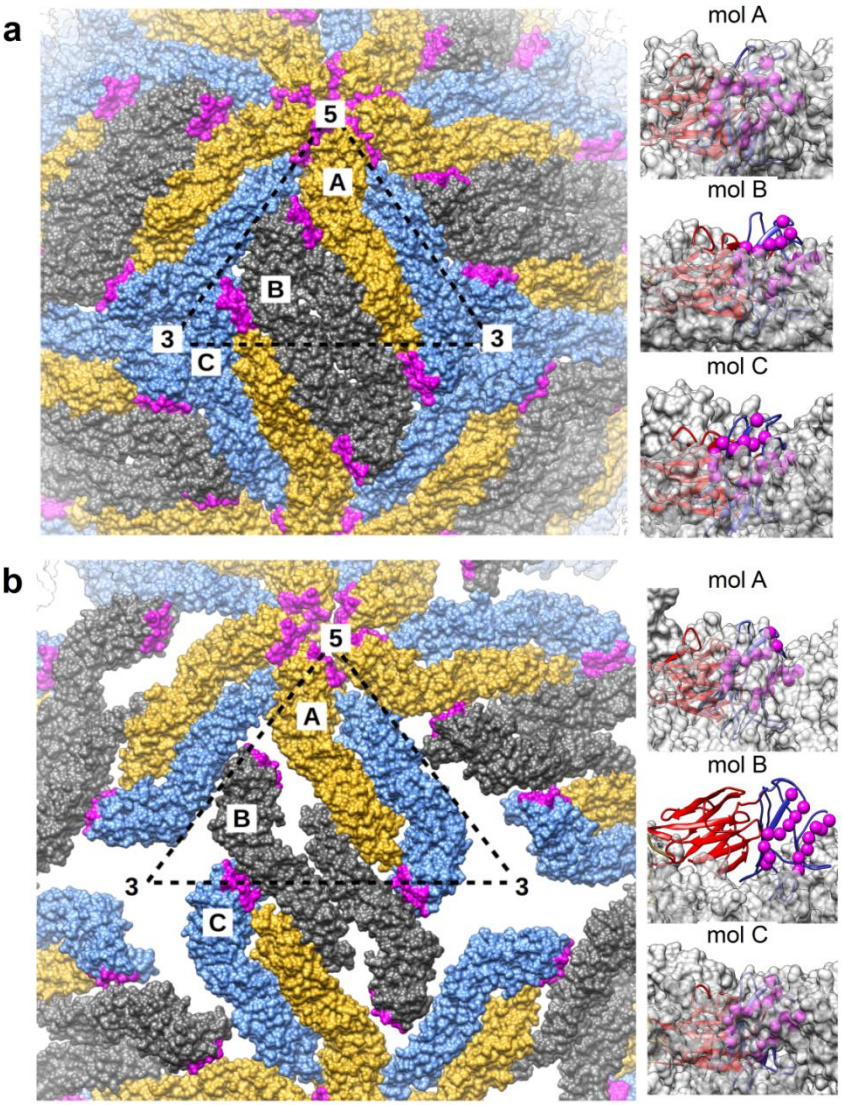

Figure 3-9 Epitope accessibility of HMAb 10.15 on DENV2 mature virus structure.

Left, the epitope of HMAb 10.15 in one asymmetric unit of (a) unexpanded and (b) expanded DENV2 mature virus structures. The E protein is shown as surface, and mols A, B and C are colored as orange, grey and blue, respectively. The epitope of HMAb 10.15 is colored magenta. The triangle indicates one asymmetric unit on virus surface with symmetric vertices numbered.

Right, mols A, B and C are represented as ribbons and colored by domains (blue for E-DIII and red for E-DI). The epitope is represented as magenta sphere. Neighboring E proteins are shown as transparent grey surface.

3.7 HMAb 10.15 binds to DENV2 in a temperature dependent manner

As expected, particles of strain NGC changed conformation after they were incubated at 37^{o}C (Fig. 3-10, bottom). However, strain PVP94/07 remained round and smooth at temperatures up to 39°C (Fig. 3-10, top). The varied structures of these two viruses at 37^{o}C were interesting, as they had different sensitivities to neutralization by HMAb 10.15. More importantly, the epitope of HMAb 10.15 only became fully accessible when the virus structure expanded, as shown in Fig 3-9b. The lack of structural changes in strain PVP94/07 raised the question of how HMAb 10.15 can bind to this virus.

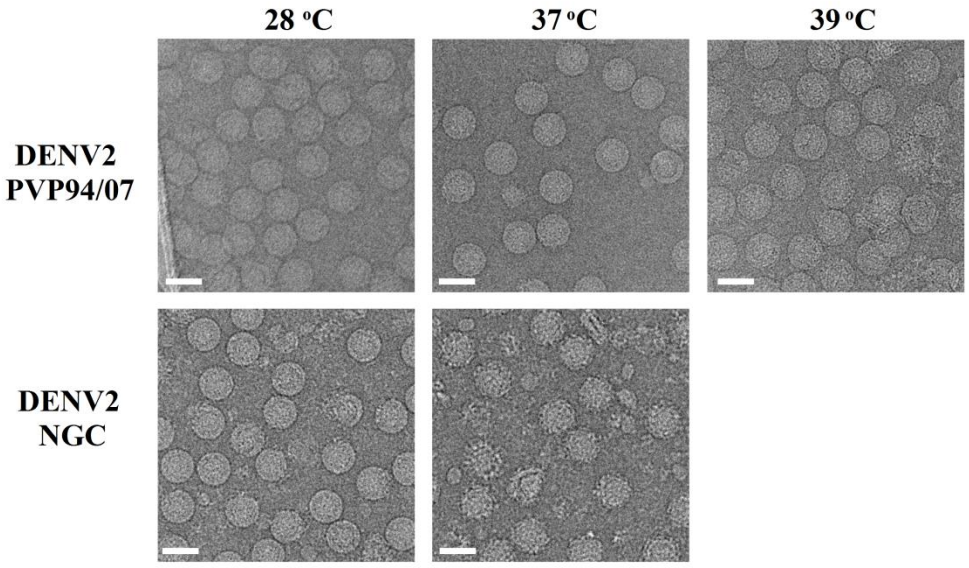

Figure 3-10 Cryo-EM images of uncomplexed DENV2 at different tempretures. The scale bar indicates 50 nm.

Very few of Fab 10.15 molecules were observed to bind to DENV2 particles of either strain at 28^{o}C (Fig. 3-11, left) but the numbers increased significantly at 37^{o}C (Fig. 3-11, right). The binding of Fab 10.15 to strain PVP94/07 which is visibly unexpanded at 37^{o}C, suggested that the E proteins on virus may still have undergone some local small changes in order to expose its epitope.

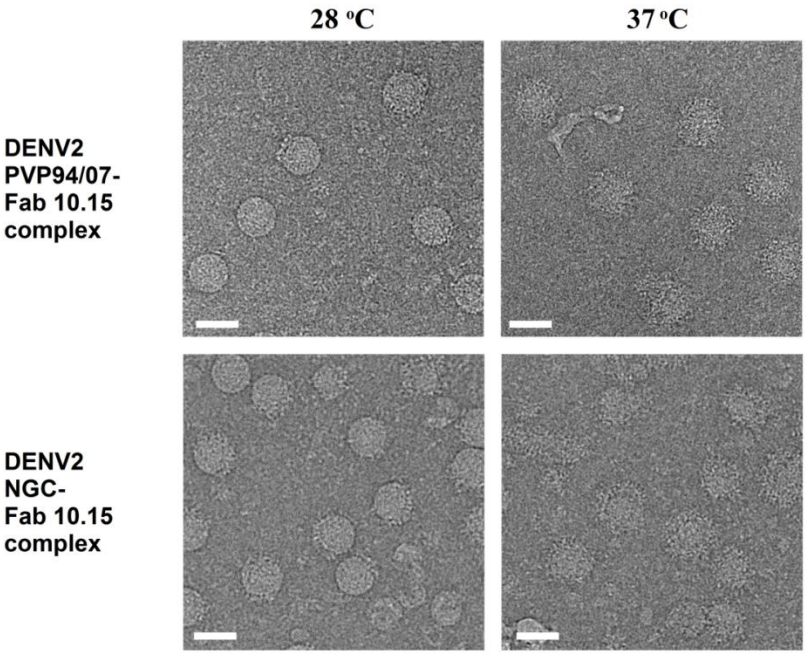

Figure 3-11 Fab 10.15 binds more efficiently to both DENV2 strains NGC and PVP94/07 at 37^{o}C than 28^{o}C. The white bar indicates a length of 50 nm.

3.8 Cryo-EM structure of DENV2 –Fab 10.15 complex

3.8.1 Single particle analysis of PVP94/07 – Fab 10.15 complex

To understand the structural basis of HMAb 10.15 binding to DENV2 PVP94/07, the sample of PVP94/07 complexed with Fab 10.15

at 37^{o}C was used for single particle analysis. Cryo-EM projections of this complex revealed that the sample was heterogeneous. As the sample of uncomplexed virus particles at 37^{o}C was homogeneous (Fig. 3-10, top middle panel), such high degree of heterogeneity was likely contributed by the binding of Fab 10.15 and thus reflecting the flexibility of this complex.

Two-dimensional classification of the particles showed two highly populated classes (class 5 and 18) with their averaged projections showing lipid bilayer separation. Together these two classes accounted for 68% of all particles. There were seven additional classes (class 1, 13, 19, 20, 21, 22, and 25), which showed averaged projections of concentric circles each representing the nucleocapsid, lipid membrane and outer protein shell layers (Fig. 3-12). In total, these nine classes accounted for 93% of all the particles. The remaining classes with small number of particles and class averages showing broken particles were excluded from subsequent steps of 3D reconstruction. Iterative alignment and reconstruction resulted in a 24-Å map (Fig. 3-13).

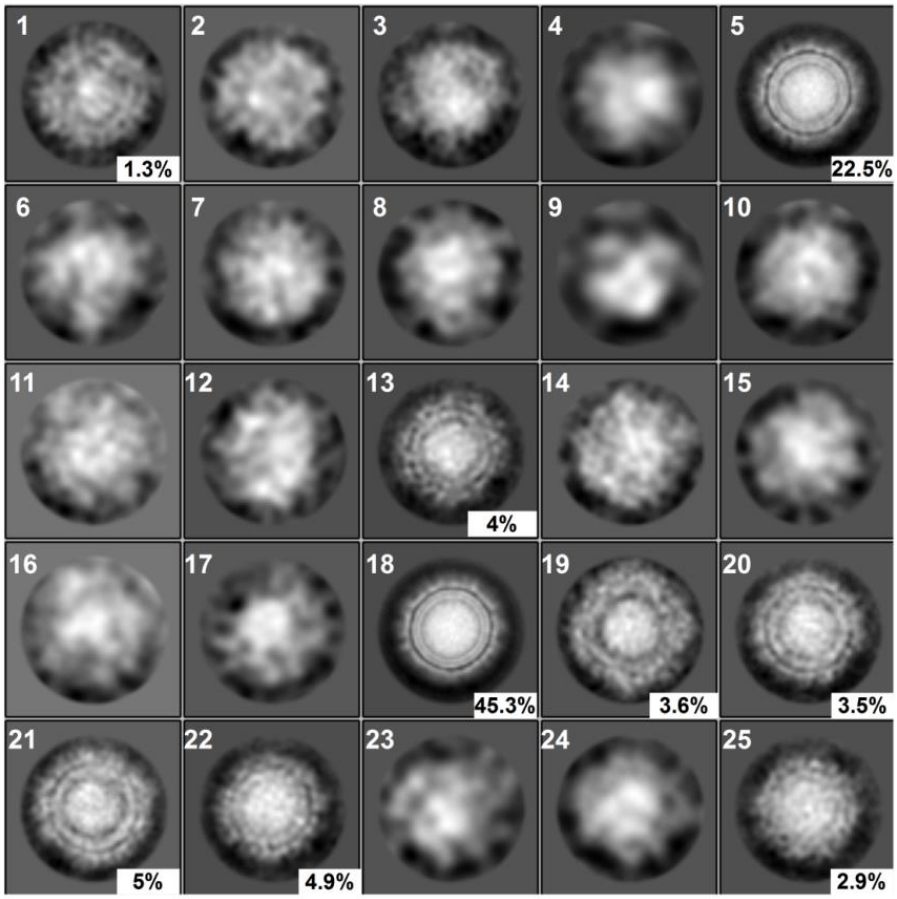

Figure 3-12 The 2D class averages of PVP94/07 – Fab 10.15 complex. The number at the right bottom corner indicates the percentages of the particles in that particular class as a proportion of all particles. Only percentages above 1% are in this figure.

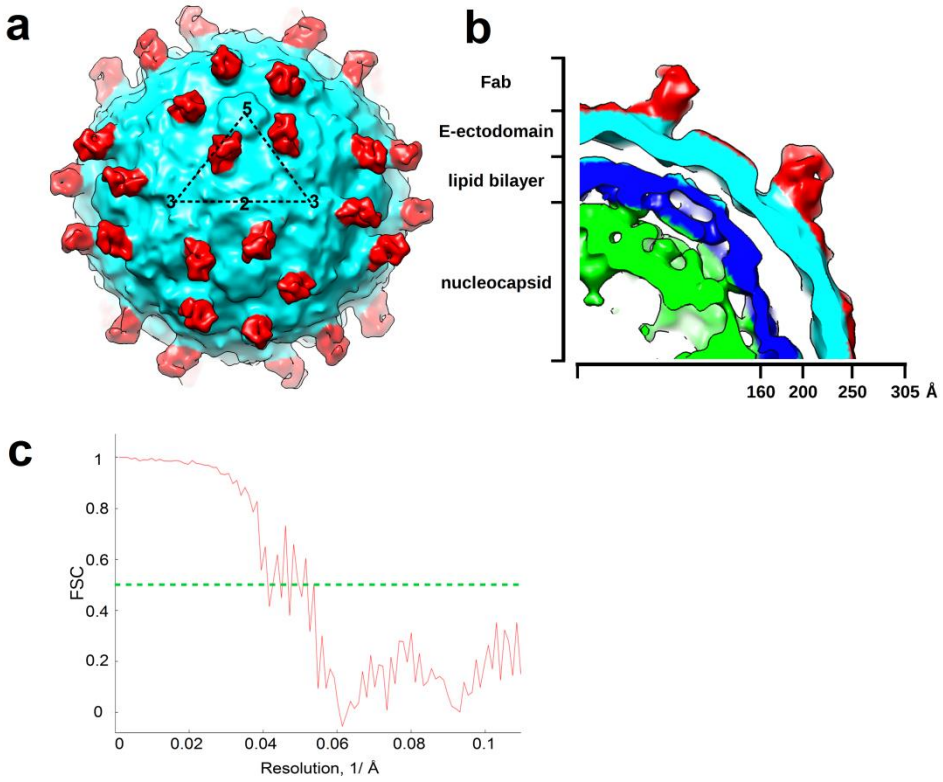

Figure 3-13 Cryo-EM density map of PVP94/07 – Fab 10.15 complex. (a) Surface representation of the cryo-EM map of Fab 10.15 – PVP94/07 complex. The black triangle represents an icosahedral asymmetric unit and the symmetry vertices are indicated (b) A quarter of the cross-section of the density map showing radial density distribution. The map is colored radially in panels A and B: up to 160 Å, green; 161 Å to 220 Å, blue; 221 Å to 250 Å, cyan; above 251, red. (c) Resolution determination of the cryo-EM map using FSC with a 0.5 cut-off value used.

3.8.2 Single particle analysis of NGC – Fab 10.15 complex

DENV2 Strain NGC has been shown to have greater structural dynamics at 37^{o}C unlike PVP94/07. Two-dimensional classification of the NGC – Fab 10.15 sample also showed greater heterogeneity compared with the PVP94/07 – Fab 10.15 sample. The sample included

two major subsets. The first subset of classes (1, 30, 32, 33, 36, 37, 38, 39, 41) (Fig. 3-14, green box), accounting for 46.2% of all the boxed particles, had similar averaged projections as those of the PVP94/07 – Fab 10.15 complex mentioned above (Fig. 3-12). The second subset of classes (class 15, 19, 20, 23, 31 and 45) had averaged projections that looked like broken particles (Fig. 3-14, red box). These classes accounted for 43.7% of all the boxed particles. A high percentage of broken particles could be due to surface disruption induced by binding of Fab 10.15, as discussed in section 3.6. 3D reconstruction using particles belonging to the first subset of classes resulted in the cryo-EM density map similar to the map obtained for PVP94/07 - Fab 10.15 complex (Fig. 3-15).

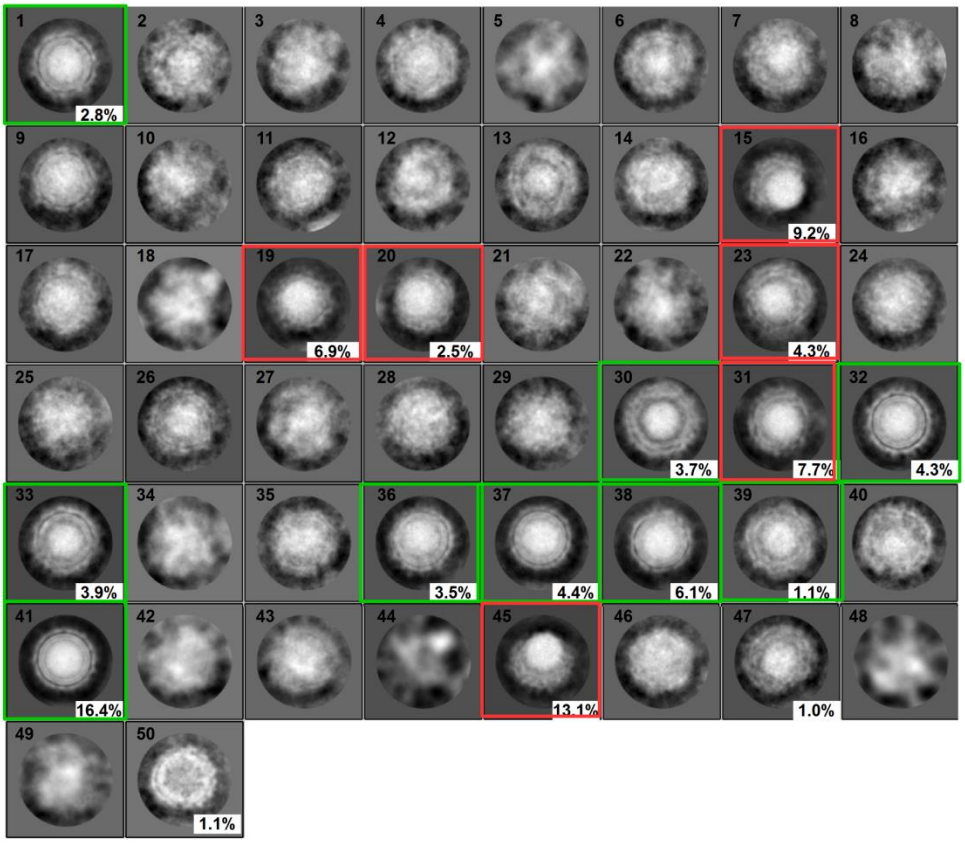

Figure 3-14 The 2D class averages of NGC – Fab 10.15 complex. The number at the right bottom corner indicates the percentages of the particles in that particular class over all particles. Only percentages above 1% are in this figure. The classes belonging to a subset that resembles PVP94/07 – Fab 10.15 are highlighted in green boxes. The classes of another subset with broken particles are highlighted in red boxes.

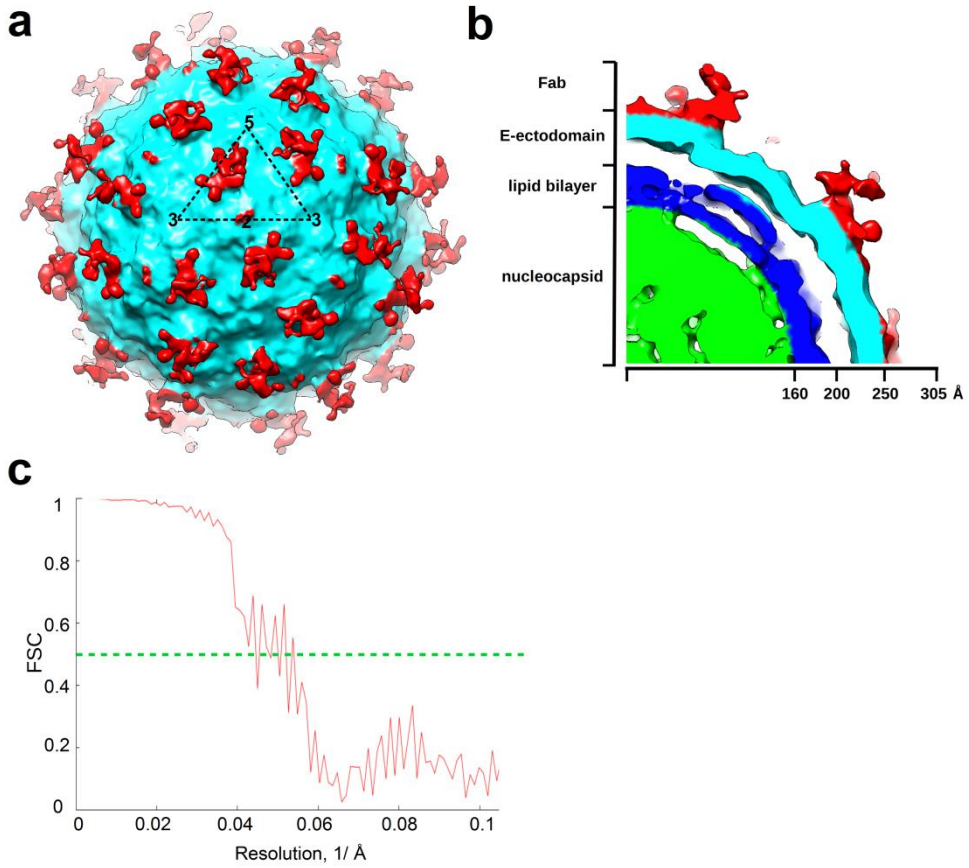

Figure 3-15 Cryo-EM density map of NGC – Fab 10.15 complex.
(a) Surface of the DENV2 NGC –Fab 10.15 cryo-EM map. The black triangle represents an icosahedral asymmetric unit and the symmetry vertices are indicated. (b) A quarter of the cross-section of the density map showing radial density distribution. The map is colored radially in panels A and B: up to 160 Å, green; 161 Å to 220 Å, blue; 221 Å to 250 Å, cyan; above 251, red. (c) Resolution determination of the cryo-EM map by using FSC with a 0.5 cut-off value used.

3.8.3 Cryo-EM structure of PVP94/07 – Fab 10.15 complex

The map obtained from the NGC – Fab 10.15 sample was similar to the PVP94/07 – Fab 10.15 sample. Cryo-EM maps of both NGC – Fab 10.15 and PVP94/07 – Fab 10.15 complexes showed protrusions of densities between 5- and 3-fold vertices, corresponding to the size of one Fab molecule, which suggested that Fab 10.15 only bound to the B molecule (Fig. 3-13a and 3-15a). The density corresponding to the E protein layer is at a radius of ~250 Å (Fig. 3-13b, Fig. 3-15b), ~10 Å higher than that of unexpanded mature virus particles. This indicates that the E protein shell may have been loosened. This is consistent with the observation that the Fab will clash with the neighboring E protein when the crystal structure Fab-E-DIII was superimposed onto the mol B in unexpanded mature virus structure (Fig. 3-16a). This suggests that if antibody is to bind to the virus, the E protein shell has to be loosened in order to fully expose the epitope. As the features in the cryo-EM map of PVP94/07 – Fab 10.15 is more obvious than NGC – Fab 10.15 complex, interpretation of the map by fitting in E-Fab crystal structures was only done for the former.

To fit the density map, the crystal structure of the Fab10.15 – E-DIII complex was superimposed onto domain III of E protein mol B. Since

the Fab density is the most obvious feature in the cryo-EM map, we first fitted the Fab molecule and this will guide the position of its bound E protein molecule B (Fig. 3-16b). The remaining density was then filled by the A-C' dimer, which was moved to a higher radius and there was minimal rotation (Fig. 3-16c, d).

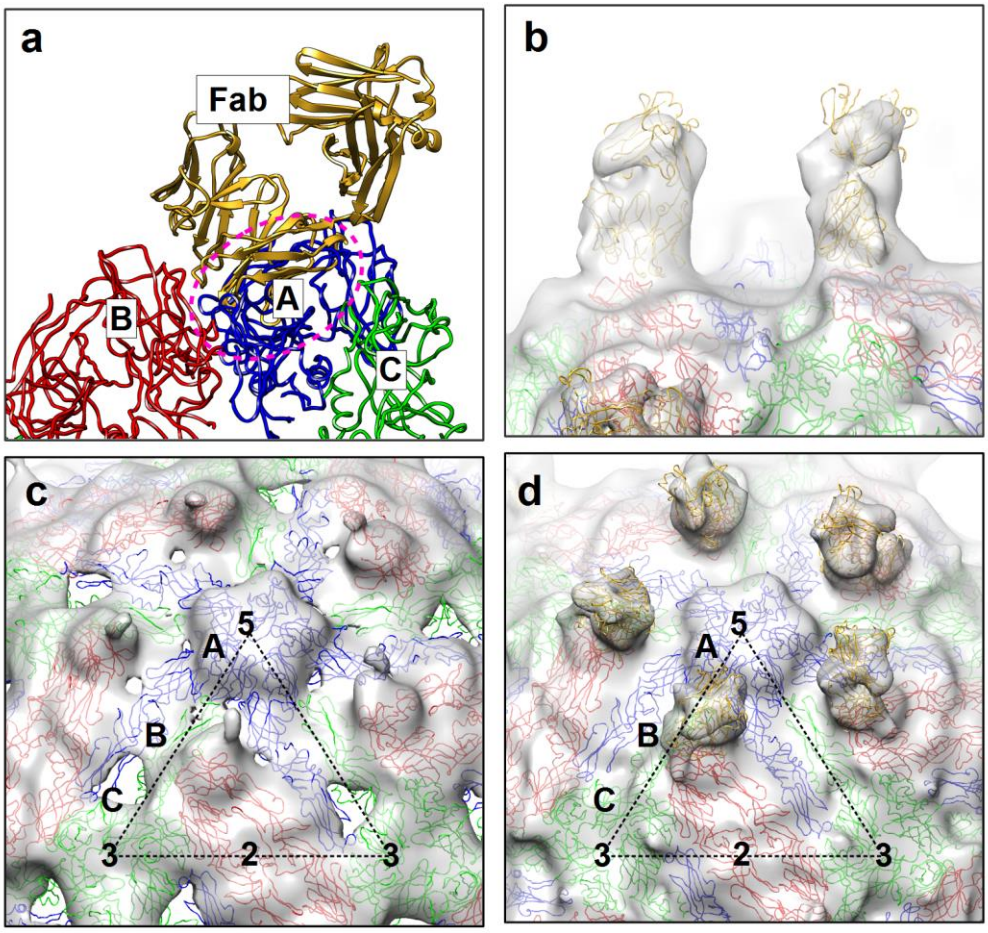

Figure 3-16 Fitting of PVP94/07- Fab10.15 into cryo-EM density map. Superimposition of the Fab 10.15 – E-DIII crystal structure to mol B in the unexpanded mature virus structure (PDB code 3J27) showed (a) clashes of the Fab with mol A, highlighted by the dotted pink circle. (b) Side view of the Fab molecule at map contour level of 2. Top views of the fitting with (c) E proteins at map contour level of 3.5 and, (d) E proteins and Fab molecules at map contour level of 2.0. The cryo-EM density map is shown as transparent grey surface. Fab 10.15 is shown

as yellow ribbon and E protein mols A, B and C on virus surface are colored in blue, red and green, respectively.

The fitted E protein suggested that upon binding of Fab 10.15 to B molecule, this E protein adopted a different conformation from that in unexpanded mature virus structure (Fig. 3-17a). In general, all E proteins had moved to a higher radius compared to the unexpanded structure. However, the E protein arrangement of the DENV2 PVP94/07 – Fab 10.15 structure was more similar to the compact unexpanded NGC structure than the expanded structure (Fig. 3-17b).

In summary, HMAb 10.15 was able to bind to B molecule, but not A and C molecules of PVP94/07. Binding of Fab 10.15 to B molecule led to the dissociation of the B-B' dimer and the loosening of the E protein shell.

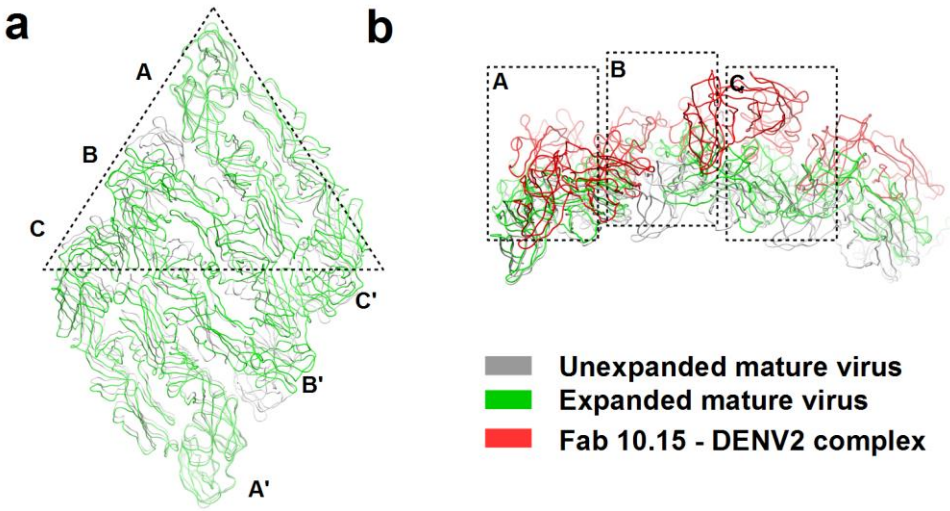

Figure 3-17 Comparison of PVP94/07 – Fab 10.15 structure with known DENV2 mature virus structures. (a) Comparison of the raft of

the fitted structure with the unexpanded mature virus structure at 28^{o}C. A, B and C molecules and A', B' and C' molecules are labeled. The triangle indicates one asymmetric unit. (b) Side view of the A, B and C molecules in different structures with the E-DIII side facing out. Different structures are colored as the color key. All molecules are shown with Cα chains.

3.9 Neutralization mechanism by HMAb 10.15

HMAb 10.15 was more potent against DENV2 strain NGC than PVP94/07 (Fig. 3-8, Table 3-4). Analysis of both cryo-EM samples revealed varied extents of structural heterogeneity of particles in the samples and DENV2 strain NGC – Fab 10.15 complex sample showed higher heterogeneity. The higher neutralization activity of HMAb 10.15 towards NGC strain than to PVP94/07 (Table 3-4) correlated with the bigger population of particles in the NGC strain that expand in structure which lead to an increased in the accessibility of epitope. The reconstructed structures for both complexes probably only represented the particles which did not expand at higher temperatures.

3.9.1 IgG 10.15 is unable to bind bivalently to PVP94/07

Distances between the CH1 domain C-termini of Fab 10.15 were measured for each pair of Fab molecules bound on the virus surface. A maximum distance between two Fab arms within the same IgG molecule is unlikely to be over 87 Å according to the currently available full-length IgG structure (PDB code 1IGT). The shortest distance of the

separation for Fab 10.15 on the cryo-EM structure was 93 Å, indicating that bivalent binding of 10.15 IgG to the same particle is unlikely to occur (Fig. 3-18a). There were about 60% of particles from the NGC – Fab 10.15 sample, which were broken or are too flexible for single particle reconstruction. It is possible that these particles may have higher Fab occupancies and thus higher number of available epitopes. Since there is a lack of structural information on these virus populations, bivalent binding of IgGs on those particles could not be analyzed.

3.9.2 IgG 10.15 is unable to aggregate PVP94/07

Since 10.15 IgG has higher neutralization activity than its Fab molecule, we investigated the ability of IgG 10.15 to aggregate PVP94/07. Dynamic light scattering (DLS) was used to measure the size of IgG – DENV2 complex. The hydrodynamic size of DENV2 (strain PVP94/07) was determined to be 71.20±2.51 nm in radius, similar to the previous finding (Watanabe et al., 2015). The size of full length IgG molecule was determined to be ~12 nm in radius.

The experiment was done using various molar ratios of IgG to individual E proteins on virions (i.e. each potential antibody binding site) ranging from 9:1 to 1:480. When another DENV2-specific neutralizing HMAb 2D22 (Fibriansah et al., 2015a) was used, the size of IgG - virus

complex increased dramatically and peaked at ~250 nm with a polydispersity index (PDI) of 0.3 at molar ratio of 3:1. There were aggregations formed at both 1:1 and 3:1 molar ratios (Fig. 3-18b). The relatively low PDI indicated formation of stable aggregates with similar sizes. At even higher IgG to E molar ratio of 9:1, the size of the immune complex decreased, suggesting that at this ratio, the excess antibodies did not cross-link virions, therefore no aggregates were formed.

In contrast, when the virus was mixed with the antibody 10.15, the size of IgG 10.15 – PVP94/07 complex only mildly increased (Fig. 3-18c). The size increase of this immune complex was modest throughout the entire range of molar ratios tested. The maximum change of the size was close to 30 nm, which corresponded to the size of IgG molecules coated on the surface of the virion. This result indicated that IgG 10.15 was unable aggregate virus particles.

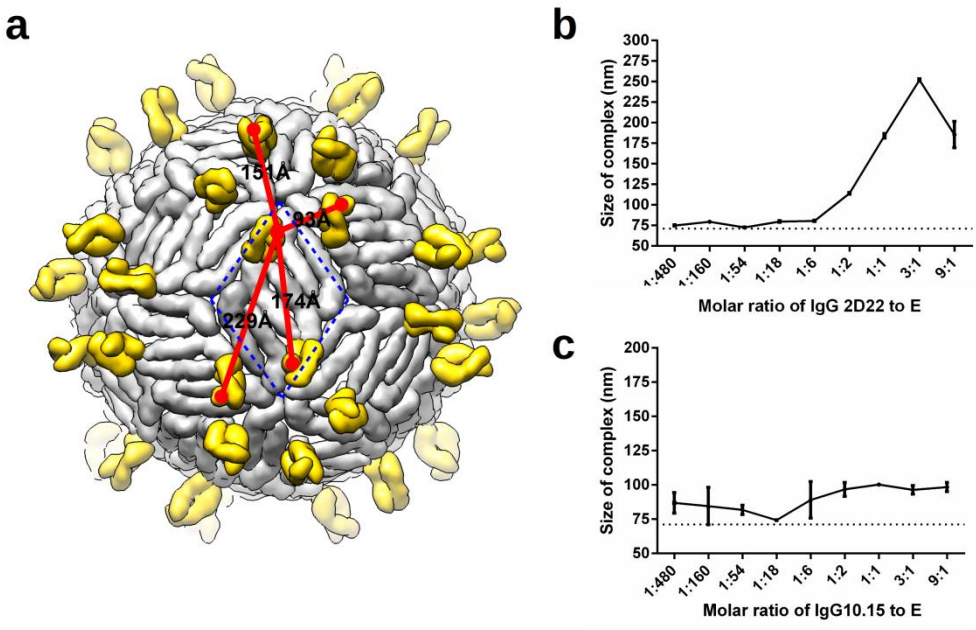

Figure 3-18 IgG 10.15 is unable to bind bivalently to PVP94/07.
(a)The possibility of bivalent binding of both Fab arms of IgG 10.15 to one PVP94/07 particle was evaluated based on the cryo-EM structure. Distances between two adjacent Fab molecules are labeled. They are all larger than the maximum distance between two Fab of an IgG molecule (approximately 87 Å, calculated from the available full-length IgG structure (PDB code 1IGT)). Size measurement of PVP94/07 complexed with IgG of (b) HMAb 10.15 and (c) 2D22 at a series of antibody-virus ratios. The size of one virus particle alone is highlighted by dashed lines.

Chapter IV. DENV2-specific Neutralizing HMAb 3F9

4.1 HMAb 3F9 could bind to recombinant DENV2 E protein but not E-DIII

HMAb 3F9 is a DENV2-specific neutralizing HMAb isolated from memory B cell of a patient recovered from a primary dengue infection (Smith et al., 2014). Preliminary data had shown that this antibody can neutralize DENV2 very efficiently in flow cytometry-based neutralization assays, with a $PRNT_{50}$ value of 30 and 3 ng/ml by using U937 cell expressing DC-SIGN and Vero-81 cell, respectively. Moreover, this antibody did not enhance viral infection at a concentration of 1.0 μg/ml in a flow cytometry-based ADE assay.

As shown in Fig. 4-1, HMAb 3F9 recognized recombinant DENV2 E protein, but did not bind to E-DIII in an indirect ELISA assay. As controls, an anti-DIII murine MAb 1A1D-2 bound to both recombinant E protein and E-DIII, whereas an anti-prM murine MAb 2H2 did not recognize either protein.

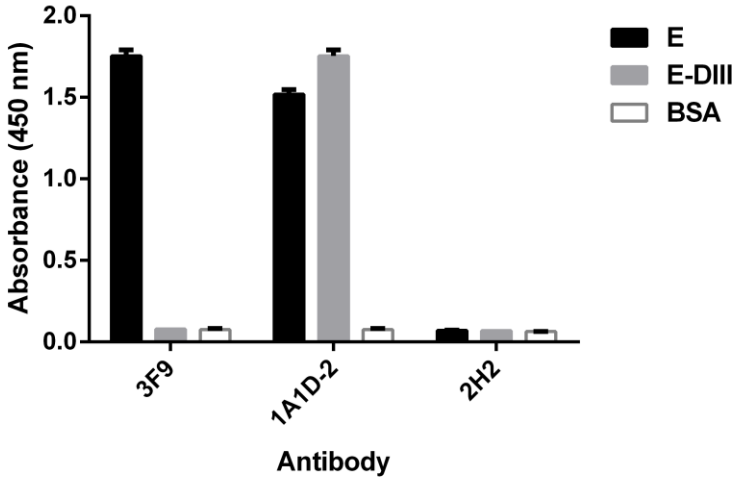

Figure 4-1 HMAb 3F9 only binds to recombinant E protein but not E-DIII. Binding of mouse monoclonal Ab 1A1D-2 and 2H2 and, HMAb 3F9 to recombinant DENV2 E and E-DIII. BSA was employed as a control antigen in this indirect ELISA.

4.2 IgG 3F9 potently neutralize both DENV2 strains NGC and PVP94/07

There was a significant difference ($P < 0.001$) in the $PRNT_{50}$ value for IgG 3F9 against DENV2 strain NGC (2.5 ± 0.2 ng/ml) and strain PVP94/07 (12.2 ± 1.7 ng/ml) (Fig. 4-2 left, Table 4-1). Comparable amounts of Fab were required to neutralize both virus strains ($PRNT_{50}$(NGC), 3.4 ± 2.5 ng/ml; $PRNT_{50}$(PVP94.07), 31.7 ± 14.7 ng/ml) (Fig. 4-2 right, Table 4-1).

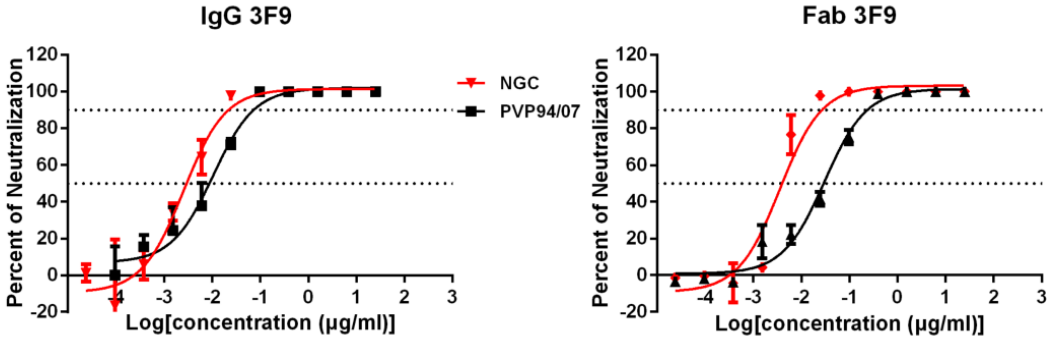

Figure 4-2 Neutralization of DENV2 strains NGC and PVP94/07 by 3F9 IgG and Fab in BHK-21 cell. Neutralizations of 50% and 90% of the infectivity were highlighted by dashed lines. All experiments were repeated at least three times with duplicates and one of the neutralization curves is shown here.

Table 4-1 Summary of $PRNT_{50}$ values for HMAb 3F9.

$PRNT_{50}$ (ng/ml) **HMAb 3F9**	**NGC**	**PVP94/07**	**(PVP94/07 : NGC)**
Fab	3.4 ± 2.5	31.7 ± 14.7	9.3
IgG	2.5 ± 0.2	12.2 ± 1.7	4.9
(Fab : IgG)	1.4	2.6	

4.3 HMAb 3F9 binds to DENV2 PVP94/07 at 4°C

DENV2 strain PVP94/07 has been previously shown to remain smooth and unexpanded at temperatures up to 39°C (Fig. 3-10). In this study, Fab 3F9 was found to bind to PVP94/07 at 4°C (Fig. 4-3), indicating that 3F9 might recognize a fully exposed epitope on the virus

surface therefore E protein motion was not required for its binding. i

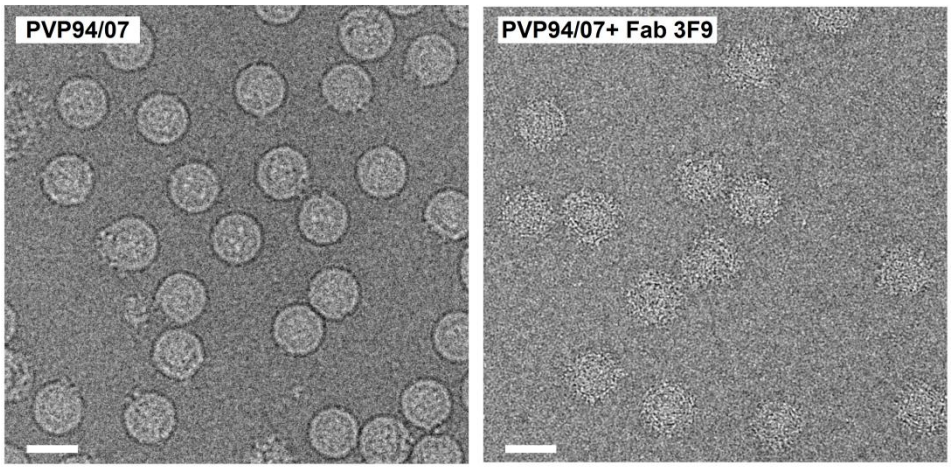

Figure 4-3 HMAb 3F9 can bind to PVP94/07 at 4^{o}C. Micrographs showing a control with DENV2 strain PVP94/07 grown at 28^{o}C followed by incubation at 4^{o}C (left) and DENV2 PVP94/07 complexed with Fab 3F9 at 4^{o}C (right). The complex appeared to be round but spiky. White bars indicate a length of 50 nm.

4.4 Cryo-EM structure of PVP94/07 – Fab 3F9 complex

The cryo-EM density map of the PVP94/07 – Fab 3F9 complex was determined to be 22-Å in resolution (Fig. 4-4e). The density corresponding to the Fab molecule was clearly resolved as a two-domain structure, representing the constant and variable regions of one Fab molecule) (Fig. 4-4a). The separation of the viral lipid bilayer was also clearly resolved (Fig. 4-4c). The E protein layer remained nearly at the same radius, ~240 Å, as the DENV2 mature virus at 28^{o}C (Fig. 4-4c). A total of 120 copies of complete Fab 3F9 molecules were

visible in this map (Fig. 4-4a). In addition, there was a bump above every 3-fold vertex, reaching a higher radius than the virus surface, which corresponded to the size of the variable region of a Fab molecule. This could be one Fab molecule binding to one of the three individual E proteins proximal to the 3-fold vertex (Fig. 4-4a). Some densities were visible at a higher radius above these bumps but only at a lower contour level (Fig. 4-4b, d). These smeared densities might correspond to the constant region of the Fab molecule. The weakened densities might be due to icosahedral averaging approach during the 3D reconstruction since each of the Fab molecules was likely to have different orientations on the virus surface if they were actually bound to different C molecules.

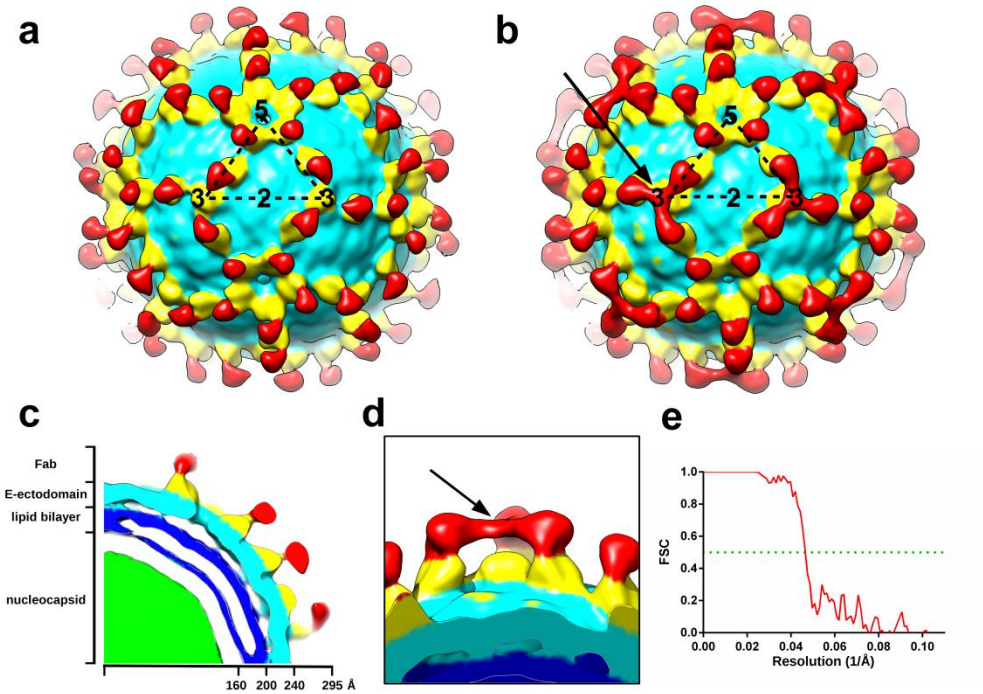

Figure 4-4 Cryo-EM density map of PVP94/07 – Fab 3F9 complex. Cryo-EM density map of PVP94/07 – Fab 3F9 complex at a contour level of (a) 2.5 and (b) 2. The virus surface is colored in cyan and the Fab 3F9 is colored in red (constant region) and yellow (variable region). The black triangle represents an icosahedral asymmetric unit and the numbers label the symmetric vertices. At (b), a slightly lower contour level showed the weaker density on top of the 3-fold vertex with the arrow pointing to it. (c) A quarter of the cross-section of the density map, showing radial density distribution. The map is colored radially in panels: green (up to 160 Å), blue (161- 200 Å), cyan (201-235 Å), yellow (235-260), red (above 261 Å). (d) Side view of the weak density on top of the 3-fold vertex with an arrow pointing to it. (e) FSC (gold-standard) versus resolution plot was shown with green line highlighted where FSC = 0.5.

Interpretation of the cryo-EM density map was carried out by fitting the DENV2 unexpanded mature virus structure (PDB code 3J27) and an atomic model for the Fab, considering that the overall shapes of the Fab molecules for HMAbs were usually conserved. The mature virus structure fitted nicely to the cryo-EM density map of PVP94/07 – Fab 3F9 complex, with the structure of E protein raft being preserved (Fig. 4-5a). In addition, the densities corresponding to the transmembrane domains of E and prM proteins matched with the unexpanded mature virus structure (Fig. 4-5c). These results together indicated that binding of Fab 3F9 did not induce significant structural changes of the virus surface. Fitting of the Fab molecule was guided by the clear separation in densities typical for its two-domain structure (Fig. 4-5d).

In this fitting, 3F9 was shown to bind to A and B molecules (Fig. 4-5b). The Fab 3F9 bound to C molecule was omitted from the fitting since its density was much poorer. Furthermore, the smeared and weaker density made the determination of its orientation ambiguous. However, the handedness of the Fab molecules (i.e. the differentiation of its heavy and light chains) relative to the E protein could not be confidently determined at this resolution. The density of the variable region was stronger than that of the constant region in our density map, indicating a greater flexibility of the constant region, similar to the previous findings (Kaufmann et al., 2010, Fibriansah et al., 2014).

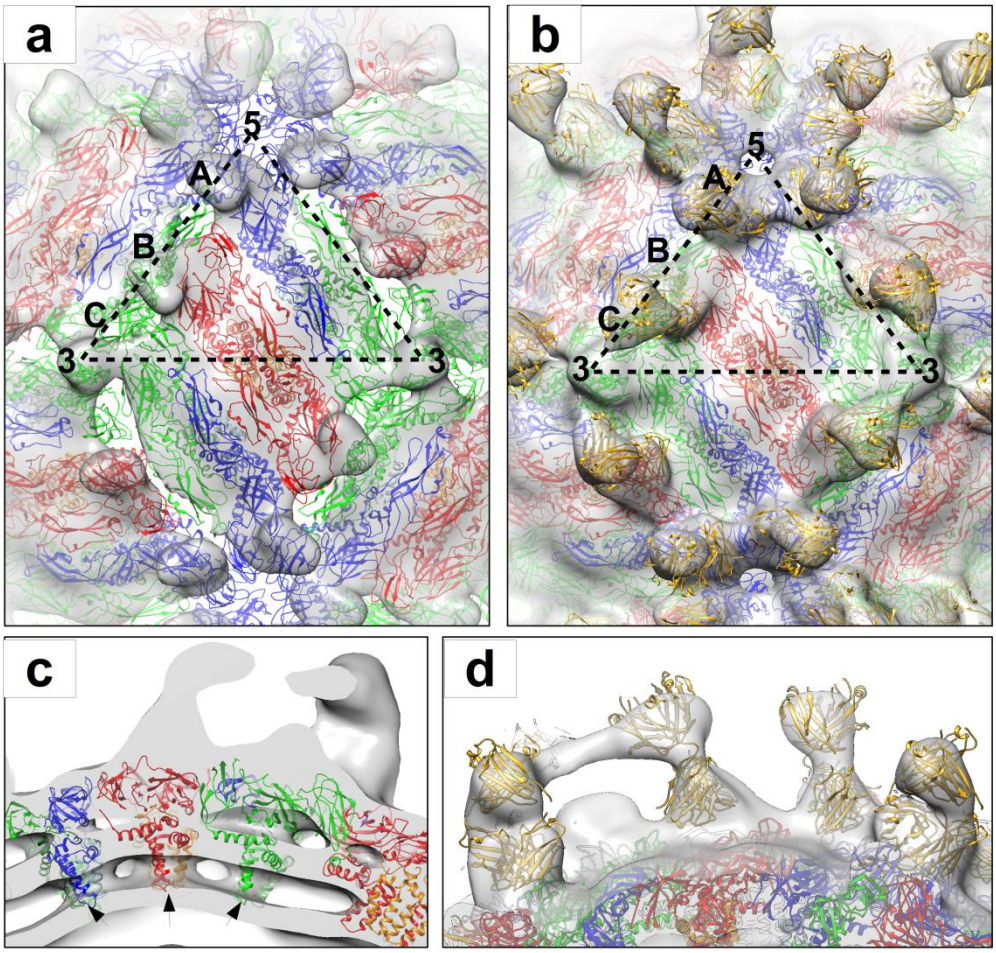

Figure 4-5 Fitting of the PVP94/07 – Fab 3F9 into the cryo-EM map. Views with the cryo-EM density map fitted with (a) the E protein raft of mature virus structure at 28^{o}C, (b, d) a model for Fab 3F9 binding on the virus surface, and (c) transmembrane domains of both E and prM proteins. The map was rendered at a contour level of 3.5 for (a) and 2 for (b, c, d), respectively. E protein A, B and C molecules within one asymmetric unit are colored in blue, red and green, respectively. The prM proteins paired with A, B and C molecules are colored in light blue, orange and dark green, respectively. The Fab molecules are colored in yellow. The black triangle labels one asymmetric unit and the arrowheads in (c) highlight the positions of the transmembrane domains.

4.5 Epitope recognized by 3F9

Fab 3F9 was found to bind to E-DI based on the fitting of atomic

models into the cryo-EM map (Fig. 4-6b, c). Footprint of the Fab was restrained to a single E protein, which was consistent with the observation that 3F9 could bind to recombinant E protein (Fig. 4-1). HMAb 3F9 largely bound to DI and possibly the linker region between E-DI and E-DIII (Fig. 4-6b, c). Since these regions in three C molecules proximal to one 3-fold vertex were close to each other, it would not be possible for the Fab 3F9 to bind to more than one of the three C molecules at the same time (Fig. 4-6d).

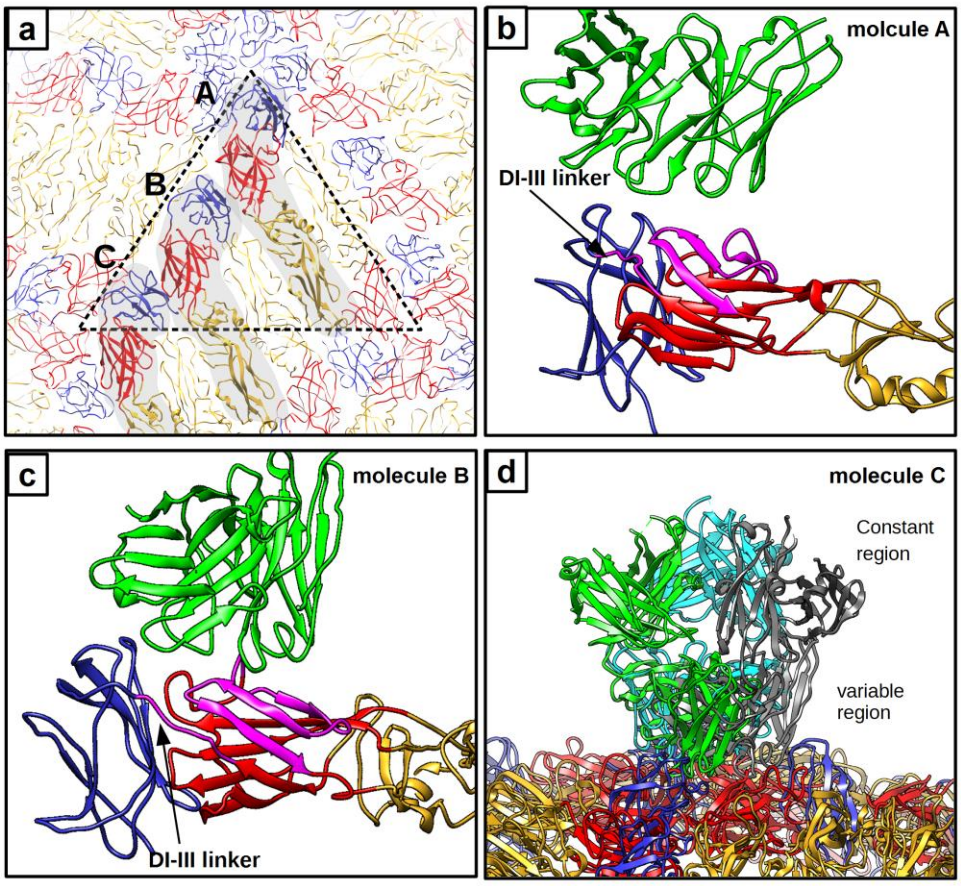

Figure 4-6 The epitope recognized by 3F9.

(a) One asymmetric unit on mature virus surface was shown with A, B and C molecules shaded. E-DI, II and III are colored as yellow, red and blue, respectively. The estimated binding areas in E-DI of (b) mol A and (c) mol B were colored as magenta with the DI-III linker labeled. The Fab molecule is colored green. (d) Clashes of three Fab molecules superimposed to three C molecules around one 3-fold vertex. The three Fab molecules are colored as green, cyan and grey, respectively with the constant and variable regions of the Fab labelled.

Chapter V. Summary, General Discussion and Future perspective

In this study, we have identified the epitope for two DENV2 specific HMAb 10.15 and 3F9 by a combination of structural and biochemical methods. Unlike previously defined epitopes for neutralizing HMAbs, both antibodies recognized epitopes which were restricted to the E protein monomer and not quaternary structure-dependent (Fig. 3-4, Fig. 4-6). While HMAb 3F9 bound to an exposed epitope located in E-DI, HMAb 10.15 recognized a partially hidden epitope on E-DIII. The study of interaction between HMAb 10.15 and DENV2 revealed that structural variation of DENV can affect the neutralizing potency of Abs. This study also showed that Fab fragment of 3F9 had a comparable potency as its IgG form, whereas Fab 10.15 was much weaker compared with its full-length IgG in neutralization. Further experiments revealed that the higher potency of IgG 10.15 was not due to its ability to aggregate virus particles. The crystal and cryo-EM structures reported in this thesis provided a structural basis for a comprehensive understanding of neutralization of DENV by HMAbs.

5.1 Neutralizing epitope

Significant number of human serotype-specific neutralizing antibodies target quaternary structure-dependent epitopes that are only present on the intact virion (Fibriansah et al., 2015b, Fibriansah et al., 2014, Teoh et al., 2012, Kaufmann et al., 2010, de Alwis et al., 2012). This type of antibodies cannot recognize recombinant E protein. Also, the binding of these antibodies depends on either the quaternary arrangement of E proteins or the specific conformation of E protein on the virus surface. In this study, we found two neutralizing HMAbs which could recognize not only intact virus but also recombinant E protein. More recently, another class of neutralizing HMAbs, which binds to the E-dimer-dependent epitopes (EDE), has been isolated and characterized (Rouvinski et al., 2015, Dejnirattisai et al., 2015, Fibriansah et al., 2015a). Epitopes for this class of antibodies typically span the E-dimer with contact residues in all three domains of the E proteins. Unlike the EDE antibodies, epitopes recognized by 3F9 and 10.15 are restrained to one E protein monomer.

HMAb 3F9 would be the third antibody that recognizes E-DI with an antigen-antibody structure available so far. The other two antibodies, 5H2 and 1F4, are isolated from chimpanzee and human, respectively (Fibriansah et al., 2014, Cockburn et al., 2012b). HMAb 3F9 has a

similar target area in E-DI as the DENV4-specific chimpanzee MAb 5H2. This is different from the DENV1-specific HMAb 1F4, which binds more to the side of the E-DI/II hinge region (Fig. 5-1). This subtle difference of their epitopes is also reflected by their binding abilities to the recombinant E protein. While 3F9 and 5H2 are able to bind to recombinant E protein, 1F4 cannot recognize recombinant E protein since it is sensitive to the DI/II hinge angle which is different between recombinant E protein and E protein on an intact virion. Because determination of the precise epitope for 3F9 could not be accomplished by the cryo-EM structure at this relatively low resolution (~22-Å), we cannot precisely compare its epitope with the epitope of 5H2. Our cryo-EM structure of PVP94/07 – Fab 3F9 complex was similar to the DENV – Fab 5H2 complex structure estimated by docking experiment. However, our cryo-EM structure also revealed unexpected occupancy of 3F9 on C molecule proximal to the three-fold vertex of the virion (Fig. 4-4). Epitope of 5H2 on molecule C was predicted to be slightly buried by neighboring E proteins. Since Fab 3F9 was observed to be able to bind to molecule C, the epitope of 3F9 might be slightly different from 5H2. There was also a possibility that even at 4^{o}C, Fab 3F9 could pull up the molecule C to expose the otherwise slightly buried epitope.

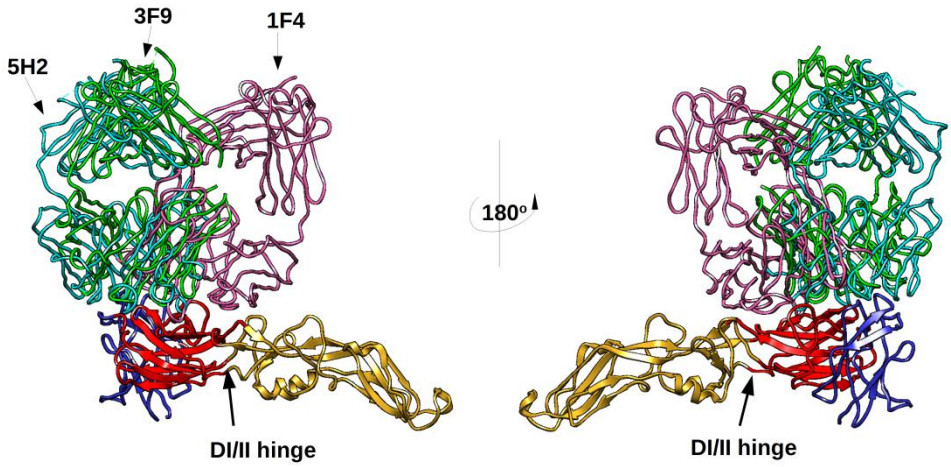

Figure 5-1 Comparison of E-DI binding antibodies.
Side views of the E protein- Fab complexes of antibody 3F9, 5H2 and 1F4. E protein was shown as ribbon with domain I, II and III colored in red, yellow and blue, respectively. Fab of 5H2, 3F9 and 1F4 are shown as cyan, green and pink ribbons, respectively. The DI/II hinge, which is critical for 1F4 binding, is highlighted.

Another antibody, HMAb 10.15, was found to bind to E-DIII (Fig. 3-1). Anti-DIII antibodies make up one category of the most highly neutralizing antibodies against flavivirus. Two well-characterized E-DIII epitopes are lateral ridge and A-strand, with crystal structures revealing the details of binding interfaces and also cryo-EM structures showing the overall arrangement of antibodies on the virus surface. Epitope of lateral ridge antibodies, for example, E16, is located on the upper face of the E-DIII and is mainly comprised of residues in four discontinuous loops (Nybakken et al., 2005). This epitope is fully exposed on all three individual E proteins within one asymmetric unit on the virus surface,

but at saturating concentration, only 120 copies of Fab molecules can bind to one virion with no Fab bound to the E-DIII close to the icosahedral 5-fold vertex (Kaufmann, 2006). A-strand epitope is mainly centered on A-strand and partially hidden from virus surface. One of the A-strand antibodies, 1A1D-2, can bind to the virus at 37^{o}C but not 28^{o}C because ~18% of its epitope is buried by neighboring E proteins (Lok et al., 2008). Binding of its Fab to the virion results in a dramatic conformational change of the virus surface with an occupancy of 120 Fab molecules per virion. The epitope of HMAb 10.15 is close to A-strand, with another major part of it located in G-strand and FG loop (Fig. 5-2a). This subtle difference of the epitope caused HMAb 10.15 to adopt a different orientation from the A-strand antibodies when bound to the E protein (Fig. 5-2b). This could potentially explain the difference of occupancies of these two antibodies on the virus surface and to which particular E proteins these two antibodies bind.

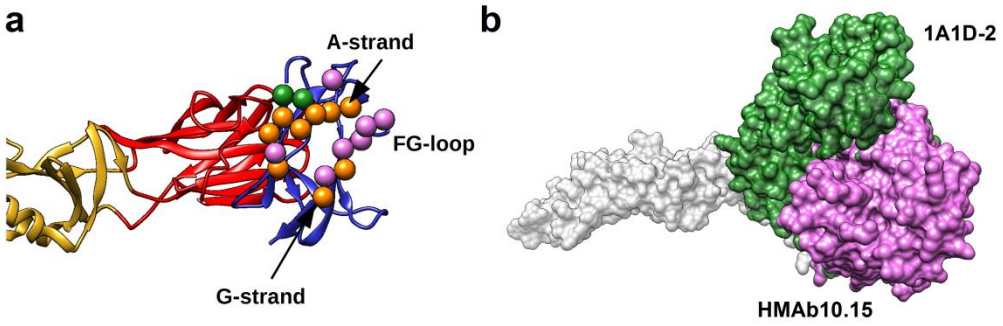

Figure 5-2 Epitope comparison between HMAb 10.15 and A-strand

antibody 1A1D-2. (a) E protein is shown as ribbon with domain I, II and III colored in blue, red and yellow, respectively. Residues only in the epitope of 1A1D-2, only in the epitope of HMAb 10.15, and shared by both epitopes are shown as green, pink and orange spheres, respectively. (b) 10.15 (pink) and 1A1D-2 (green) bind to E protein (grey) at different orientations. All proteins are shown as surfaces. Crystal structure of Fab 1A1D-2 – E-DIII (PDB code 2R69) and Fab 10.15 – E-DIII are superimposed to the E protein structure (PDB code 1OAN).

5.2 Structural basis for antibody neutralization

Anti-flavivirus antibodies have been shown to neutralize the virus by mechanisms such as blockage of virion attachment to target cells, destabilization of the virion, and inhibition of fusion between viral and host cell lipid membranes. Neutralization mechanism is determined by the properties of both antibody and its epitope on the virion.

The epitope of HMAb 10.15 in E-DIII has been suggested to have important functions in virus infection. Residues located in A-strand have been suggested to be involved in attachment and receptor recognition since mutations of some of these residues can greatly attenuate the virus (Holzmann et al., 1990, Mandl et al., 2000, Lee et al., 2013). Residues 383-384 (located in FG loop) that is only present in mosquito-borne but not tick-borne flaviviruses have also been proven to be critical for infection (Erb et al., 2010). Therefore, HMAb 10.15 might block two important sites for virus-receptor recognition at the same time.

Moreover, binding of HMAb 10.15 to the virus forced the B-B' dimer to fall apart, resulting in changes of the relative position between A, B and C molecules. This might affect the binding of the virus to its attachment factors or receptors. For example, binding of DENV to DC-SIGN, one of the receptors in dendritic cells, requires the glycans subtly arrayed on the neighboring E proteins, which depends on the quaternary structure of the virion (Pokidysheva et al., 2006).

Mechanisms of fusion inhibition have been postulated based on the crystal structures of E protein homotrimers at low pH with and without the presence of the stem region (Modis et al., 2004, Bressanelli et al., 2004, Nayak et al., 2009, Klein et al., 2013) and some *in-vitro* fusion assays with synthetic liposome (Stiasny et al., 2007). The proposed mechanisms include interference with the relocation of DIII for hairpin formation, trimer formation, cooperative interactions of E homotrimers (suggested for enlargement of the fusion pore) and direct blocking of the fusion loop (Stiasny et al., 2007) (Fig 5-3a). E-DIII relocates in the fusogenic conformation by a substantial swing-around movement of the DI-III linker (Fig. 5-3b). Since the 3F9 contacted residues located in the DI-III linker region, it may be able to stabilize the DI-III linker to prevent it from adopting the post-fusion conformation. Moreover, superposition of

DI in the Fab 3F9 – E protein from the cryo-EM structure to the post-fusion trimeric E protein structure (PDB code 1OK8) showed significant clashes of the Fab molecule with the DIII from one of the adjacent E protein (Fig. 5-3c). This suggested that once Fab 3F9 was bound to the virus, the E protein would not be able to form the fusogenic post-fusion trimeric spike. This hypothesis is supported by the fact that anti-DI antibody 5H2, which recognizes a similar epitope, has been shown to inhibit virus fusion with lipid membrane at low pH (Cockburn et al., 2012b). In summary, binding of HMAb 3F9 would prevent the formation of the fusogenic trimer, therefore neutralizing the virus by inhibiting its fusion process. In contrast, for HMAb 10.15, superimposition of the Fab 10.15 – E-DIII co-crystal structure with E-DIII to the post-fusion E protein trimeric structure did not show any clashes between the Fab molecule and adjacent E proteins within the same trimer (Fig. 5-3d). However, the possibility that binding of HMAb 10.15 might interfere with fusion in other steps, such as clashes with adjacent trimeric spikes during the process of enlargement of the fusion pore, could not be ruled out completely.

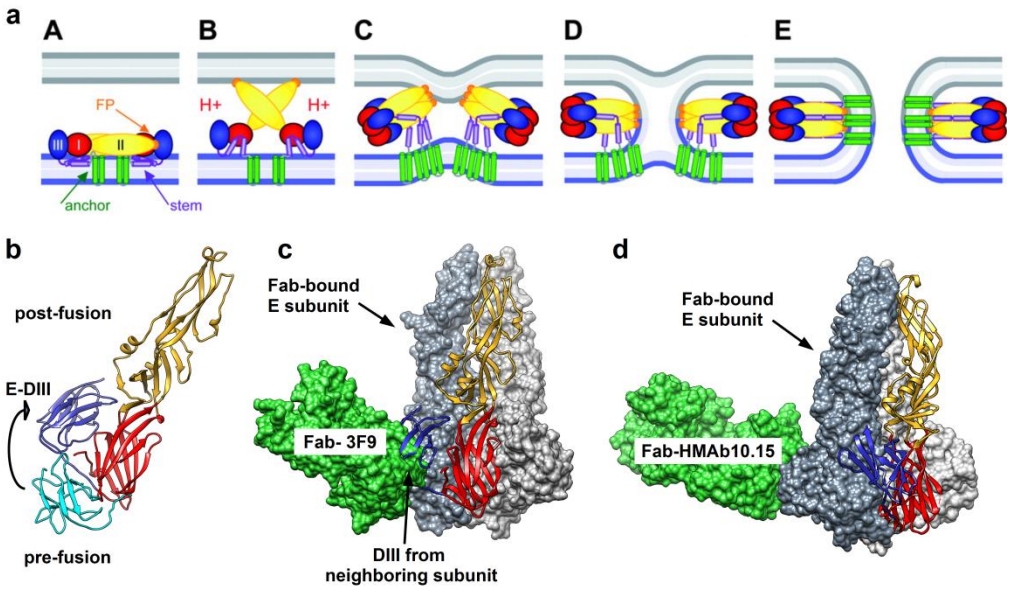

Figure 5-3 Interference of the fusion process by 3F9 and 10.15

(a) Schematic model of the flavivirus fusion process (A to E). E-DI, red; E-DII, yellow; E-DIII, blue; fusion loop, orange; stem, purple; transmembrane anchor, green; viral membrane, blue; target membrane, grey. (A) E dimer on the mature virus surface. (B) Low pH-induced dissociation of the dimer and insertion of the fusion loop into the target membrane. (C) Relocation of DIII leading to hairpin formation, trimerization, and zippering of the stem along the trimer. (D) Hemifusion intermediate. (E) Fusion pore formation. Figure extracted from Stiasny, K., et al. J Virol (2007).

(b)The DI-DIII linker flexes and the DIII was relocated in the post-fusion trimeric structure of E protein (PDB code 1OK8). DI, II and III of E protein on the mature virus surface (PDB code 3J27) are colored in red, yellow and cyan, respectively. E-DIII in the post-fusion crystal structure is colored in blue. (c) Superposition of DI in the Fab 3F9 – E protein cryo-EM structure to the post-fusion trimeric E protein structure showed significant clashes between the Fab and DIII of a neighboring E protein. Two E proteins are shown as surfaces (colored in light and dark gray) and another is shown as ribbons. Fab 3F9 is drawn as a green surface. (d) Superimposition of Fab 10.15 - E-DIII crystal structure onto the post-fusion trimeric spike. The Fab molecule points away from the trimeric E protein. Three individual E proteins in the trimer are shown as (c) and Fab 10.15 is drawn as a green surface.

5.3 Structural dynamics, epitope accessibility, occupancy and antibody potency

DENV2 undergoes structural changes at temperatures above 33^{o}C (Zhang et al., 2013). One class of expanded structures, shows an expansion of the E protein layer, lifting up of DIII of molecule B and formation of holes at the 3-fold vertices of the virion (Fig. 3-9b). Previous studies have suggested a role of structural dynamics of DENV in antibody-mediated neutralization (Austin et al., 2012, Zhou et al., 2013).

The impact of the structural dynamics on antibody recognition has been discussed for some antibodies recognizing hidden epitopes (Fibriansah et al., 2013). In this study, the epitope of HMAb 10.15 was mapped to one of the expanded structures, showing that the epitope on B molecule have become fully exposed (Fig. 3-9b). Surprisingly, although DENV2 PVP94/07 does not seem to change its structure at 37^{o}C, Fab 10.15 could still bind to the virus particle (Fig. 3-11). Binding of Fab 10.15 to NGC strain is easier to understand since this virus is expanded at a higher temperature, leading to exposure of the otherwise partially hidden epitope. On the other hand, the explanation of how Fab 10.15 could bind to PVP94/07 is not as straightforward as its structure is

less dynamic and insensitive to temperature change. There are two hypotheses to explain the binding of HMAb 10.15 to these unexpanded virus particles.

The first hypothesis is that these unexpanded virus particles do expand, but their expansions are reversible, so the epitopes are only exposed transiently. In our cryo-EM experiment, incubations of the viruses at different temperatures were typically followed by a 2-hrs 4^{o}C-cooling step before the sample was plunged-frozen to liquid nitrogen temperature. This step was included to equilibrate the sample to lower temperatures to facilitate formation of vitrified ice which can preserve the native structure of the sample. During this cooling step, it is possible that the virus particles alone can recover to the unexpanded state.

There is also another possible explanation for the binding of HMAb 10.15 to the unexpanded virus particles of DENV2 strain PVP94/07. The second hypothesis is that the interaction between Fab 10.15 and its epitope is much stronger than that between the E proteins. As a result, upon binding, Fab 10.15 was able to pull out and rotate the E protein B molecule on the virus surface. This exposed the previously partially hidden epitope.

DENV2 strains NGC and PVP94/07 have different susceptibilities to HMAb 10.15 neutralization. The neutralization of the structurally more stable strain, PVP94/07, requires at least 10 times higher antibody concentration, regardless of IgG or Fab used (Table 3-4). This difference in potencies was proved to be only due to the structural difference between these two viruses instead of the variation in their binding affinities.

All previously-characterized neutralizing antibodies against flavivirus have an occupancy of at least 120 Fab molecules per virion (Kaufmann, 2006, Kaufmann et al., 2010, Lok et al., 2008, Teoh et al., 2012, Fibriansah et al., 2014, Fibriansah et al., 2015b, Fibriansah et al., 2015a, Dejnirattisai et al., 2015). One exception is a DENV3-specific HMAb, 5J7, which binds to the virion at an occupancy of 60 Fab molecules per virion at saturation levels but can grabs three E proteins at the same time by one single Fab molecule (Fibriansah et al., 2015b). As a result, this antibody is able to lock the virus and prevent it from undergoing conformational changes required for viral fusion process. In our study, the cryo-EM structure of PVP94/07 – Fab 10.15 complex revealed an occupancy of 60 Fab molecules on one virus particle at saturation (Fig. 3-13a, Fig. 3-16d). A subset of the NGC – Fab 10.15

sample also showed the same occupancy (Fig. 3-15a). It should be noted that not all particles in strain NGC undergo conformational changes at 37^{o}C. In previous study, there are still about 20% of the particles which are not expanded (Fibriansah et al., 2013). However, for the expanded virus particles of DENV2 strain NGC, as the E protein layer on the virus surface is loosened, the antibody has a higher chance of binding to more E proteins on the virus surface. Binding of the antibody on these particles might be able to disrupt the E protein structure since the surface protein interaction in these particles is weaker. This might contribute to the formation of the broken particles observed in the experiment (Fig. 3-14). Moreover, there is another class of virus particles in which their E proteins have probably flexed up (Fibriansah et al., 2013). This class might have more binding sites available for HMAb 10.15. Thus, HMAb 10.15 might be able to bind to strain NGC at a higher occupancy, but the structures of these particles were probably too heterogeneous to be resolved.

5.4 IgG of HMAb 10.15 is more potent than its Fab

To our knowledge, the neutralizing ability of IgG against virus is typically better than its Fab and the difference between their potencies

can vary widely. For example, HMAbs 1F4 and 5J7, neutralize the virus 4-fold and 8-fold more potently in their full-length IgG forms than their Fab fragments (Fibriansah et al., 2014, Fibriansah et al., 2015b). However, for antibody E106, the potency of its Fab is 18150-fold lower than its IgG (Edeling et al., 2014). The bivalent binding ability of IgG E106 was demonstrated to be important for its neutralizing ability, as the affinity of its Fab is only at micromolar range. The epitope of E106 in molecules A, B and C within one asymmetric unit are all exposed on the virus surface and close to each other, allowing for bivalent binding of its IgG form, which compensates for the relatively low affinity of its Fab.

In this study, there was an approximately 100-fold difference in the potencies of HMAb 10.15 between its IgG and Fab (Table 3-4). In comparison, the Fab fragment of 3F9 could neutralize the virus as well as its full-length IgG. Fab 3F9 was apparently much more potent compared to Fab 10.15 against the same virus strain. For example, $PRNT_{50}$ of Fab 3F9 against NGC was 3.4 ± 2.5 ng/ml, whereas for Fab 10.15, $PRNT_{50}$ value was 293.6 ± 67.5 ng/ml (Table 3-4). The fact that Fab 3F9 neutralized better compared to Fab 10.15 could be possibly due to its higher occupancy on the virus surface, as shown by the cryo-EM structures, and the step in which it neutralized the virus.

The higher potency of IgG 10.15 compared with its Fab fragment could be due to several reasons: (1) bivalent binding to single virion and cross-link the virus surface; (2) aggregation of virus particles; (3) increase of the steric hindrance to virus – host interactions (such as receptor binding or virus fusion) due to its larger size; (4) bivalency of the IgG which can increase the chance for a second binding to an otherwise hidden epitope site. It should be noted that cryo-EM structures of antibody – virus complexes which have been solved so far were mostly using Fab or scFv (single chain variable fragment) instead of full-length IgG. This might not reveal the real binding situation which happens in the virus –IgG complex since IgG has two Fab arms and is also larger in size.

Whether the IgG can bind bivalently to the same virion depends on several factors: the span of its two Fab arms, the distance between its epitopes on the virus and the dynamics of the virus structure. Our analysis showed that IgG 10.15 is unlikely to bind bivalently to the same virion at least for particles of strain PVP94/07 (Fig. 3-18a) whereas for HMAb 3F9, IgG bivalent binding is possible for a few neighboring binding sites on individual E proteins (Fig. 5-4), which might cross-link the virus surface to restrain structural changes required for fusion

process.

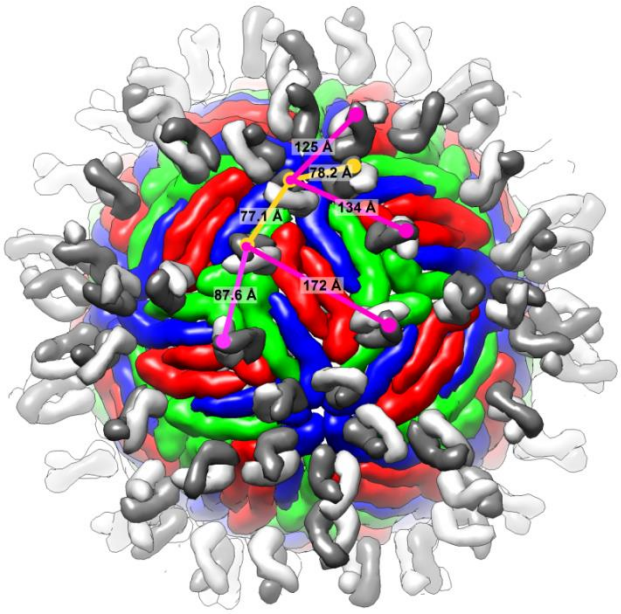

Figure 5-4 The possibility of bivalent binding of IgG 3F9 to DENV2. Orange lines indicate epitope that are close enough there likely to allow both Fab arms to be engaged simultaneously. Magenta lines indicate epitopes that are further apart therefore unlikely to allow bivalent binding. Distances of both orange and magenta lines are indicated. The maximum distance between two Fab of an IgG molecule (approximately 87 Å) is calculated from the available IgG structure (PDB code 1IGT). Measurement was based on the Fab 3F9- PVP94/07 complex cryo-EM structure. The handedness of the Fab was arbitrarily chosen and distances between two CH1 termini were measured.

Aggregation is another important potential neutralization mechanism, which reduces the number of virions able to initiate an infection. Aggregates form when many virus particles are stably cross-linked by multivalent antibodies. IgG can aggregate viruses by binding its two arms to different particles but it is only possible for some

antibodies. Measuring the size profile of PVP94/07 in complex with IgG 10.15 showed that IgG 10.15 is unable to aggregate PVP94/07, in contrast with another potent DENV2 specific HMAb 2D22 (Fig. 3-18b, c). Since IgG 10.15 does not bind bivalently to the same virion according to the current cryo-EM structure or aggregate the viruses, the increase of its potency comparing to Fab can be purely due to its larger size. When one arm of the IgG binds to the virus, the rest of the antibody can cover a larger area of the virus surface, leading to a greater steric obstruction, which can prevent the virus from binding to its attachment factor or receptor. This could be particularly important for antibodies like HMAb 10.15, which could not bind to virus at high occupancy. Another potential explanation is that due to the bivalency of the IgG molecule, binding of one Fab arm to the virus can increase the chances of binding of the other arm to a previously-hidden epitope site, therefore resulting in bivalent binding, which is not captured in our current cryo-EM structure of virus – Fab 10.15 complex.

5.5 Future perspectives

Some studies have observed strain/genotype -wide differences of antibody potencies (Brien et al., 2010, Shrestha et al., 2010, Wahala et

al., 2010). We have found in this study that an antibody which targets a partially hidden epitope was less neutralizing against a structurally more stable virus strain PVP94/07 compared with the more dynamic strain NGC. This finding provides direct evidence that structural dynamics of DENV affects antibody potency. Considering that the neutralization assay for evaluation of antibody neutralizing ability often only includes very limited virus strains with unclear structural backgrounds, this thesis highlights the structural variation of different DENV strains and emphasizes the importance of accounting for structural differences of virus strains in the future design of antibody function assay.

In this study, both HMAb 10.15 and 3F9 target epitopes on E-monomer and their bindings are not dependent on either the E protein dimeric structure or the quaternary arrangement of the whole virion. As DENV particles have been shown to be heterogeneous in structure: the unexpanded mature virus, the expanded mature virus, the partially mature virus and fully immature virus. Further studies need to be conducted to investigate whether the antibodies characterized so far can neutralize these structurally different DENV particles. The results will be constructive in answering the question of whether a single type of neutralizing antibodies would be sufficient for protection against

DENV infection. The two E-monomer targeting DENV2-specific neutralizing HMAbs in this study might be a good supplement to the arsenal of DENV antibody therapeutics.

Since the structural variation of different DENV strains can affect antibody potency, it would be interesting to investigate the extent of its impact not only with isolated monoclonal antibodies, but also with polyclonal antibodies or even human serum from DENV-infected patients. This could help answer the question of whether antibody response stimulated by virus strains with one particular structure can also potently neutralize structurally different strains and protect human from re-infection with these strains. These studies can potentially contribute to DENV vaccine or therapeutic development.

Bibliography

Afonine, P. V., R. W. Grosse-Kunstleve, N. Echols, J. J. Headd, N. W. Moriarty, M. Mustyakimov, T. C. Terwilliger, A. Urzhumtsev, P. H. Zwart and P. D. Adams (2012), "Towards automated crystallographic structure refinement with phenix. refine", *Acta Crystallographica Section D: Biological Crystallography,* Vol. 68, No. 4.

Akey, D. L., W. C. Brown, S. Dutta, J. Konwerski, J. Jose, T. J. Jurkiw, J. Delproposto, C. M. Ogata, G. Skiniotis and R. J. Kuhn (2014), "Flavivirus NS1 structures reveal surfaces for associations with membranes and the immune system", *Science,* Vol. 343, No. 6173.

Amberg, S. M., A. Nestorowicz, D. W. Mccourt and C. M. Rice (1994), "NS2B-3 proteinase-mediated processing in the yellow fever virus structural region: in vitro and in vivo studies", *Journal of virology,* Vol. 68, No. 6.

Anderson, R. (2003), "Manipulation of cell surface macromolecules by flaviviruses", *Advances in virus research,* Vol. 59.

Ashour, J., M. Laurent-Rolle, P.-Y. Shi and A. García-Sastre (2009), "NS5 of dengue virus mediates STAT2 binding and degradation", *Journal of virology,* Vol. 83, No. 11.

Aslanidis, C. and P. J. De Jong (1990), "Ligation-independent cloning of PCR products (LIC-PCR)", *Nucleic acids research,* Vol. 18, No. 20.

Austin, S. K., K. A. Dowd, B. Shrestha, C. A. Nelson, M. A. Edeling, S. Johnson, T. C. Pierson, M. S. Diamond and D. H. Fremont (2012), "Structural basis of differential neutralization of DENV-1 genotypes by an antibody that recognizes a cryptic epitope", *PLoS pathogens,* Vol. 8, No. 10.

Avirutnan, P., A. Fuchs, R. E. Hauhart, P. Somnuke, S. Youn, M. S. Diamond and J. P. Atkinson (2010), "Antagonism of the complement component C4 by flavivirus nonstructural protein NS1", *The Journal of experimental medicine,* Vol. 207, No. 4.

Baerga‐Ortiz, A., C. A. Hughes, J. G. Mandell and E. A. Komives (2002), "Epitope mapping of a monoclonal antibody against human thrombin by H/D‐exchange mass spectrometry reveals selection of a diverse sequence in a highly conserved protein", *Protein science,* Vol. 11, No. 6.

Bai, X.-C., G. Mcmullan and S. H. Scheres (2014), "How cryo-EM is revolutionizing structural biology", *analysis,* Vol. 968.

Baker, T., N. Olson and S. Fuller (1999), "Adding the third dimension to virus life cycles: three-dimensional reconstruction of icosahedral viruses from cryo-electron micrographs", *Microbiology and Molecular Biology Reviews,* Vol. 63, No. 4.

Balsitis, S. J., K. L. Williams, R. Lachica, D. Flores, J. L. Kyle, E. Mehlhop, S. Johnson, M. S. Diamond, P. R. Beatty and E. Harris (2010), "Lethal antibody enhancement of dengue disease in mice is prevented by Fc modification", *PLoS Pathog,* Vol. 6, No. 2.

Bartesaghi, A., A. Merk, S. Banerjee, D. Matthies, X. Wu, J. L. Milne and S. Subramaniam (2015), "2.2 Å resolution cryo-EM structure of β-galactosidase in complex with a cell-permeant inhibitor", *Science*.

Beckett, C. G., J. Tjaden, T. Burgess, J. R. Danko, C. Tamminga, M. Simmons, S.-J. Wu, P. Sun, T. Kochel and K. Raviprakash (2011), "Evaluation of a prototype dengue-1 DNA vaccine in a Phase 1 clinical trial", *Vaccine,* Vol. 29, No. 5.

Beltramello, M., K. L. Williams, C. P. Simmons, A. Macagno, L. Simonelli, N. T. H. Quyen, S. Sukupolvi-Petty, E. Navarro-Sanchez, P. R. Young and A. M. De Silva (2010), "The human immune response to Dengue virus is dominated by highly cross-reactive antibodies endowed with neutralizing and enhancing activity", *Cell host & microbe,* Vol. 8, No. 3.

Bera, A. K., R. J. Kuhn and J. L. Smith (2007), "Functional characterization of cis and trans activity of the Flavivirus NS2B-NS3 protease", *Journal of Biological Chemistry,* Vol. 282, No. 17.

Bernardo, L., A. Izquierdo, M. Alvarez, D. Rosario, I. Prado, C. López, R. Martínez, J. Castro, E. Santana and L. Hermida (2008), "Immunogenicity and protective efficacy of a recombinant fusion protein containing the domain III of the dengue 1 envelope protein in non-human primates", *Antiviral research,* Vol. 80, No. 2.

Bhamarapravati, N. and Y. Sutee (2000), "Live attenuated tetravalent dengue vaccine", *Vaccine,* Vol. 18.

Bhatt, S., P. W. Gething, O. J. Brady, J. P. Messina, A. W. Farlow, C. L. Moyes, J. M. Drake, J. S. Brownstein, A. G. Hoen and O. Sankoh (2013), "The global distribution and burden of dengue", *Nature*.

Bressanelli, S., K. Stiasny, S. L. Allison, E. A. Stura, S. Duquerroy, J. Lescar, F. X. Heinz and F. A. Rey (2004), "Structure of a flavivirus envelope glycoprotein in its low-pH-induced membrane fusion conformation", *The EMBO journal,* Vol. 23, No. 4.

Brien, J. D., S. K. Austin, S. Sukupolvi-Petty, K. M. O'brien, S. Johnson, D. H. Fremont and M. S. Diamond (2010), "Genotype-specific neutralization and protection by antibodies against dengue virus type 3", *Journal of virology,* Vol. 84, No. 20.

Butrapet, S., C. Y.-H. Huang, D. J. Pierro, N. Bhamarapravati, D. J. Gubler and R. M. Kinney (2000), "Attenuation markers of a candidate dengue type 2 vaccine virus, strain 16681 (PDK-53), are defined by mutations in the 5′ noncoding region and nonstructural proteins 1 and 3", *Journal of virology,* Vol. 74, No. 7.

Campbell, M. G., D. Veesler, A. Cheng, C. S. Potter and B. Carragher (2015), "2.8 Å resolution reconstruction of the Thermoplasma acidophilum 20S proteasome using cryo-electron microscopy", *eLife,* Vol. 4.

Capeding, M. R., N. H. Tran, S. R. S. Hadinegoro, H. I. H. M. Ismail, T. Chotpitayasunondh, M. N. Chua, C. Q. Luong, K. Rusmil, D. N. Wirawan and R. Nallusamy (2014), "Clinical efficacy and safety of a novel tetravalent dengue vaccine in healthy children in Asia:

a phase 3, randomised, observer-masked, placebo-controlled trial", *The Lancet,* Vol. 384, No. 9951.

Capeding, R. Z., I. A. Luna, E. Bomasang, S. Lupisan, J. Lang, R. Forrat, A. Wartel and D. Crevat (2011), "Live-attenuated, tetravalent dengue vaccine in children, adolescents and adults in a dengue endemic country: randomized controlled phase I trial in the Philippines", *Vaccine,* Vol. 29, No. 22.

Carragher, B., N. Kisseberth, D. Kriegman, R. A. Milligan, C. S. Potter, J. Pulokas and A. Reilein (2000), "Leginon: an automated system for acquisition of images from vitreous ice specimens", *Journal of structural biology,* Vol. 132, No. 1.

Chan, K. R., S. L.-X. Zhang, H. C. Tan, Y. K. Chan, A. Chow, A. P. C. Lim, S. G. Vasudevan, B. J. Hanson and E. E. Ooi (2011), "Ligation of Fc gamma receptor IIB inhibits antibody-dependent enhancement of dengue virus infection", *Proceedings of the National Academy of Sciences,* Vol. 108, No. 30.

Chen, S.-T., Y.-L. Lin, M.-T. Huang, M.-F. Wu, S.-C. Cheng, H.-Y. Lei, C.-K. Lee, T.-W. Chiou, C.-H. Wong and S.-L. Hsieh (2008), "CLEC5A is critical for dengue-virus-induced lethal disease", *Nature,* Vol. 453, No. 7195.

Chen, V. B., W. B. Arendall, J. J. Headd, D. A. Keedy, R. M. Immormino, G. J. Kapral, L. W. Murray, J. S. Richardson and D. C. Richardson (2009), "MolProbity: all-atom structure validation for macromolecular crystallography", *Acta Crystallographica Section D: Biological Crystallography,* Vol. 66, No. 1.

Chen, Y.-C., S.-Y. Wang and C.-C. King (1999), "Bacterial lipopolysaccharide inhibits dengue virus infection of primary human monocytes/macrophages by blockade of virus entry via a CD14-dependent mechanism", *Journal of virology,* Vol. 73, No. 4.

Chen, Y., T. Maguire, R. E. Hileman, J. R. Fromm, J. D. Esko, R. J. Linhardt and R. M. Marks (1997), "Dengue virus infectivity depends on envelope protein binding to target cell heparan sulfate", *Nature medicine,* Vol. 3, No. 8.

Cheng, Y. (2015), "Single-particle cryo-EM at crystallographic resolution", *Cell,* Vol. 161, No. 3.

Cherrier, M. V., B. Kaufmann, G. E. Nybakken, S. M. Lok, J. T. Warren, B. R. Chen, C. A. Nelson, V. A. Kostyuchenko, H. A. Holdaway and P. R. Chipman (2009), "Structural basis for the preferential recognition of immature flaviviruses by a fusion‐loop antibody", *The EMBO journal,* Vol. 28, No. 20.

Chung, K. M., M. K. Liszewski, G. Nybakken, A. E. Davis, R. R. Townsend, D. H. Fremont, J. P. Atkinson and M. S. Diamond (2006), "West Nile virus nonstructural protein NS1 inhibits complement activation by binding the regulatory protein factor H", *Proceedings of the National Academy of Sciences,* Vol. 103, No. 50.

Clements, D. E., B.-a. G. Coller, M. M. Lieberman, S. Ogata, G. Wang, K. E. Harada, J. R. Putnak, J. M. Ivy, M. Mcdonell and G. S. Bignami (2010), "Development of a recombinant tetravalent dengue virus vaccine: immunogenicity and efficacy studies in mice and monkeys", *Vaccine,* Vol. 28, No. 15.

Cockburn, J. J., M. E. Navarro Sanchez, N. Fretes, A. Urvoas, I. Staropoli, C. M. Kikuti, L. L. Coffey, F. Arenzana Seisdedos, H. Bedouelle and F. A. Rey (2012a), "Mechanism of dengue virus broad cross-neutralization by a monoclonal antibody", *Structure,* Vol. 20, No. 2.

Cockburn, J. J., M. E. Navarro Sanchez, A. P. Goncalvez, E. Zaitseva, E. A. Stura, C. M. Kikuti, S. Duquerroy, P. Dussart, L. V. Chernomordik and C. J. Lai (2012b), "Structural insights into the neutralization mechanism of a higher primate antibody against dengue virus", *The EMBO journal,* Vol. 31, No. 3.

Coller, B.-a. G., D. E. Clements, A. J. Bett, S. L. Sagar and J. H. Ter Meulen (2011), "The development of recombinant subunit envelope-based vaccines to protect against dengue virus induced disease", *Vaccine,* Vol. 29, No. 42.

Costin, J. M., E. Zaitseva, K. M. Kahle, C. O. Nicholson, D. K. Rowe, A. S. Graham, L. E. Bazzone, G. Hogancamp, M. F. Sierra and R. H. Fong (2013), "Mechanistic study of broadly neutralizing human monoclonal antibodies against dengue virus that target the fusion loop", *Journal of virology,* Vol. 87, No. 1.

Crill, W. D., H. R. Hughes, M. J. Delorey and G.-J. J. Chang (2009), "Humoral immune responses of dengue fever patients using epitope-specific serotype-2 virus-like particle antigens", *PLoS One,* Vol. 4, No. 4.

Crill, W. D. and J. T. Roehrig (2001), "Monoclonal antibodies that bind to domain III of dengue virus E glycoprotein are the most efficient blockers of virus adsorption to Vero cells", *Journal of Virology,* Vol. 75, No. 16.

Crowther, R., L. Amos, J. Finch, D. De Rosier and A. Klug (1970), "Three dimensional reconstructions of spherical viruses by fourier synthesis from electron micrographs", *Nature,* Vol. 226, No. 5244.

De Alwis, R., M. Beltramello, W. B. Messer, S. Sukupolvi-Petty, W. M. Wahala, A. Kraus, N. P. Olivarez, Q. Pham, J. Brian and W.-Y. Tsai (2011), "In-depth analysis of the antibody response of individuals exposed to primary dengue virus infection", *PLoS neglected tropical diseases,* Vol. 5, No. 6.

De Alwis, R., S. A. Smith, N. P. Olivarez, W. B. Messer, J. P. Huynh, W. M. Wahala, L. J. White, M. S. Diamond, R. S. Baric and J. E. Crowe (2012), "Identification of human neutralizing antibodies that bind to complex epitopes on dengue virions", *Proceedings of the National Academy of Sciences,* Vol. 109, No. 19.

Dejnirattisai, W., A. Jumnainsong, N. Onsirisakul, P. Fitton, S. Vasanawathana, W. Limpitikul, C. Puttikhunt, C. Edwards, T. Duangchinda and S. Supasa (2010), "Cross-reacting antibodies enhance dengue virus infection in humans", *Science Signaling,* Vol. 328, No. 5979.

Dejnirattisai, W., W. Wongwiwat, S. Supasa, X. Zhang, X. Dai, A. Rouvinsky, A. Jumnainsong, C. Edwards, N. T. H. Quyen and T. Duangchinda (2015), "A new class of highly potent, broadly neutralizing antibodies isolated from viremic patients infected with dengue virus", *Nature immunology,* Vol. 16, No. 2.

Dowd, K. A., S. Mukherjee, R. J. Kuhn and T. C. Pierson (2014), "Combined effects of the structural heterogeneity and dynamics of flaviviruses on antibody recognition", *Journal of virology,* Vol. 88, No. 20.

Dowd, K. A. and T. C. Pierson (2011), "Antibody-mediated neutralization of flaviviruses: a reductionist view", *Virology,* Vol. 411, No. 2.

Duangchinda, T., W. Dejnirattisai, S. Vasanawathana, W. Limpitikul, N. Tangthawornchaikul, P. Malasit, J. Mongkolsapaya and G. Screaton (2010), "Immunodominant T-cell responses to dengue virus NS3 are associated with DHF", *Proceedings of the National Academy of Sciences,* Vol. 107, No. 39.

Dung, N. T. P., H. T. Le Duyen, N. T. Van Thuy, T. Van Ngoc, N. V. V. Chau, T. T. Hien, S. L. Rowland-Jones, T. Dong, J. Farrar and B. Wills (2010), "Timing of CD8+ T cell responses in relation to commencement of capillary leakage in children with dengue", *The Journal of Immunology,* Vol. 184, No. 12.

Durbin, A. P., B. D. Kirkpatrick, K. K. Pierce, D. Elwood, C. J. Larsson, J. C. Lindow, C. Tibery, B. P. Sabundayo, D. Shaffer and K. R. Talaat (2013), "A single dose of any of four different live attenuated tetravalent dengue vaccines is safe and immunogenic in flavivirus-naive adults: a randomized, double-blind clinical trial", *Journal of Infectious Diseases,* Vol. 207, No. 6.

Durbin, A. P., M. J. Vargas, K. Wanionek, S. N. Hammond, A. Gordon, C. Rocha, A. Balmaseda and E. Harris (2008), "Phenotyping of peripheral blood mononuclear cells during acute dengue illness demonstrates infection and increased activation of monocytes in severe cases compared to classic dengue fever", *Virology,* Vol. 376, No. 2.

Edeling, M. A., S. K. Austin, B. Shrestha, K. A. Dowd, S. Mukherjee, C. A. Nelson, S. Johnson, M. N. Mabila, E. A. Christian and J. Rucker (2014), "Potent Dengue virus neutralization by a therapeutic antibody with low monovalent affinity requires bivalent engagement", *PLoS pathogens,* Vol. 10, No. 4.

Edelman, R., S. S. Wasserman, S. A. Bodison, R. J. Putnak, K. H. Eckels, D. Tang, N. Kanesa-Thasan, D. W. Vaughn, B. L. Innis and W. Sun (2003), "Phase I trial of 16 formulations of a tetravalent live-attenuated dengue vaccine", *The American journal of tropical medicine and hygiene,* Vol. 69, No. 6 suppl.

Egloff, M. P., D. Benarroch, B. Selisko, J. L. Romette and B. Canard (2002), "An RNA cap (nucleoside‐2′‐O‐)‐methyltransferase in the flavivirus RNA polymerase NS5: crystal structure and functional characterization", *The EMBO journal,* Vol. 21, No. 11.

Emsley, P., B. Lohkamp, W. G. Scott and K. Cowtan (2010), "Features and development of Coot", *Acta Crystallographica Section D: Biological Crystallography,* Vol. 66, No. 4.

Englander, S. W. and N. R. Kallenbach (1983), "Hydrogen exchange and structural dynamics of proteins and nucleic acids", *Quarterly reviews of biophysics,* Vol. 16, No. 04.

Erb, S. M., S. Butrapet, K. J. Moss, B. E. Luy, T. Childers, A. E. Calvert, S. J. Silengo, J. T. Roehrig, C. Y.-H. Huang and C. D. Blair (2010), "Domain-III FG loop of the dengue virus type 2

envelope protein is important for infection of mammalian cells and< i> Aedes aegypti</i> mosquitoes", *Virology,* Vol. 406, No. 2.

Fibriansah, G., K. D. Ibarra, T.-S. Ng, S. A. Smith, J. L. Tan, X.-N. Lim, J. S. Ooi, V. A. Kostyuchenko, J. Wang and A. M. De Silva (2015a), "Cryo-EM structure of an antibody that neutralizes dengue virus type 2 by locking E protein dimers", *Science,* Vol. 349, No. 6243.

Fibriansah, G., T.-S. Ng, V. A. Kostyuchenko, J. Lee, S. Lee, J. Wang and S.-M. Lok (2013), "Structural Changes in Dengue Virus When Exposed to a Temperature of 37° C", *Journal of virology,* Vol. 87, No. 13.

Fibriansah, G., J. L. Tan, S. A. Smith, A. R. Alwis, T. S. Ng, V. A. Kostyuchenko, K. D. Ibarra, J. Wang, E. Harris and A. Silva (2014), "A potent anti‐dengue human antibody preferentially recognizes the conformation of E protein monomers assembled on the virus surface", *EMBO molecular medicine*.

Fibriansah, G., J. L. Tan, S. A. Smith, R. De Alwis, T.-S. Ng, V. A. Kostyuchenko, R. S. Jadi, P. Kukkaro, A. M. De Silva and J. E. Crowe (2015b), "A highly potent human antibody neutralizes dengue virus serotype 3 by binding across three surface proteins", *Nature communications,* Vol. 6.

Fischer, N., P. Neumann, A. L. Konevega, L. V. Bock, R. Ficner, M. V. Rodnina and H. Stark (2015), "Structure of the E. coli ribosome-EF-Tu complex at< 3 A resolution by Cs-corrected cryo-EM", *Nature*.

Goncalvez, A. P., R. E. Engle, M. S. Claire, R. H. Purcell and C.-J. Lai (2007), "Monoclonal antibody-mediated enhancement of dengue virus infection in vitro and in vivo and strategies for prevention", *Proceedings of the National Academy of Sciences,* Vol. 104, No. 22.

Grant, T. and N. Grigorieff (2015), "Measuring the optimal exposure for single particle cryo-EM using a 2.6 Å reconstruction of rotavirus VP6", *eLife*.

Gromowski, G. D. and A. D. Barrett (2007), "Characterization of an antigenic site that contains a dominant, type-specific neutralization determinant on the envelope protein domain III (ED3) of dengue 2 virus", *Virology,* Vol. 366, No. 2.

Gubler, D. J. (1988), "Dengue", *The arboviruses: epidemiology and ecology,* Vol. 2.

Gubler, D. J. (1998), "Dengue and dengue hemorrhagic fever", *Clinical microbiology reviews,* Vol. 11, No. 3.

Guirakhoo, F., J. Arroyo, K. Pugachev, C. Miller, Z.-X. Zhang, R. Weltzin, K. Georgakopoulos, J. Catalan, S. Ocran and K. Soike (2001), "Construction, safety, and immunogenicity in nonhuman primates of a chimeric yellow fever-dengue virus tetravalent vaccine", *Journal of virology,* Vol. 75, No. 16.

Gutsche, I., F. Coulibaly, J. E. Voss, J. Salmon, J. D'alayer, M. Ermonval, E. Larquet, P. Charneau, T. Krey and F. Mégret (2011), "Secreted dengue virus nonstructural protein NS1 is an atypical barrel-shaped high-density lipoprotein", *Proceedings of the National Academy of Sciences*.

Guttman, M., A. Cupo, J.-P. Julien, R. W. Sanders, I. A. Wilson, J. P. Moore and K. K. Lee (2015), "Antibody potency relates to the ability to recognize the closed, pre-fusion form of HIV Env", *Nature communications,* Vol. 6.

Guy, B., B. Barrere, C. Malinowski, M. Saville, R. Teyssou and J. Lang (2011), "From research to phase III: preclinical, industrial and clinical development of the Sanofi Pasteur tetravalent dengue vaccine", *Vaccine,* Vol. 29, No. 42.

Guzman, M. G., S. B. Halstead, H. Artsob, P. Buchy, J. Farrar, D. J. Gubler, E. Hunsperger, A. Kroeger, H. S. Margolis and E. Martínez (2010), "Dengue: a continuing global threat", *Nature Reviews Microbiology,* Vol. 8.

Hadinegoro, S. R., J. L. Arredondo-García, M. R. Capeding, C. Deseda, T. Chotpitayasunondh, R. Dietze, H. Hj Muhammad Ismail, H. Reynales, K. Limkittikul and D. M. Rivera-Medina (2015), "Efficacy and long-term safety of a dengue vaccine in regions of endemic disease", *New England Journal of Medicine,* Vol. 373, No. 13.

Halstead, S. and E. O'rourke (1977a), "Antibody-enhanced dengue virus infection in primate leukocytes".

Halstead, S. and E. O'rourke (1977b), "Dengue viruses and mononuclear phagocytes. I. Infection enhancement by non-neutralizing antibody", *The Journal of experimental medicine,* Vol. 146, No. 1.

Halstead, S. B. (1988), "Pathogenesis of dengue: challenges to molecular biology", *Science,* Vol. 239, No. 4839.

Henchal, E., J. Mccown, D. Burke, M. Seguin and W. Brandt (1985), "Epitopic analysis of antigenic determinants on the surface of dengue-2 virions using monoclonal antibodies", *The American journal of tropical medicine and hygiene,* Vol. 34, No. 1.

Henderson, R., A. Sali, M. L. Baker, B. Carragher, B. Devkota, K. H. Downing, E. H. Egelman, Z. Feng, J. Frank and N. Grigorieff (2012), "Outcome of the first electron microscopy validation task force meeting", *Structure,* Vol. 20, No. 2.

Hermida, L., L. Bernardo, J. Martín, M. Alvarez, I. Prado, C. López, B. D. L. C. Sierra, R. Martínez, R. Rodríguez and A. Zulueta (2006), "A recombinant fusion protein containing the domain III of the dengue-2 envelope protein is immunogenic and protective in nonhuman primates", *Vaccine,* Vol. 24, No. 16.

Hoke, C. H., A. Nisalak, N. Sangawhipa, S. Jatanasen, T. Laorakapongse, B. L. Innis, S.-O. Kotchasenee, J. B. Gingrich, J. Latendresse and K. Fukai (1988), "Protection against Japanese encephalitis by inactivated vaccines", *New England Journal of Medicine,* Vol. 319, No. 10.

Holzmann, H., F. X. Heinz, C. Mandl, F. Guirakhoo and C. Kunz (1990), "A single amino acid substitution in envelope protein E of tick-borne encephalitis virus leads to attenuation in the mouse model", *Journal of virology,* Vol. 64, No. 10.

Huang, C. Y.-H., S. Butrapet, K. R. Tsuchiya, N. Bhamarapravati, D. J. Gubler and R. M. Kinney (2003), "Dengue 2 PDK-53 virus as a chimeric carrier for tetravalent dengue vaccine development", *Journal of virology,* Vol. 77, No. 21.

Innis, B., A. Nisalak, S. Nimmannitya, S. Kusalerdchariya, V. Chongswasdi, S. Suntayakorn, P. Puttisri and C. Hoke (1989), "An enzyme-linked immunosorbent assay to characterize dengue infections where dengue and Japanese encephalitis co-circulate", *The American journal of tropical medicine and hygiene,* Vol. 40, No. 4.

Jessie, K., M. Y. Fong, S. Devi, S. K. Lam and K. T. Wong (2004), "Localization of dengue virus in naturally infected human tissues, by immunohistochemistry and in situ hybridization", *Journal of Infectious Diseases,* Vol. 189, No. 8.

Jiang, J., B. L. Pentelute, R. J. Collier and Z. H. Zhou (2015), "Atomic structure of anthrax protective antigen pore elucidates toxin translocation", *Nature,* Vol. 521, No. 7553.

Jindadamrongwech, S., C. Thepparit and D. Smith (2004), "Identification of GRP 78 (BiP) as a liver cell expressed receptor element for dengue virus serotype 2", *Archives of virology,* Vol. 149, No. 5.

John, A. L. S., S. N. Abraham and D. J. Gubler (2013), "Barriers to preclinical investigations of anti-dengue immunity and dengue pathogenesis", *Nature Reviews Microbiology*.

Jones, C. T., L. Ma, J. W. Burgner, T. D. Groesch, C. B. Post and R. J. Kuhn (2003), "Flavivirus capsid is a dimeric alpha-helical protein", *Journal of virology,* Vol. 77, No. 12.

Jones, T. A., J.-Y. Zou, S. T. Cowan and M. Kjeldgaard (1991), "Improved methods for building protein models in electron density maps and the location of errors in these models", *Acta Crystallographica Section A: Foundations of Crystallography,* Vol. 47, No. 2.

Kanesa-Thasan, N., W. Sun, G. Kim-Ahn, S. Van Albert, J. Putnak, A. King, B. Raengsakulsrach, H. Christ-Schmidt, K. Gilson and J. Zahradnik (2001), "Safety and immunogenicity of attenuated dengue virus vaccines (Aventis Pasteur) in human volunteers", *Vaccine,* Vol. 19, No. 23.

Kaufmann, B. (2006), "WNV in complex with the Fab fragment of a neutralizing MAb", *PNAS*.

Kaufmann, B., M. R. Vogt, J. Goudsmit, H. A. Holdaway, A. A. Aksyuk, P. R. Chipman, R. J. Kuhn, M. S. Diamond and M. G. Rossmann (2010), "Neutralization of West Nile virus by cross-linking of its surface proteins with Fab fragments of the human monoclonal antibody CR4354", *Proceedings of the National Academy of Sciences,* Vol. 107, No. 44.

Kim, M., Z.-Y. J. Sun, K. D. Rand, X. Shi, L. Song, Y. Cheng, A. F. Fahmy, S. Majumdar, G. Ofek and Y. Yang (2011), "Antibody mechanics on a membrane-bound HIV segment essential for GP41-targeted viral neutralization", *Nature structural & molecular biology,* Vol. 18, No. 11.

Kirkpatrick, B. D., A. P. Durbin, K. K. Pierce, M. P. Carmolli, C. M. Tibery, P. L. Grier, N. Hynes, S. A. Diehl, D. Elwood and A. P. Jarvis (2015), "Robust and balanced immune responses to all 4 dengue virus serotypes following administration of a single dose of a live attenuated tetravalent dengue vaccine to healthy, flavivirus-naive adults", *Journal of Infectious Diseases*.

Kitchener, S., M. Nissen, P. Nasveld, R. Forrat, S. Yoksan, J. Lang and J.-F. Saluzzo (2006), "Immunogenicity and safety of two live-attenuated tetravalent dengue vaccine formulations in healthy Australian adults", *Vaccine,* Vol. 24, No. 9.

Klein, D. E., J. L. Choi and S. C. Harrison (2013), "Structure of a dengue virus envelope protein late-stage fusion intermediate", *Journal of virology,* Vol. 87, No. 4.

Kliks, S. C., S. Nimmanitya, A. Nisalak and D. S. Burke (1988), "Evidence that maternal dengue antibodies are important in the development of dengue hemorrhagic fever in infants", *The American journal of tropical medicine and hygiene,* Vol. 38, No. 2.

Kostyuchenko, V. A., Q. Zhang, J. L. Tan, T.-S. Ng and S.-M. Lok (2013), "Immature and mature dengue serotype 1 virus structures provide insight into the maturation process", *Journal of virology,* Vol. 87, No. 13.

Krissinel, E. and K. Henrick (2007), "Inference of macromolecular assemblies from crystalline state", *Journal of molecular biology,* Vol. 372, No. 3.

Kuhn, R. J., W. Zhang, M. G. Rossmann, S. V. Pletnev, J. Corver, E. Lenches, C. T. Jones, S. Mukhopadhyay, P. R. Chipman and E. G. Strauss (2002), "Structure of dengue virus: implications for flavivirus organization, maturation, and fusion", *Cell,* Vol. 108, No. 5.

Kuno, G., G.-J. J. Chang, K. R. Tsuchiya, N. Karabatsos and C. B. Cropp (1998), "Phylogeny of the genus Flavivirus", *Journal of virology,* Vol. 72, No. 1.

Kurane, I., B. L. Innis, A. Nisalak, C. Hoke, S. Nimmannitya, A. Meager and F. A. Ennis (1989), "Human T cell responses to dengue virus antigens. Proliferative responses and interferon gamma production", *Journal of Clinical Investigation,* Vol. 83, No. 2.

Lai, C.-Y., W.-Y. Tsai, S.-R. Lin, C.-L. Kao, H.-P. Hu, C.-C. King, H.-C. Wu, G.-J. Chang and W.-K. Wang (2008), "Antibodies to envelope glycoprotein of dengue virus during the natural course of infection are predominantly cross-reactive and recognize epitopes containing highly conserved residues at the fusion loop of domain II", *Journal of virology,* Vol. 82, No. 13.

Lawrence, M. C. and P. M. Colman (1993), "Shape complementarity at protein/protein interfaces", *Journal of molecular biology,* Vol. 234, No. 4.

Lee, E., R. C. Weir and L. Dalgarno (1997), "Changes in the dengue virus major envelope protein on passaging and their localization on the three-dimensional structure of the protein", *Virology,* Vol. 232, No. 2.

Lee, P. D., S. Mukherjee, M. A. Edeling, K. A. Dowd, S. K. Austin, C. J. Manhart, M. S. Diamond, D. H. Fremont and T. C. Pierson (2013), "The Fc region of an antibody impacts the neutralization of West Nile viruses in different maturation states", *Journal of virology,* Vol. 87, No. 24.

Leng, C.-H., S.-J. Liu, J.-P. Tsai, Y.-S. Li, M.-Y. Chen, H.-H. Liu, S.-P. Lien, A. Yueh, K.-N. Hsiao and L.-W. Lai (2009), "A novel dengue vaccine candidate that induces cross-neutralizing antibodies and memory immunity", *Microbes and Infection,* Vol. 11, No. 2.

Li, H., S. Clum, S. You, K. E. Ebner and R. Padmanabhan (1999), "The serine protease and RNA-stimulated nucleoside triphosphatase and RNA helicase functional domains of dengue virus type 2 NS3 converge within a region of 20 amino acids", *Journal of virology,* Vol. 73, No. 4.

Li, L., S.-M. Lok, I.-M. Yu, Y. Zhang, R. J. Kuhn, J. Chen and M. G. Rossmann (2008), "The flavivirus precursor membrane-envelope protein complex: structure and maturation", *Science,* Vol. 319, No. 5871.

Lin, C.-F., S.-C. Chiu, Y.-L. Hsiao, S.-W. Wan, H.-Y. Lei, A.-L. Shiau, H.-S. Liu, T.-M. Yeh, S.-H. Chen and C.-C. Liu (2005), "Expression of cytokine, chemokine, and adhesion molecules during endothelial cell activation induced by antibodies against dengue virus nonstructural protein 1", *The Journal of Immunology,* Vol. 174, No. 1.

Lin, C. F., H. Y. Lei, A. L. Shiau, C. C. Liu, H. S. Liu, T. M. Yeh, S. H. Chen and Y. S. Lin (2003), "Antibodies from dengue patient sera cross‐react with endothelial cells and induce damage", *Journal of medical virology,* Vol. 69, No. 1.

Lindenbach, B. D. and C. Rice (2001), "Flaviviridae: the viruses and their replication", *Fields virology,* Vol. 1.

Lindenbach, B. D. and C. M. Rice (1997), "trans-Complementation of yellow fever virus NS1 reveals a role in early RNA replication", *Journal of virology,* Vol. 71, No. 12.

Lindenbach, B. D. and C. M. Rice (1999), "Genetic interaction of flavivirus nonstructural proteins NS1 and NS4A as a determinant of replicase function", *Journal of virology,* Vol. 73, No. 6.

Lindenbach, B. D. and C. M. Rice (2003), "Molecular biology of flaviviruses", *Advances in virus research,* Vol. 59.

Liu, J. and S. C. Thorp (2002), "Cell surface heparan sulfate and its roles in assisting viral infections", *Medicinal research reviews,* Vol. 22, No. 1.

Liu, X. (2007), "Averaging tens to hundreds of icosahedral particle images to resolve protein secondary structure elements using a MPSA optimization algorithm", *J Struct Biol*.

Liu, X., W. Jiang, J. Jakana and W. Chiu (2007), "Averaging tens to hundreds of icosahedral particle images to resolve protein secondary structure elements using a Multi-Path Simulated Annealing optimization algorithm", *Journal of structural biology,* Vol. 160, No. 1.

Lok, S.-M., V. Kostyuchenko, G. E. Nybakken, H. A. Holdaway, A. J. Battisti, S. Sukupolvi-Petty, D. Sedlak, D. H. Fremont, P. R. Chipman and J. T. Roehrig (2008), "Binding of a neutralizing antibody to dengue virus alters the arrangement of surface glycoproteins", *Nature structural & molecular biology,* Vol. 15, No. 3.

Low, J. G., E. Ooi, T. Tolfvenstam, Y.-S. Leo, M. L. Hibberd, L.-C. Ng, Y.-L. Lai, G. Yap, C. Li and S. G. Vasudevan (2006), "Early Dengue infection and outcome study (EDEN)-study design and preliminary findings", *ANNALS-ACADEMY OF MEDICINE SINGAPORE,* Vol. 35, No. 11.

Lozach, P.-Y., L. Burleigh, I. Staropoli, E. Navarro-Sanchez, J. Harriague, J.-L. Virelizier, F. A. Rey, P. Desprès, F. Arenzana-Seisdedos and A. Amara (2005), "Dendritic cell-specific intercellular adhesion molecule 3-grabbing non-integrin (DC-SIGN)-mediated enhancement of dengue virus infection is independent of DC-SIGN internalization signals", *Journal of Biological Chemistry,* Vol. 280, No. 25.

Ludtke, S. J., P. R. Baldwin and W. Chiu (1999), "EMAN: semiautomated software for high-resolution single-particle reconstructions", *Journal of structural biology,* Vol. 128, No. 1.

Ma, L., C. T. Jones, T. D. Groesch, R. J. Kuhn and C. B. Post (2004), "Solution structure of dengue virus capsid protein reveals another fold", *Proceedings of the National Academy of Sciences of the United States of America,* Vol. 101, No. 10.

Mackenzie, J. M., M. K. Jones and P. R. Young (1996), "Immunolocalization of the dengue virus nonstructural glycoprotein NS1 suggests a role in viral RNA replication", *Virology,* Vol. 220, No. 1.

Mandl, C. W., S. L. Allison, H. Holzmann, T. Meixner and F. X. Heinz (2000), "Attenuation of tick-borne encephalitis virus by structure-based site-specific mutagenesis of a putative flavivirus receptor binding site", *Journal of virology,* Vol. 74, No. 20.

Markoff, L., B. Falgout and A. Chang (1997), "A conserved internal hydrophobic domain mediates the stable membrane integration of the dengue virus capsid protein", *Virology,* Vol. 233, No. 1.

Mccoy, A. J., R. W. Grosse-Kunstleve, P. D. Adams, M. D. Winn, L. C. Storoni and R. J. Read (2007), "Phaser crystallographic software", *Journal of applied crystallography,* Vol. 40, No. 4.

Men, R., M. Bray, D. Clark, R. M. Chanock and C.-J. Lai (1996), "Dengue type 4 virus mutants containing deletions in the 3'noncoding region of the RNA genome: analysis of growth restriction in cell culture and altered viremia pattern and immunogenicity in rhesus monkeys", *Journal of virology,* Vol. 70, No. 6.

Midgley, C. M., A. Flanagan, H. B. Tran, W. Dejnirattisai, K. Chawansuntati, A. Jumnainsong, W. Wongwiwat, T. Duangchinda, J. Mongkolsapaya and J. M. Grimes (2012), "Structural analysis of a dengue cross-reactive antibody complexed with envelope domain III reveals the molecular basis of cross-reactivity", *The Journal of Immunology,* Vol. 188, No. 10.

Miller, J. L., B. J. M Dewet, L. Martinez-Pomares, C. M. Radcliffe, R. A. Dwek, P. M. Rudd and S. Gordon (2008), "The mannose receptor mediates dengue virus infection of macrophages", *PLoS pathogens,* Vol. 4, No. 2.

Miller, S., S. Kastner, J. Krijnse-Locker, S. Bühler and R. Bartenschlager (2007), "The non-structural protein 4A of dengue virus is an integral membrane protein inducing membrane alterations in a 2K-regulated manner", *Journal of Biological Chemistry,* Vol. 282, No. 12.

Miller, S., S. Sparacio and R. Bartenschlager (2006), "Subcellular localization and membrane topology of the dengue virus type 2 non-structural protein 4B", *Journal of Biological Chemistry,* Vol. 281, No. 13.

Mindell, J. A. and N. Grigorieff (2003), "Accurate determination of local defocus and specimen tilt in electron microscopy", *Journal of structural biology,* Vol. 142, No. 3.

Modis, Y., S. Ogata, D. Clements and S. C. Harrison (2003), "A ligand-binding pocket in the dengue virus envelope glycoprotein", *Proceedings of the National Academy of Sciences,* Vol. 100, No. 12.

Modis, Y., S. Ogata, D. Clements and S. C. Harrison (2004), "Structure of the dengue virus envelope protein after membrane fusion", *Nature,* Vol. 427, No. 6972.

Monath, T. P., R. Nichols, W. T. Archambault, L. Moore, R. Marchesani, J. Tian, R. E. Shope, N. Thomas, R. Schrader and D. Furby (2002), "Comparative safety and immunogenicity of two yellow fever 17D vaccines (ARILVAX and YF-VAX) in a phase III multicenter, double-blind clinical trial", *The American journal of tropical medicine and hygiene,* Vol. 66, No. 5.

Mongkolsapaya, J., W. Dejnirattisai, X.-N. Xu, S. Vasanawathana, N. Tangthawornchaikul, A. Chairunsri, S. Sawasdivorn, T. Duangchinda, T. Dong and S. Rowland-Jones (2003), "Original antigenic sin and apoptosis in the pathogenesis of dengue hemorrhagic fever", *Nature medicine,* Vol. 9, No. 7.

Moreland, N. J., P. Susanto, E. Lim, M. Y. Tay, R. Rajamanonmani, B. J. Hanson and S. G. Vasudevan (2012), "Phage Display Approaches for the Isolation of Monoclonal Antibodies Against Dengue Virus Envelope Domain III from Human and Mouse Derived Libraries", *International journal of molecular sciences,* Vol. 13, No. 3.

Morens, D. M., S. Halstead, P. Repik, R. Putvatana and N. Raybourne (1985), "Simplified plaque reduction neutralization assay for dengue viruses by semimicro methods in BHK-21 cells: comparison of the BHK suspension test with standard plaque reduction neutralization", *Journal of clinical microbiology,* Vol. 22, No. 2.

Muñoz-Jordán, J. L., M. Laurent-Rolle, J. Ashour, L. Martínez-Sobrido, M. Ashok, W. I. Lipkin and A. García-Sastre (2005), "Inhibition of alpha/beta interferon signaling by the NS4B protein of flaviviruses", *Journal of virology,* Vol. 79, No. 13.

Muñoz-Jordán, J. L., G. G. Sánchez-Burgos, M. Laurent-Rolle and A. García-Sastre (2003), "Inhibition of interferon signaling by dengue virus", *Proceedings of the National Academy of Sciences,* Vol. 100, No. 24.

Mukhopadhyay, S., W. Zhang, S. Gabler, P. R. Chipman, E. G. Strauss, J. H. Strauss, T. S. Baker, R. J. Kuhn and M. G. Rossmann (2006), "Mapping the structure and function of the E1 and E2 glycoproteins in alphaviruses", *Structure,* Vol. 14, No. 1.

Muller, D. A. and P. R. Young (2013), "The flavivirus NS1 protein: molecular and structural biology, immunology, role in pathogenesis and application as a diagnostic biomarker", *Antiviral research,* Vol. 98, No. 2.

Navarro‐Sanchez, E., R. Altmeyer, A. Amara, O. Schwartz, F. Fieschi, J. L. Virelizier, F. Arenzana‐Seisdedos and P. Desprès (2003), "Dendritic‐cell‐specific ICAM3‐grabbing non‐integrin is essential for the productive infection of human dendritic cells by mosquito‐cell‐derived dengue viruses", *EMBO reports,* Vol. 4, No. 7.

Nayak, V., M. Dessau, K. Kucera, K. Anthony, M. Ledizet and Y. Modis (2009), "Crystal structure of dengue virus type 1 envelope protein in the postfusion conformation and its implications for membrane fusion", *Journal of virology,* Vol. 83, No. 9.

Nybakken, G. E., T. Oliphant, S. Johnson, S. Burke, M. S. Diamond and D. H. Fremont (2005), "Structural basis of West Nile virus neutralization by a therapeutic antibody", *Nature,* Vol. 437, No. 7059.

Oliphant, T., G. E. Nybakken, S. K. Austin, Q. Xu, J. Bramson, M. Loeb, M. Throsby, D. H. Fremont, T. C. Pierson and M. S. Diamond (2007), "Induction of epitope-specific neutralizing antibodies against West Nile virus", *Journal of virology,* Vol. 81, No. 21.

Osorio, J. E., I. D. Velez, C. Thomson, L. Lopez, A. Jimenez, A. A. Haller, S. Silengo, J. Scott, K. L. Boroughs and J. L. Stovall (2014), "Safety and immunogenicity of a recombinant live attenuated tetravalent dengue vaccine (DENVax) in flavivirus-naive healthy adults in Colombia: a randomised, placebo-controlled, phase 1 study", *The Lancet Infectious Diseases,* Vol. 14, No. 9.

Otwinowski, Z., W. Minor and C. C. W Jr (1997), "Processing of X-ray diffraction data collected in oscillation mode".

Pandit, D., S. J. Tuske, S. J. Coales, A. Liu, J. E. Lee, J. A. Morrow, J. F. Nemeth and Y. Hamuro (2012), "Mapping of discontinuous conformational epitopes by amide hydrogen/deuterium exchange mass spectrometry and computational docking", *Journal of Molecular Recognition,* Vol. 25, No. 3.

Paterson, Y., S. W. Englander and H. Roder (1990), "An antibody binding site on cytochrome c defined by hydrogen exchange and two-dimensional NMR", *Science,* Vol. 249, No. 4970.

Patkar, C. G. and R. J. Kuhn (2008), "Yellow fever virus NS3 plays an essential role in virus assembly independent of its known enzymatic functions", *Journal of virology,* Vol. 82, No. 7.

Penczek, P., J. Zhu, R. Schröder and J. Frank (1997), "Three dimensional reconstruction with contrast transfer compensation from defocus series", *Scanning Microsc,* Vol. 11.

Pettersen, E. F., T. D. Goddard, C. C. Huang, G. S. Couch, D. M. Greenblatt, E. C. Meng and T. E. Ferrin (2004), "UCSF Chimera—a visualization system for exploratory research and analysis", *Journal of computational chemistry,* Vol. 25, No. 13.

Pickett, B. E., E. L. Sadat, Y. Zhang, J. M. Noronha, R. B. Squires, V. Hunt, M. Liu, S. Kumar, S. Zaremba and Z. Gu (2012), "ViPR: an open bioinformatics database and analysis resource for virology research", *Nucleic acids research,* Vol. 40, No. D1.

Pierson, T. C., Q. Xu, S. Nelson, T. Oliphant, G. E. Nybakken, D. H. Fremont and M. S. Diamond (2007), "The stoichiometry of antibody-mediated neutralization and enhancement of West Nile virus infection", *Cell host & microbe,* Vol. 1, No. 2.

Pokidysheva, E., Y. Zhang, A. J. Battisti, C. M. Bator-Kelly, P. R. Chipman, C. Xiao, G. G. Gregorio, W. A. Hendrickson, R. J. Kuhn and M. G. Rossmann (2006), "Cryo-EM reconstruction of dengue virus in complex with the carbohydrate recognition domain of DC-SIGN", *Cell,* Vol. 124, No. 3.

Putnak, R., D. A. Barvir, J. M. Burrous, D. R. Dubois, V. M. D'andrea, C. H. Hoke, J. C. Sadoff and K. H. Eckels (1996), "Development of a purified, inactivated, dengue-2 virus vaccine prototype in Vero cells: immunogenicity and protection in mice and rhesus monkeys", *Journal of Infectious Diseases,* Vol. 174, No. 6.

Raviprakash, K., D. Ewing, M. Simmons, K. R. Porter, T. R. Jones, C. G. Hayes, R. Stout and G. S. Murphy (2003), "Needle-free Biojector injection of a dengue virus type 1 DNA vaccine with human immunostimulatory sequences and the GM-CSF gene increases immunogenicity and protection from virus challenge in Aotus monkeys", *Virology,* Vol. 315, No. 2.

Ray, D., A. Shah, M. Tilgner, Y. Guo, Y. Zhao, H. Dong, T. S. Deas, Y. Zhou, H. Li and P.-Y. Shi (2006), "West Nile virus 5′-cap structure is formed by sequential guanine N-7 and ribose 2′-O methylations by nonstructural protein 5", *Journal of virology,* Vol. 80, No. 17.

Rey, F. A., F. X. Heinz, C. Mandl, C. Kunz and S. C. Harrison (1995), "The envelope glycoprotein from tick-borne encephalitis virus at 2 Å resolution".

Reyes-Del Valle, J., S. Chávez-Salinas, F. Medina and R. M. Del Angel (2005), "Heat shock protein 90 and heat shock protein 70 are components of dengue virus receptor complex in human cells", *Journal of virology,* Vol. 79, No. 8.

Rico-Hesse, R. (1990), "Molecular evolution and distribution of dengue viruses type 1 and 2 in nature", *Virology,* Vol. 174, No. 2.

Rico-Hesse, R. (2003), "Microevolution and virulence of dengue viruses", *Advances in virus research,* Vol. 59.

Rivino, L., E. A. Kumaran, V. Jovanovic, K. Nadua, E. W. Teo, S. W. Pang, G. H. Teo, V. C. H. Gan, D. C. Lye and Y. S. Leo (2012), "Differential Targeting of Viral Components by CD4+ versus CD8+ T Lymphocytes in Dengue Infection", *Journal of virology*.

Rodenhuis-Zybert, I. A., H. M. Van Der Schaar, J. M. Da Silva Voorham, H. Van Der Ende-Metselaar, H.-Y. Lei, J. Wilschut and J. M. Smit (2010), "Immature dengue virus: a veiled pathogen?", *PLoS pathogens,* Vol. 6, No. 1.

Rodenhuis-Zybert, I. A., J. Wilschut and J. M. Smit (2011), "Partial maturation: an immune-evasion strategy of dengue virus?", *Trends in microbiology,* Vol. 19, No. 5.

Roehrig, J. T., R. A. Bolin and R. G. Kelly (1998), "Monoclonal antibody mapping of the envelope glycoprotein of the dengue 2 virus, Jamaica", *Virology,* Vol. 246, No. 2.

Romero-Brey, I. and R. Bartenschlager (2014), "Membranous replication factories induced by plus-strand RNA viruses", *Viruses,* Vol. 6, No. 7.

Rosenthal, P. B. and R. Henderson (2003), "Optimal determination of particle orientation, absolute hand, and contrast loss in single-particle electron cryomicroscopy", *Journal of molecular biology,* Vol. 333, No. 4.

Rothman, A. L. (2004), "Dengue: defining protective versus pathologic immunity", *Journal of Clinical Investigation,* Vol. 113, No. 7.

Rothman, A. L. (2011), "Immunity to dengue virus: a tale of original antigenic sin and tropical cytokine storms", *Nature Reviews Immunology,* Vol. 11, No. 8.

Rouvinski, A., P. Guardado-Calvo, G. Barba-Spaeth, S. Duquerroy, M.-C. Vaney, C. M. Kikuti, M. E. N. Sanchez, W. Dejnirattisai, W. Wongwiwat and A. Haouz (2015), "Recognition determinants of broadly neutralizing human antibodies against dengue viruses", *Nature*.

Sabchareon, A., J. Lang, P. Chanthavanich, S. Yoksan, R. Forrat, P. Attanath, C. Sirivichayakul, K. Pengsaa, C. Pojjaroen-Anant and L. Chambonneau (2004), "Safety and immunogenicity of a three dose regimen of two tetravalent live-attenuated dengue vaccines in five-to twelve-year-old Thai children", *The Pediatric infectious disease journal,* Vol. 23, No. 2.

Sabchareon, A., D. Wallace, C. Sirivichayakul, K. Limkittikul, P. Chanthavanich, S. Suvannadabba, V. Jiwariyavej, W. Dulyachai, K. Pengsaa and T. A. Wartel (2012), "Protective efficacy of the recombinant, live-attenuated, CYD tetravalent dengue vaccine in Thai schoolchildren: a randomised, controlled phase 2b trial", *The Lancet,* Vol. 380, No. 9853.

Sabin, A. B. (1952), "Research on dengue during World War II", *The American journal of tropical medicine and hygiene,* Vol. 1, No. 1.

Scheres, S. H. (2010a), "Chapter Eleven-Classification of Structural Heterogeneity by Maximum-Likelihood Methods", *Methods in enzymology,* Vol. 482.

Scheres, S. H. (2010b), "Maximum-likelihood methods in cryo-EM. Part II: application to experimental data", *Methods in enzymology,* Vol. 482.

Scheres, S. H. (2012), "RELION: implementation of a Bayesian approach to cryo-EM structure determination", *Journal of structural biology*.

Scheres, S. H., H. Gao, M. Valle, G. T. Herman, P. P. Eggermont, J. Frank and J.-M. Carazo (2007), "Disentangling conformational states of macromolecules in 3D-EM through likelihood optimization", *Nature Methods,* Vol. 4, No. 1.

Scheres, S. H., M. Valle, R. Nuñez, C. O. Sorzano, R. Marabini, G. T. Herman and J.-M. Carazo (2005), "Maximum-likelihood multi-reference refinement for electron microscopy images", *Journal of molecular biology,* Vol. 348, No. 1.

Shen, Z., P. Li, R.-J. Ni, M. Ritchie, C.-P. Yang, G.-F. Liu, W. Ma, G.-J. Liu, L. Ma and S.-J. Li (2009), "Label-free quantitative proteomics analysis of etiolated maize seedling leaves during greening", *Molecular & Cellular Proteomics,* Vol. 8, No. 11.

Shrestha, B., J. D. Brien, S. Sukupolvi-Petty, S. K. Austin, M. A. Edeling, T. Kim, K. M. O'brien, C. A. Nelson, S. Johnson and D. H. Fremont (2010), "The development of therapeutic antibodies that neutralize homologous and heterologous genotypes of dengue virus type 1", *PLoS pathogens,* Vol. 6, No. 4.

Smith, S. A., A. R. De Alwis, N. Kose, R. S. Jadi, A. M. De Silva and J. E. Crowe (2014), "Isolation of dengue virus-specific memory B cells with live virus antigen from human subjects following natural infection reveals the presence of diverse novel functional groups of antibody clones", *Journal of virology,* Vol. 88, No. 21.

Smith, S. A., R. De Alwis, N. Kose, A. P. Durbin, S. S. Whitehead, A. M. De Silva and J. E. Crowe (2013), "Human monoclonal antibodies derived from memory B cells following live attenuated dengue virus vaccination or natural infection exhibit similar characteristics", *Journal of Infectious Diseases,* Vol. 207, No. 12.

Smith, S. A., Y. Zhou, N. P. Olivarez, A. H. Broadwater, A. M. De Silva and J. E. Crowe (2012), "Persistence of circulating memory B cell clones with potential for dengue virus disease enhancement for decades following infection", *Journal of virology,* Vol. 86, No. 5.

Stadler, K., S. L. Allison, J. Schalich and F. X. Heinz (1997), "Proteolytic activation of tick-borne encephalitis virus by furin", *Journal of Virology,* Vol. 71, No. 11.

Stiasny, K., S. Brandler, C. Kössl and F. X. Heinz (2007), "Probing the flavivirus membrane fusion mechanism by using monoclonal antibodies", *Journal of virology,* Vol. 81, No. 20.

Stieh, D. J., D. F. King, K. Klein, P. Liu, X. Shen, K. K. Hwang, G. Ferrari, D. C. Montefiori, B. Haynes and P. Pitisuttithum (2014), "Aggregate complexes of HIV-1 induced by multimeric antibodies", *Retrovirology,* Vol. 11, No. 1.

Sukupolvi-Petty, S., S. K. Austin, W. E. Purtha, T. Oliphant, G. E. Nybakken, J. J. Schlesinger, J. T. Roehrig, G. D. Gromowski, A. D. Barrett and D. H. Fremont (2007), "Type-and subcomplex-specific neutralizing antibodies against domain III of dengue virus type 2 envelope protein recognize adjacent epitopes", *Journal of virology,* Vol. 81, No. 23.

Sun, W., D. Cunningham, S. S. Wasserman, J. Perry, J. R. Putnak, K. H. Eckels, D. W. Vaughn, S. J. Thomas, N. Kanesa-Thasan and B. L. Innis (2009), "Phase 2 clinical trial of three formulations of tetravalent live-attenuated dengue vaccine in flavivirus-naive adults", *Human Vaccines,* Vol. 5, No. 1.

Sun, W., R. Edelman, N. Kanesa-Thasan, K. H. Eckels, J. R. Putnak, A. D. King, H.-S. Houng, D. Tang, J. M. Scherer and C. H. Hoke (2003), "Vaccination of human volunteers with monovalent and tetravalent live-attenuated dengue vaccine candidates", *The American journal of tropical medicine and hygiene,* Vol. 69, No. 6 suppl.

Tang, G., L. Peng, P. R. Baldwin, D. S. Mann, W. Jiang, I. Rees and S. J. Ludtke (2007), "EMAN2: an extensible image processing suite for electron microscopy", *Journal of structural biology,* Vol. 157, No. 1.

Tassaneetrithep, B., T. H. Burgess, A. Granelli-Piperno, C. Trumpfheller, J. Finke, W. Sun, M. A. Eller, K. Pattanapanyasat, S. Sarasombath and D. L. Birx (2003), "DC-SIGN (CD209) mediates dengue virus infection of human dendritic cells", *The Journal of experimental medicine,* Vol. 197, No. 7.

Teo, E. W. (2014), "Generation and Characterization of Human Monoclonal Antibodies with Neutralizing Activity for Dengue Virus", (ed)^(eds).

Teoh, E. P., P. Kukkaro, E. W. Teo, A. P. Lim, T. T. Tan, A. Yip, W. Schul, M. Aung, V. A. Kostyuchenko, Y. S. Leo, S. H. Chan, K. G. Smith, A. H. Chan, G. Zou, E. E. Ooi, D. M. Kemeny, G. K. Tan, J. K. Ng, M. L. Ng, S. Alonso, D. Fisher, P. Y. Shi, B. J. Hanson, S. M. Lok and P. A. Macary (2012), "The structural basis for serotype-specific neutralization of dengue virus by a human antibody", *Sci Transl Med,* Vol. 4, No. 139, Jun 20.

Thepparit, C. and D. R. Smith (2004), "Serotype-specific entry of dengue virus into liver cells: identification of the 37-kilodalton/67-kilodalton high-affinity laminin receptor as a dengue virus serotype 1 receptor", *Journal of virology,* Vol. 78, No. 22.

Thomas, S. J. (2014), "Developing a dengue vaccine: progress and future challenges", *Annals of the New York Academy of Sciences,* Vol. 1323, No. 1.

Thompson, B. S., B. Moesker, J. M. Smit, J. Wilschut, M. S. Diamond and D. H. Fremont (2009), "A therapeutic antibody against West Nile virus neutralizes infection by blocking fusion within endosomes", *PLoS pathogens,* Vol. 5, No. 5.

Tsai, W.-Y., C.-Y. Lai, Y.-C. Wu, H.-E. Lin, C. Edwards, A. Jumnainsong, S. Kliks, S. Halstead, J. Mongkolsapaya and G. R. Screaton (2013), "High-avidity and potently neutralizing cross-reactive human monoclonal antibodies derived from secondary dengue virus infection", *Journal of virology,* Vol. 87, No. 23.

Van Der Schaar, H. M., M. J. Rust, C. Chen, H. Van Der Ende-Metselaar, J. Wilschut, X. Zhuang and J. M. Smit (2008), "Dissecting the cell entry pathway of dengue virus by single-particle tracking in living cells", *PLoS pathogens,* Vol. 4, No. 12.

Van Der Schaar, H. M., M. J. Rust, B.-L. Waarts, H. Van Der Ende-Metselaar, R. J. Kuhn, J. Wilschut, X. Zhuang and J. M. Smit (2007), "Characterization of the early events in dengue virus cell entry by biochemical assays and single-virus tracking", *Journal of virology,* Vol. 81, No. 21.

Wahala, W., A. A. Kraus, L. B. Haymore, M. A. Accavitti-Loper and A. M. De Silva (2009), "Dengue virus neutralization by human immune sera: role of envelope protein domain III-reactive antibody", *Virology,* Vol. 392, No. 1.

Wahala, W. M., E. F. Donaldson, R. De Alwis, M. A. Accavitti-Loper, R. S. Baric and A. M. De Silva (2010), "Natural strain variation and antibody neutralization of dengue serotype 3 viruses", *PLoS pathogens,* Vol. 6, No. 3.

Wang, E., H. Ni, R. Xu, A. D. Barrett, S. J. Watowich, D. J. Gubler and S. C. Weaver (2000), "Evolutionary relationships of endemic/epidemic and sylvatic dengue viruses", *Journal of virology,* Vol. 74, No. 7.

Wang, L. C., L. K. Morgan, P. Godakumbura, L. J. Kenney and G. S. Anand (2012), "The inner membrane histidine kinase EnvZ senses osmolality via helix-coil transitions in the cytoplasm", *The EMBO journal,* Vol. 31, No. 11.

Wang, S.-H., W.-J. Syu, K.-J. Huang, H.-Y. Lei, C.-W. Yao, C.-C. King and S.-T. Hu (2002), "Intracellular localization and determination of a nuclear localization signal of the core protein of dengue virus", *Journal of general virology,* Vol. 83, No. 12.

Watanabe, S., K. W. K. Chan, J. Wang, L. Rivino, S.-M. Lok and S. G. Vasudevan (2015), "Dengue Virus Infection with Highly Neutralizing Levels of Cross-Reactive Antibodies Causes Acute Lethal Small Intestinal Pathology without a High Level of Viremia in Mice", *Journal of virology,* Vol. 89, No. 11.

Weiskopf, D., M. A. Angelo, E. L. De Azeredo, J. Sidney, J. A. Greenbaum, A. N. Fernando, A. Broadwater, R. V. Kolla, A. D. De Silva and A. M. De Silva (2013), "Comprehensive analysis of dengue virus-specific responses supports an HLA-linked protective role for CD8+ T cells", *Proceedings of the National Academy of Sciences,* Vol. 110, No. 22.

Whitehead, S. S., B. Falgout, K. A. Hanley, J. E. Blaney Jr, L. Markoff and B. R. Murphy (2003), "A live, attenuated dengue virus type 1 vaccine candidate with a 30-nucleotide deletion in the 3′ untranslated region is highly attenuated and immunogenic in monkeys", *Journal of virology,* Vol. 77, No. 2.

Who (2009), "Guidelines for diagnosis, Treatment", *Prevention and Control. Geneva: World Health Organization*.

Williams, K. L., W. M. Wahala, S. Orozco, A. M. De Silva and E. Harris (2012), "Antibodies targeting dengue virus envelope domain III are not required for serotype-specific protection or prevention of enhancement< i> in vivo</i>", *Virology*.

Xie, X., S. Gayen, C. Kang, Z. Yuan and P.-Y. Shi (2013), "Membrane topology and function of dengue virus NS2A protein", *Journal of virology,* Vol. 87, No. 8.

Xie, X., J. Zou, Q.-Y. Wang, C. G. Noble, J. Lescar and P.-Y. Shi (2014), "Generation and characterization of mouse monoclonal antibodies against NS4B protein of dengue virus", *Virology,* Vol. 450.

Yamada, N., E. I. Suzuki and K. Hirayama (2002), "Identification of the interface of a large protein–protein complex using H/D exchange and Fourier transform ion cyclotron resonance mass spectrometry", *Rapid communications in mass spectrometry,* Vol. 16, No. 4.

Yamshchikov, V. F. and R. W. Compans (1995), "Formation of the flavivirus envelope: role of the viral NS2B-NS3 protease", *Journal of virology,* Vol. 69, No. 4.

Yap, T. L., T. Xu, Y.-L. Chen, H. Malet, M.-P. Egloff, B. Canard, S. G. Vasudevan and J. Lescar (2007), "Crystal structure of the dengue virus RNA-dependent RNA polymerase catalytic domain at 1.85-angstrom resolution", *Journal of virology,* Vol. 81, No. 9.

Youn, S., T. Li, B. T. Mccune, M. A. Edeling, D. H. Fremont, I. M. Cristea and M. S. Diamond (2012), "Evidence for a genetic and physical interaction between nonstructural

proteins NS1 and NS4B that modulates replication of West Nile virus", *Journal of virology,* Vol. 86, No. 13.

Yu, I.-M., W. Zhang, H. A. Holdaway, L. Li, V. A. Kostyuchenko, P. R. Chipman, R. J. Kuhn, M. G. Rossmann and J. Chen (2008), "Structure of the immature dengue virus at low pH primes proteolytic maturation", *Science,* Vol. 319, No. 5871.

Zaitseva, E., S.-T. Yang, K. Melikov, S. Pourmal and L. V. Chernomordik (2010), "Dengue virus ensures its fusion in late endosomes using compartment-specific lipids", *PLoS pathogens,* Vol. 6, No. 10.

Zellweger, R. M., T. R. Prestwood and S. Shresta (2010), "Enhanced infection of liver sinusoidal endothelial cells in a mouse model of antibody-induced severe dengue disease", *Cell host & microbe,* Vol. 7, No. 2.

Zhang, W., P. R. Chipman, J. Corver, P. R. Johnson, Y. Zhang, S. Mukhopadhyay, T. S. Baker, J. H. Strauss, M. G. Rossmann and R. J. Kuhn (2003), "Visualization of membrane protein domains by cryo-electron microscopy of dengue virus", *Nature Structural & Molecular Biology,* Vol. 10, No. 11.

Zhang, X., J. Sheng, P. Plevka, R. J. Kuhn, M. S. Diamond and M. G. Rossmann (2013), "Dengue structure differs at the temperatures of its human and mosquito hosts", *Proceedings of the National Academy of Sciences,* Vol. 110, No. 17.

Zhou, Y., S. K. Austin, D. H. Fremont, B. L. Yount, J. P. Huynh, A. M. De Silva, R. S. Baric and W. B. Messer (2013), "The mechanism of differential neutralization of dengue serotype 3 strains by monoclonal antibody 8A1", *Virology,* Vol. 439, No. 1.

Zhou, Y., D. Ray, Y. Zhao, H. Dong, S. Ren, Z. Li, Y. Guo, K. A. Bernard, P.-Y. Shi and H. Li (2007), "Structure and function of flavivirus NS5 methyltransferase", *Journal of virology,* Vol. 81, No. 8.

Zuest, R., I. Valdes, D. Skibinski, Y. Lin, Y. X. Toh, K. Chan, L. Hermida, J. Connolly, G. Guillen and K. Fink (2015), "Tetravalent dengue DIIIC protein together with alum and ODN elicits a Th1 response and neutralizing antibodies in mice", *Vaccine,* Vol. 33, No. 12.